Automated detection of river morphodynamics for large multithreaded rivers with satellite imagery

A case study on the Ayeyarwady river

Automated detection of river morphodynamics for large multithreaded rivers with satellite imagery

A case study on the Ayeyarwady river

Master Thesis Civil Engineering and Management

University of Twente

Faculty of Engineering Technology

Water Engineering and Management

Author: Joep Rawee (s1590138)

Supervision: Dr. ir. D.C.M. Augustijn
University of Twente, Department of Water Engineering and Management

Dr. F. Huthoff
University of Twente, Department of Water Engineering and Management
HKV- Lijn in water

Date: 28-02-2020

PREFACE

This thesis marks the end of my master Civil Engineering and Management at the University of Twente. In my thesis I applied remote sensing to study river planform dynamics. Remote sensing was a new topic for me. During the past months, I learned a lot about the potential, but also about the challenges, of applying remote sensing to study rivers and their dynamics.

I would like to thank HKV for giving me the opportunity to execute this research project as an intern in Lelystad. I experienced a great time as an intern due to the nice working atmosphere. Furthermore, I would like to thank Mattijn van Hoek for the excellent help he provided by answering technical questions about remote sensing and scripting in Python. Also, I would like to thank Carolien Wegman for introducing me into the topic of remote sensing to study river morphodynamics.

Finally, I would like to thank my supervisors at the University of Twente: Denie Augustijn and Freek Huthoff. They provided valuable feedback on the research structure but also on potential directions for the study.

Joep Rawee, February 2020

SUMMARY

Understanding planform dynamics is a difficult task as they are controlled by complex interactions between the discharge variability, sediment transport, floodplain characteristics and the valley geometry. The difficulties in understanding planform dynamics especially become clear in multithreaded river planforms, whose existence is still poorly understood. Multithreaded river planforms are characterized by a complex geometry with multiple channels separated by bars or islands. Satellite imagery combined with automated detection techniques might be key to generate a better understanding of planform dynamics, due to their ability to study large spatial scales. However, automated detection and quantification of planform dynamics is challenging, especially in complex multithreaded rivers. The main goal of this thesis is therefore to investigate the possibilities of automated detection techniques with satellite imagery to characterize, quantify and explain planform dynamics for large multithreaded rivers

There exist several ways to consistently identify the river surface. The main challenge is to eliminate the effect of a varying water level, as the water level affects the extent of the water surface. To eliminate this effect two techniques are applied. The first is to automatically detect the vegetation boundary, which is assumed to be the river bankline. The second method uses water level measurements to select images with a similar water level and automatically detects the water surface. To study planform dynamics there is opted to use yearly intervals, in which images are selected in each dry season. This limits cloud cover in the study area and allows to study the effect of yearly occurring flood seasons on planform dynamics. The final step is to quantify yearly changes in river planform, which is done by differencing the detected river masks. This allows to quantify areas of change in metrics such as erosion and deposition.

Next, the methods are applied at a case study of the multithreaded Ayeyarwady river (Myanmar). A roughly 250 km long river section located in the lower Ayeyarwady river is studied. Strong variability in planform dynamics over time is detected. Some years measure up to 3 times the amount of erosion as other years. The intensity of the planform dynamics is found to be strongly correlated to the average water level in the 4-month lasting flood season. Thus, yearly variations in average flood season intensity explain the large yearly variability in the measured intensity of the planform dynamics. Besides, the active surface area of the river, or the total area between the river banklines, is investigated. A decreasing trend is found in the study period of 1988-2019, indicating the abandonment of channels and a reduction in the overall river width. A plausible explanation that is found is a reduction in the long-term average intensity of flood seasons. The reduced intensity especially becomes clear between 1998 and 2010, in which relatively calm flood seasons are measured. This caused the abandonment of some of the active channels which resulted in a strong decrease in active channel area in the study period.

The results of the case study show that even in complex multithreaded rivers, the usage of automatic detection on satellite imagery allows to quantify and characterize planform dynamics. The ability of automated detection techniques to quantify planform dynamics on large spatial scales, allowed to quantitatively study the controls of observed planform dynamics. In this way, the large impact of flood season intensity and its yearly variations could be identified. Some difficulties and limits remain, such as the uncertainty in detection, the spatial resolution of satellite images, and the remaining challenges to consistently derive river banklines. Nevertheless, this study shows the potential of automated detection techniques to better understand planform dynamics in rivers with complex multithreaded planforms. With ever-increasing pressure on river systems due to climate change or human interventions such as river dams, understanding the controls of planform dynamics is key to successfully manage rivers and their dynamics in the future.

TABLE OF CONTENTS

1 INTRODUCTION

1.1 GENERAL INTRODUCTION

Worldwide river systems are essential by providing fresh water, transportation and important natural habitats. At the same time, they also pose risks. The river planform, or the river geometry as seen from above, is generally unstable and various planform dynamics take place. Examples are the migration of channels, the creation of new channels by avulsion and the formation of bars and islands. These dynamics can have unwanted effects on infrastructure, flood safety and shipping. Successful management is largely dependent on a good understanding of the processes leading to river dynamics (Ward, 1994).

To get an understanding of the existence of different planform geometries (or channel patterns) and their dynamics, classification schemes were proposed. A well-known classification of channel planforms is straight, meandering and braided (Leopold & Wolman, 1957). Furthermore, anabranching is often added, which is generally described as a large multithreaded river with stable vegetated islands (Latrubesse, 2008). Some examples of the different channel patterns are given in Figure 1. A common approach to classify different channel patterns is creating empirical models, which use parameters such as the bankfull discharge, channel slope and sediment size (e.g. Leopold & Wolman, 1957; Schumm, 1985; Van den Berg, 1995). These parameters can be used to get an understanding of the controls of planforms and their dynamics. Nevertheless, creating a thorough understanding of the controls of channel patterns and the planform dynamics remains difficult, as it depends on a large number of factors such as discharge variability, sediment transport, floodplain characteristics and the valley geometry (Harmar & Clifford, 2006; Słowik, 2018). The difficulties especially become clear in multithreaded anabranching rivers, whose existence is still poorly understood (Carling et al., 2014; Latrubesse, 2008).

Remote sensing is a very effective tool to identify planform changes (Gupta, 2012). Recent developments in automated detection techniques allow to identify planform dynamics on unprecedented scales (Monegaglia et al., 2018). These techniques can quantify planform changes, which can help in improving the understanding of drivers and conditions leading to these dynamics. Furthermore, as planform dynamics give rise to different channel patterns (Gupta, 2012), this can possibly help to identify the controls of channel patterns. This thesis will, therefore, investigate the possibilities of satellite imagery to improve the understanding of planform dynamics for large multithreaded rivers. To this end, satellite imagery will be combined with automated detection techniques in Google Earth Engine.

Figure 1: From left to right: Meandering single-thread river (Coghlan, 2014), multithreaded braided river (Geological Survey of Canada, 2008) and a multithreaded anabranching river with stable vegetated islands (Cruciat, 2010).

1.2 CASE DESCRIPTION: AYEYARWADY RIVER

As a case study a roughly 250 km long section of the Ayeyarwady river in Myanmar is studied (see Figure 2). Like many of the other large rivers of the world, the Ayeyarwady river is characterised by a multithreaded anabranching river planform, recognised by the large vegetated islands. With a mean annual discharge of approximately 13,000 m^3/s (Jansen et al., 1994), it is one of the larger rivers of Asia. Furthermore, it is one of the last long free-flowing rivers in Asia (WWF, 2019), which means the natural variation in discharge and sediment transport is still present. The hydrology in the Ayeyarwady basin shows distinct dry and wet seasons, with relatively steady low water levels during the months December-April (dry season), and high water level peaks in the months June-October (wet season). The study area ranges from Pyay to Nyaungdon, which is the lower section of the Ayeyarwady river. The studied river section can be considered as the start of the delta. Just like many other parts of the Ayeyarwady river, it is characterised by intense morphological changes, including significant channel shifts, bar movements and avulsions on a year-to-year basis.

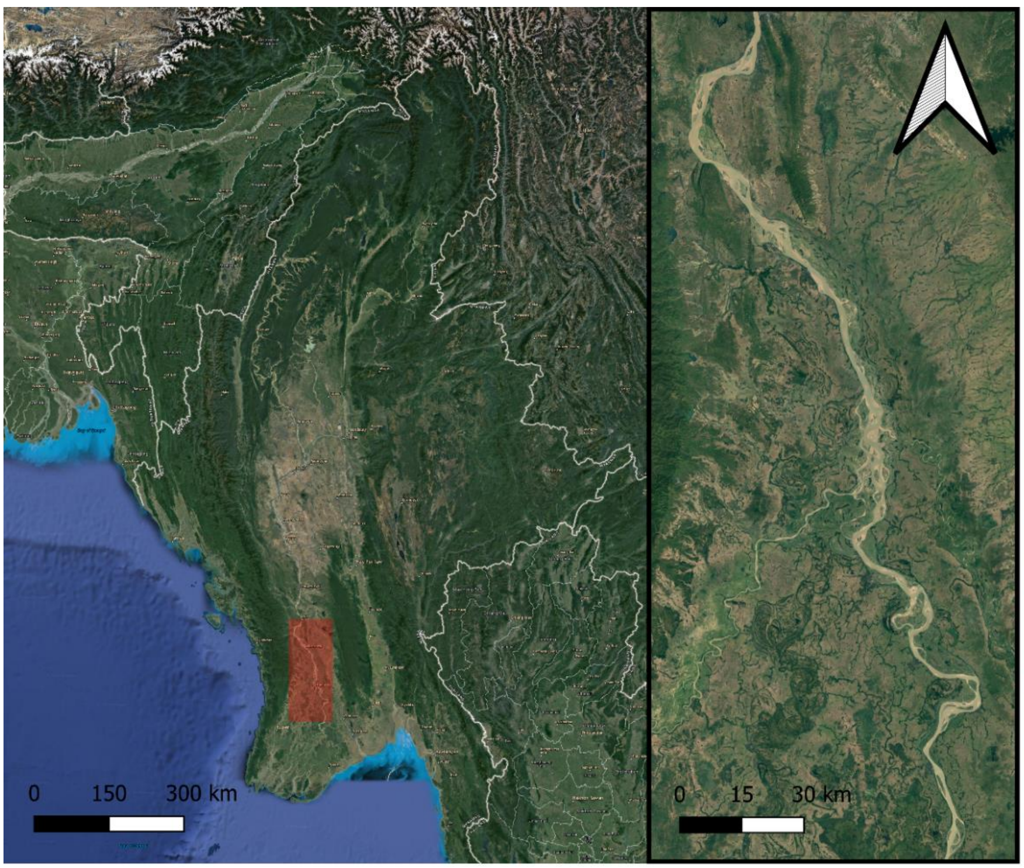

Figure 2: Study area and its location within Myanmar. Satellite images from Google Earth (2019).

1.3 RESEARCH ON PLANFORM DYNAMICS IN MULTITHREADED RIVERS

Over the last decades, there have been a wide variety of studies on river planform changes and their drivers. In the past, a common method to improve the understanding of planforms and their dynamics were flume studies. For example, both Leopold & Wolman (1957) and Ashmore (1991) used flume experiments to study the conditions and processes that lead to the formation of multithreaded braided rivers. By being able to control the conditions, the controls of channel patterns and planform dynamics could be studied extensively. However, the scale of the experiments is often limited, which comes with abstraction from reality (Kleinhans, 2010). A different method to study planform changes are field studies, which have an advantage by using actual observations of river morphodynamics. A downside of field studies for highly dynamic rivers is that a large number of samples in time and space are needed to create a reliable dataset (Ferguson, 1993), which is difficult and costly. More recently numerical modelling is being applied to multithreaded rivers to improve the understanding of drivers of the channel planform and its dynamics (e.g. Moron et al., 2017; Nicholas et al., 2013). Numerical models offer large opportunities by being able to control processes and conditions, which allows to generate a better understanding of the existence of different planform geometries and their dynamics. However, numerical modelling comes with abstractions from reality and some important processes that influence the morphology might not be included (Kleinhans, 2010). This is for example illustrated by the fact that the predicting capability of planform changes, such as lateral mobility, is still limited (Surian, 2015).

Lastly, remote sensing with satellite images is a method that has gained more ground in the last decades to study river planform properties and its dynamics. Although satellite imagery can only be used to study past changes of river planforms, it offers large opportunities by being able to track the river geometry and its changes over time periods of up to 40 years. Satellite images can help improve the understanding of the presence of different planforms, by investigating the planform dynamics and their drivers on large spatial scales. Traditionally, satellite images were digitized by hand for complex tasks such as detecting surface water or river banklines (Rowland, et al., 2016). A recent trend in remote sensing is the use of automatic detection techniques to detect surface water. With techniques like water indices, supervised or unsupervised classification, the water surface can be automatically detected (Yang, et al., 2015). Semi-automated methods and a large amount of freely available imagery provide the opportunity to perform large spatial and temporal scale analysis of rivers without being severely limited by processing time (Fisher et al., 2013). In recent years the development of applications like Google Earth Engine accelerates this type of analysis by providing cloud computing. Cloud computing provides the ability to analyse satellite imagery on a large scale (Kumar & Mutanga, 2018). This, for example, allowed to detect global surface water changes (e.g. Donchyts, 2018). Compared to the other mentioned methods to study planform changes, satellite data thus facilitates the investigation of actually measured planform dynamics and possible drivers of these dynamics on large spatial and temporal scales.

1.4 PROBLEM DEFINITION

The difficulties in understanding the controls of different planform patterns and their dynamics especially become clear in multithreaded anabranching rivers, whose existence is still poorly understood (Carling et al., 2014; Latrubesse, 2008). Remote sensing might be a key instrument to understand the controls of planform patterns and its dynamics. Actual planform dynamics can be quantified, and their key drivers can be quantitatively investigated on large scales. Manual digitization of satellite images is already used for decades to map and study river morphodynamics (e.g. Mertes et al., 1996; Poxeito et al. 2009). However, the possible scale of these methods is limited due to long processing times. Semi-automated methods for detecting surface water have become popular in the analysis of river morphodynamics (e.g. Fisher et al., 2013; Rowland et al., 2016; Schwenk et al., 2017). Nevertheless, even though there are large quantities of satellite data, such as Landsat, Sentinel and MODIS, there is still limited research on how to process this data for systematic analysis of river morphodynamics (Monegaglia et al., 2018). Furthermore, many remote sensing studies of rivers focus on single-thread meandering rivers, which resulted in methods to extract river change metrics that are generally not transferable to multithreaded rivers (Schwenk et al., 2017).

1.5 Research objective and research questions

The objective of this research is to investigate the possibilities of Google Earth Engine combined with automated detection techniques to characterize, quantify and explain planform dynamics for large multithreaded rivers. The main research question is defined as follows:

Main question: *How and to what extent can automated detection techniques on satellite imagery, combined with commonly available data, be used to characterise and explain planform dynamics for large multithreaded rivers?*

The main research question mentions commonly available data, which requires some elaboration. With commonly available data there is aimed at data sources that are available for most large rivers, such as water level measurements or discharge measurements. Besides, other remotely sensed datasets that are available globally or can be derived globally such as elevation maps also fit in this category. Excluded are datasets that require extensive field measurements of the flow, sediment transport and hydraulic geometry. This limit was set to not limit the large benefit satellite images offer, which is its potential to study rivers on a large scale, and globally.

Several sub-questions will help to answer the main research question, which are divided into two separate parts. The first part assists in developing a method to detect and investigate planform changes in multithreaded rivers. The second part focusses on the application of the developed method to the case study. In the end, the combination of developing a method to extract planform changes and applying it to the case study will help to answer the main research question.

Part 1: Background for developing a method to detect planform change

1. In what ways can satellite images combined with commonly available data assist in creating a better understanding of planform dynamics and their controls in multithreaded rivers?

2. How can river planform dynamics be automatically detected and quantified with satellite imagery on a large scale for multithreaded rivers?

Part 2: Applying the method to the case study

3. Which planform dynamics and drivers of these dynamics can be identified in the lower Ayeyarwady river with automated classification on satellite imagery and other commonly available data?

1.6 THESIS OUTLINE

Chapter two describes the literature review, which gives the background for developing a method to automatically detect planform dynamics. The chapter is divided in two parts. The first part focusses on different planform dynamics observed in multithreaded river planforms and their controls. This will give insights on how satellite images and other commonly available data can be used to create a better understanding of planform dynamics. This will assist in answering the first research question. The second part focusses on remote sensing and detection techniques, which assists in answering the second research question. Chapter 3 describes the developed method that is used to study planform dynamics with satellite imagery. In chapter 4 the method is applied to the case study of the Ayeyarwady river, which focusses on answering the third research question. Chapter 5 discusses the methods and the results of the case study. Finally, in chapter 6, the research questions will be answered and recommendations for further research are given. The outline of this thesis and its relationship with the research questions are illustrated in Figure 3.

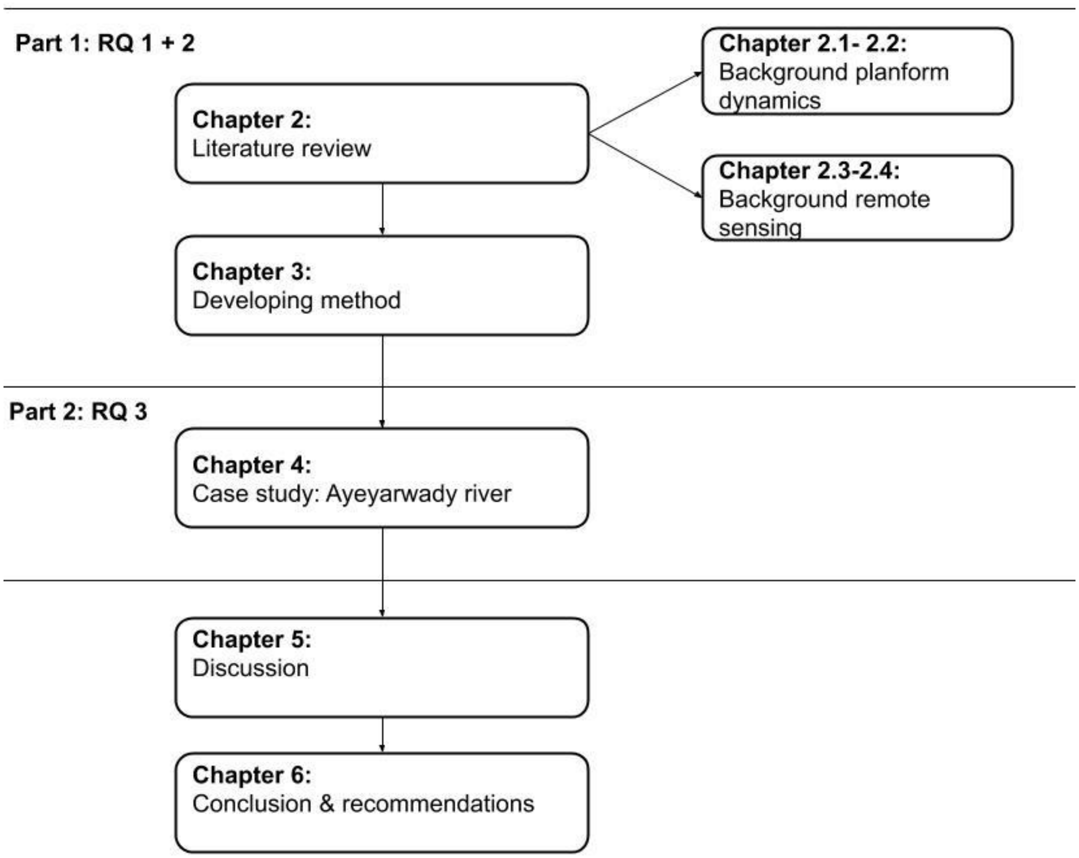

Figure 3: Outline of the thesis and its relationship with the research questions

2 BACKGROUND AND LITERATURE REVIEW

This chapter can be divided into two parts. This first part of this chapter discusses planform dynamics and their drivers on different scales (sections 1 and 2). The second part focusses on remote sensing (sections 3 and 4). The final section gives a summary of the literature review and gives some concluding remarks that are relevant for the next chapter (developing a method).

2.1 CHANNEL PATTERNS AND THEIR CONTROLS

On a reach scale (10s-100s km's) the channel planform geometries are often described in terms of channel patterns. Planform changes on these spatial scales involve transitions of channel patterns or large scale changes in the river geometry. For example, a transition from a multithreaded planform to a single-threaded planform. The planform geometry is often described as a dynamic equilibrium, and to study changes in channel pattern it needs to be considered over a period of years to decades (Blom et al., 2017). Understanding observed changes in channel patterns requires insights into the controls of channel patterns and channel geometry. The different channel patterns and their controls are discussed in the next sections.

2.1.1 Classifying channel patterns

Over the last decades, there have been various attempts at classifying river planforms. One of the first widely used categorizations of channel patterns is straight, meandering or braided (Leopold & Wolman, 1957). Braided rivers are characterized by multiple channels or braids, whilst meandering rivers mostly consist of a single sinuous channel. For straight channels, it holds that they are not common in nature (Leopold & Wolman, 1957).

It was later realized that in many cases the distinction between meandering and braided is not exclusive and various intermediate styles exist (Nanson & Knighton, 1996). For example, within multi-channel or multithreaded river planforms, various classes have been proposed, of which braiding is only one of the classes. Both anabranching and anastomosing rivers are used to describe a more stable form of braiding (Carling et al., 2014). They are characterised by stable vegetated islands that separate the different channels. Nanson & Knighton (1996) use the following definition for anabranching rivers: "A*n anabranching river is defined as a system of multiple channels characterized by vegetated or otherwise stable alluvial islands that divide flows at discharges up to nearly bankfull"*. In terms of morphological characteristics anabranching or anastomosing channel planforms are characterized by a relatively low stream power and/or more stable banks compared to braided rivers (Nanson & Knighton, 1996). Also, the channels in the river planform are more stable compared to braided rivers (Eaton et al., 2010). Stable banks can, for example, be the result of vegetation, the cohesion of the soil, low stream power or a combination of the three.

Next to different classes that are proposed in literature, the methods for the classification also vary. Generally, two divergent groups can be identified: Qualitative and quantitative approaches (Eaton et al., 2010). Qualitative classification schemes use observed characteristics of the river planform. Classifying can be aided by characteristics such as the channel sinuosity or the number of channels (braiding index) in the river planform. For example, meandering rivers are more sinuous than braiding rivers, which are often relatively straight over its length. A downside of these qualitative classifications is that they provide limited insight into the morphodynamics which characterize the planform (Eaton et al., 2010). Furthermore, similar planforms might be present, whilst the underlying morphodynamics are different (Nanson & Knighton, 1996). This led to different ways of classifying channel patterns. An important method that is commonly found is the creation of empirical models, which allows to quantify the classification process. Furthermore, it allowed to improve the understanding of different controls of channel patterns and patterning processes (Eaton et al., 2010). More information on these empirical models and the controls of channel patterns is given in the next section.

2.1.2 Controls of channel patterns

The empirical models often include different parameters, such as the slope, the bankfull discharge and the median grain size, which allowed to identify controls of channel patterns. An example of such an approach is the one of Leopold & Wolman (1957), who derived the following empirical equation to distinguish between braiding and meandering rivers:

$$S_b = 0.013 Q_b^{-0.44} \tag{1}$$

In the equation Q_b is the bankfull discharge and S_b is the channel slope. The equation gives a critical slope for the transition between meandering and braided. An example of the classification with the empirical equations is given in Figure 4. Later it was realized that the grain size also plays a key role in this threshold. Ferguson (1987) added the median grain size to a similar equation. Eaton et al. (2010) used an empirical model to distinguish between anastomosing and braiding rivers. To discriminate these two classes an additional parameter of the bank strength was used. A disadvantage of these types of relations for the classification is the difficulty in quantifying all parameters that can play an important role in the formation of the river planform (Nanson & Knighton, 1996). An example of a difficult to quantify variable is the presence of vegetation.

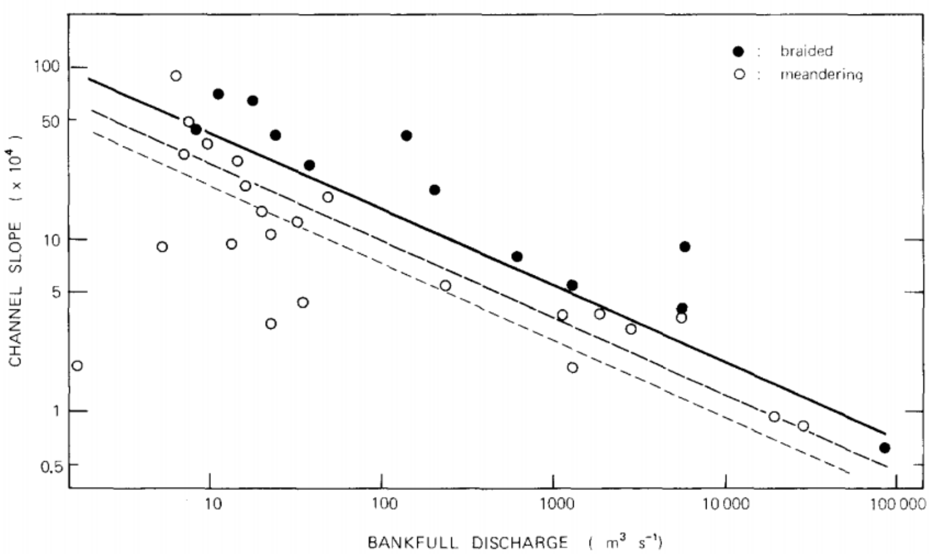

Figure 4: Characterisation of braiding and meandering by defining a relation between the bankfull discharge and the slope (Leopold & Wolman, 1957). The solid line represents equation 1.

If one describes the commonly parameterised drivers of the channel planform they generally fit in the following categories: The supply and transport of sediment, the channel geometry and the flow characteristics, which are often interrelated. Many of the empirical equations use a combination of parameters from these categories (see Table 1). An attempt to visualise the relationships between key drivers of planform formation is given in Figure 5. A problem that is mentioned by for example Kleinhans & Van den Berg (2011) is that often pattern dependent parameters are used, which leaves some problems in the predictive value of such relations. For example, flow characteristics already depend on the planform shape or geometry. This relationship is indicated in Figure 5 by the yellow boxes.

Table 1: An overview of some of the often-used parameters to distinguish channel planforms

Geometry characteristics	Flow characteristics	Transport characteristics
Channel slope (e.g. Leopold and Wolman, 1957) **Width-to-depth ratio (**e.g. Schumm, 1985**)**	**Stream power** (e.g. Van den Berg, 1995) **Bankfull discharge** (e.g. Leopold & Wolman, 1957)	**D50** (e.g. Ferguson, 1987) **Sediment load (**e.g. Schumm, 1985)

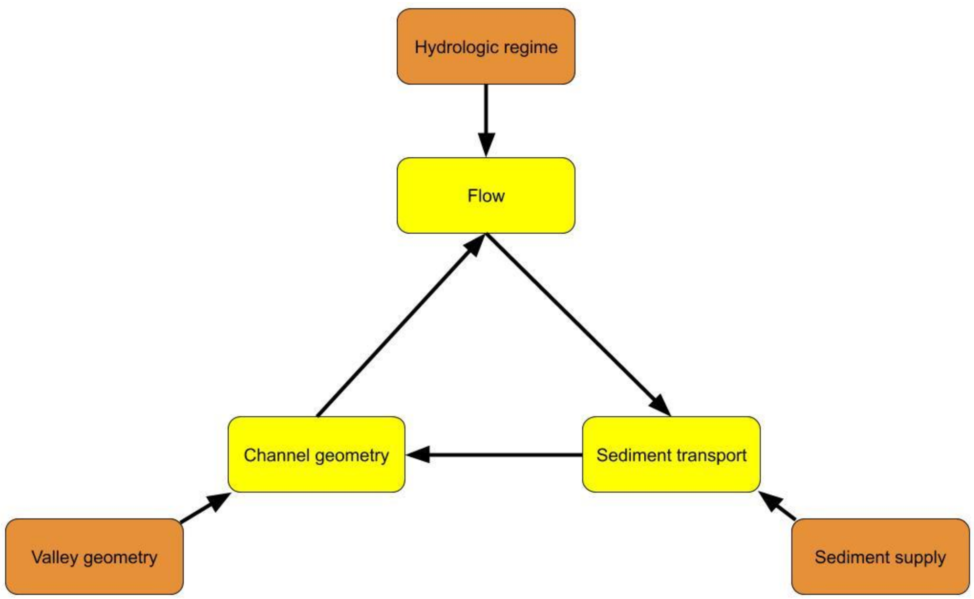

Figure 5: Attempt at generalizing categories of influence on the channel planform. The yellow parameters are dependent on the channel planform, orange parameters are generally independent.

A different representation of the controls of the planform geometry is given in Figure 6. In this figure also different aspects of the valley context are included such as vegetation and the floodplain substrate. Furthermore, it is important to note that both the discharge and sediment transport are variable over time. This variability is hard to describe with parameters used in the empirical models. The empirical models often try to characterize the hydrologic regime with a single steady parameter. For example, a concept that is commonly applied is the bankfull discharge (e.g. Leopold & Wolman, 1957). However, this can miss the importance of for example flood waves which can be essential in the creation of cut-offs, and the ability of plants to colonize exposed bars (Blom et al., 2017). More information on the difficulties in the empirical models is given in the next section.

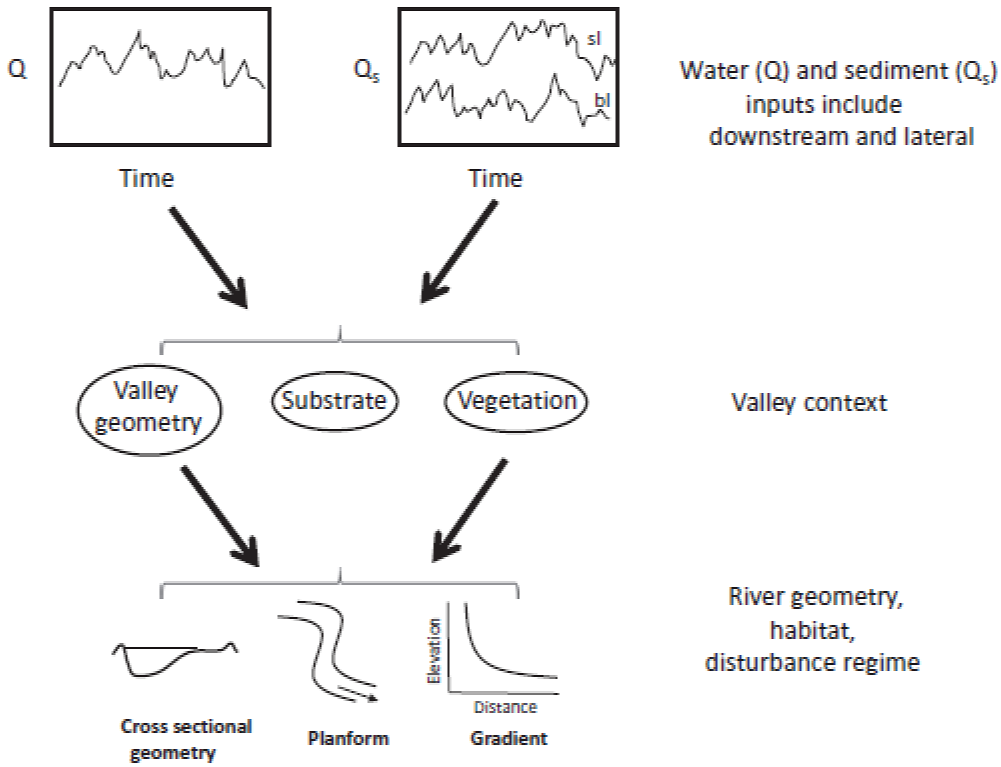

Figure 6: Controls of the river geometry, including the planform geometry (Wohl, et al., 2015). The water and sediment interact with the valley context to govern the river geometry.

2.1.3 Difficulties in characterising channel planforms

Although in many cases empirical models with parameters such as those in Table 1 can distinguish between planforms, anabranching rivers are often not well characterised by these parameters (Latrubresse, 2008). For example, a problem with the empirical relations is that anabranching rivers seem to be unrelated to streampower (Kleinhans & Van den Berg, 2011), which is often in some form included in these relations. Carling et al. (2014) mention that an important way forward in the planform classification is to determine the conditions and processes under which the planforms form. They distinguished braiding and anastomosing rivers based on the way the bars or islands are formed. Islands that are formed by channel avulsion were characterised as anastomosing, whilst islands/bars that were formed as a result of accretion are characterized as braided rivers. The classification technique is illustrated in Figure 7. Key to improving the understanding of the existence of different channel patterns is therefore to determine the conditions under which the planform dynamics such as avulsion and accretion of bars and islands occur (Carling et al., 2014).

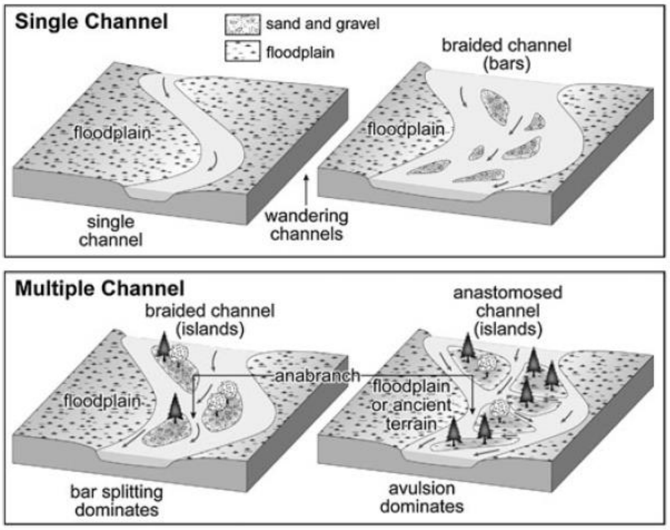

Figure 7: Classification technique used by Carling et al. (2014). Anastomosed channels are dominated by avulsion processes

2.1.4 The anabranching planform and its controls

Due to recent advances in numerical modelling, new insights into the controls of planform dynamics and channel patterns could be generated. As most of the largest rivers of the world are characterised by anabranching river patterns (Latrubresse, 2008), there has been an interest in discovering conditions that lead to the formation of this type of river planform. Numerical models have a large benefit compared to the empirical models described in the last sections. They allow studying actual causal relationships between the conditions, such as the discharge regime, and the observed channel pattern and planform dynamics.

First of all, in terms of channel geometry, large rivers with anabranching planforms have low slopes and are often characterised by wide (unconfined) floodplains (Latrubresse, 2008; Kleinhans et al, 2010). A wide floodplain as a key condition for the formation of anabranching planforms has also been identified by numerical modelling. By simulating various sand bed rivers with different floodplain widths, Moron et al (2017) describe that for narrower floodplains braided planforms tend to form. On the other hand, wider floodplains can accommodate flood discharges, which favours stabilization of bars to islands. In terms of sediment transport characteristics, a key characteristic of many large rivers seems to be that under some conditions they can transport a relatively large amount of coarse sediment in suspension (Latrubresse, 2008). Although the exact role of suspended sediment in the planform formation in anabranching planforms is still not completely understood, Nicholas et al. (2013) found that the suspension of bed material had a large impact on channel bifurcation dynamics and vertical rates of bar aggradation in anabranching river planforms.

In terms of flow, an important driver for anabranching river planform is the hydrologic regime and its variability (Kleinhans & Van den Berg, 2010; Nicholas et al., 2013). Numerical modelling of sand bed anabranching rivers revealed the importance of the variability in the hydrologic regime. A large yearly variability in flood magnitude encourages the formation of emergent bars that can be converted to stable islands (Nicholas et al, 2013). In the conversion to stable islands, vegetation growth is considered to be an important factor. On the other hand, an often mentioned driver of anabranching rivers is avulsions caused by an exceptional flood (Wang et al., 2019). These avulsions are sometimes linked to influences such as local blockage of debris flow or accumulation of bed material (Nanson, 2013).

In terms of planform dynamics responsible for the anabranching planform, two planform dynamics are mentioned: Avulsions or accretion within the channel as a dominating driver. Specifically, the distinction between avulsion as a dominant driver or accretion within the channel as a dominant driver of the anabranching planform was already identified by Nanson & Knighton (1996). Important in this distinction is that in rivers where banks are relatively resistant to erosion, avulsion is mentioned as dominant. The importance of floodplain strength and bank strength was also identified by Kleinhans & Van den Berg (2011). Furthermore, the classification technique by Carling et al. (2014) used a similar distinction between avulsion and accretion (see Figure 7) to distinguish between braiding with multiple channels and anastomosing.

2.1.5 Planform and channel pattern changes

Channel patterns and the large-scale planform geometry are subject to change. The last sections gave an extensive view of the controls of channel patterns. A transition of channel pattern or large-scale changes in the geometry requires one of the controlling factors of channel geometry to change. Of the controlling factors of the channel patterns, both the discharge and sediment regime are most susceptible to change. It is therefore not surprising that changes in the discharge and sediment regime are often mentioned as dominant drivers of large changes in the planform geometry (Nanson & Knighton, 1996; Xia et al., 2014). The discharge and sediment regime can be impacted by climate change, but especially in the last century, human interventions started to have a large influence on the discharge and sediment regimes of rivers. A key example is a river dam, which can have significant impact on the flow and sediment regime. River dams are often linked to large changes in the channel geometry (e.g. Surian, 1998, Wang et al. 2019, Xia et al., 2014)

2.2 PLANFORM DYNAMICS WITHIN MULTITHREADED RIVER PLANFORMS

Within the multithreaded river planform, various dynamics take place which contribute to planform dynamics. With planform dynamics, there is aimed at dynamics such as the formation of bars and islands, channel avulsion and channel migration. Said differently, there is mostly focussed on dynamics that are visible on satellite images. A key difference with the planform changes discussed in the previous section, is the spatial scale and the time scale on which they occur. The planform dynamics discussed in this section occur at spatial scales of 100's of meters to multiple km's and take place at timescales of several days to years. The next sections discuss the different planform dynamics observed in multithreaded river planforms and their drivers.

2.2.1 Formation and migration of bars and islands

The reason for a braided pattern or a multithreaded river planform is the presence of bars or islands. Depending on the type of river planform there is a large variety of bars that can be present (see Figure 8). A key condition for the formation of multithreaded patterns is the existence of mid-channel bars or braid bars. These bars can be emergent during bankfull flow conditions but can also be submerged. Furthermore, they can be vegetated. Islands are often characterised as being more stable than bars. Vegetated islands can be either formed by cutting in the flood plain or by a stabilized braid bar (Carling et al., 2014).

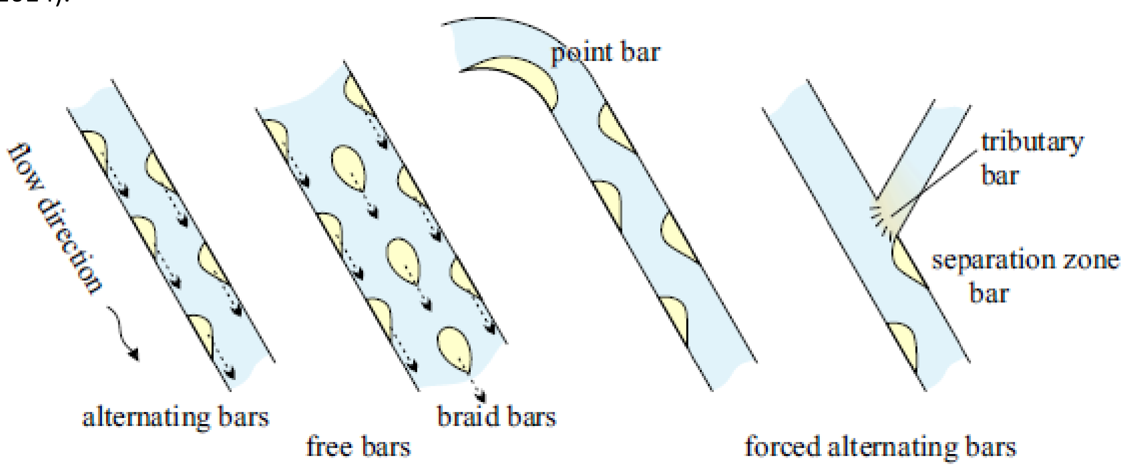

Figure 8: Examples of bars that can be present in river planforms (Jagers, 2003)

The formation of braid bars can originate from different processes. Leopold and Wolman (1957), identified that coarse bedload transport can be stalled in the middle of the channel where the local transport capacity is not sufficient. As a result, the flow bifurcates, which favours more deposition of bedload on the central bar. This eventually leads to the development of a braid bar. Ashmore (1991) used flume experiments to identify different processes that lead to the formation of a braiding pattern. One of the processes is also related to the loss of capacity identified by Leopold and Wolman (1957), which forms a central bar. Other processes identified by Ashmore (1991) are described by erosional mechanisms of existing bars. For example, by incising a bar two channels form. Lastly, Robert (2003) mentions channel avulsion as a braiding mechanism. A new channel is incised in the floodplain. This process can be distinguished from the erosional mechanisms of bars as it takes place on a larger scale. The described mechanisms lead to both the formation and the maintenance of a braided pattern. Which of the mechanisms leads to braiding depends on the sediment mobility and the channel instability (Ashmore, 1991).

After bars and/or islands are formed they are seldomly stable. A common phenomenon in multithreaded rivers is the migration of bars. The bars migrate in the downstream direction by upstream erosion and deposition at their lee (Schuurman, 2015).

2.2.2 Channel migration

For braiding, anabranching and especially for meandering rivers, channel migration is an important characteristic of the morphodynamics. As meandering rivers are mostly single-channel rivers, the channel migration is relatively predictable compared to braided rivers. In river meanders the flows are concentrated in the outer bends, which generally leads to bank erosion. On the other hand, processes like secondary circulation cause the deposition of point bars in the inner bend (Robert, 2003). This process generally continuous which results in a migrating channel. In this process, the channel length increases and therefore the gradient decreases. Eventually, a cut-off and channel avulsion cause a relatively rapid shift of the channel and abandonment of the former channel.

For braiding or anabranching rivers, secondary circulation also plays a key role (Ashworth et al., 1992). The braid bar or island diverts the flow outwards, which leads to erosion in the outer bend and deposition in the inner bend. Therefore, also in the individual channels of a multithreaded planform, a transverse slope can be present. Some of the coarse bedload transport ends up on the head of the bar, whilst the finer material ends up in the distributaries (Ashworth et al., 1992). The secondary circulation and the wake of the bars allow the deposition of finer sediment. This causes lateral sorting of the material, with finer sediments downstream than upstream. The process is illustrated in Figure 9.

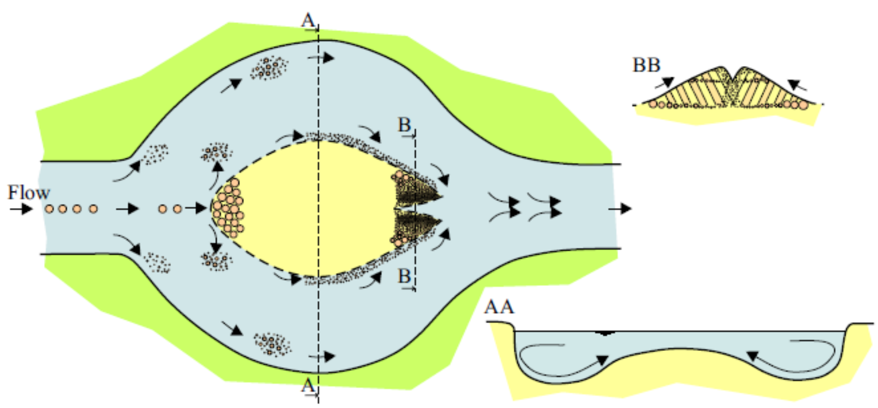

Figure 9: Sediment sorting and secondary circulation near the braid bar (Ashworth et al., 1992)

Therefore, in the individual channels of the river planform in multithreaded rivers, similar processes of bank erosion in the outer bend and deposition in the inner bend take place, which leads to migration (Jagers, 2003). However, it is important to note that bars often migrate and new bars form in the channels. The migration is therefore not as continuous as in meandering rivers. If a new bar forms or the bar migrates, this will cause a redistribution of both water and sediment and changes of the flow angle (Klaassen & Masselink, 1992). This can cause migration of the channel downstream of the bars.

One of the key conditions for channel migration is bank erosion, which is defined as erosion in the horizontal or lateral direction. There exist a wide variety of processes and mechanisms that cause bank erosion. The first distinction that can be made is between semi-continuous erosion of the bank and erosion that takes place during discrete events. The former being referred to as fluvial erosion whilst the latter is referred to as mass failure (Rinaldi & Darby, 2007). Semi-continuous erosion of the bank occurs when the shear stress exceeds the critical shear stress of the soil, which means that particles are entrained in the flow. For erosion during discrete events or mass failure, there exist various mechanisms and processes that play a role. In cohesive soils, undercutting might occur, which eventually leads to mass failure of the overhanging soil. For non-cohesive soils, which are present in many braided rivers, shear failure is more common (Coleman, 1969). Shear failure can be seen as a form of mass failure. The shear resistance of the bank might become too small due to the saturation of the soil, which can occur when the water level drops after a flood. Also, rainfall might saturate the soil which can lead to bank instability. Furthermore, the banks might become too steep due to fluvial erosion. Some of the different types of mass failure are illustrated in Figure 10.

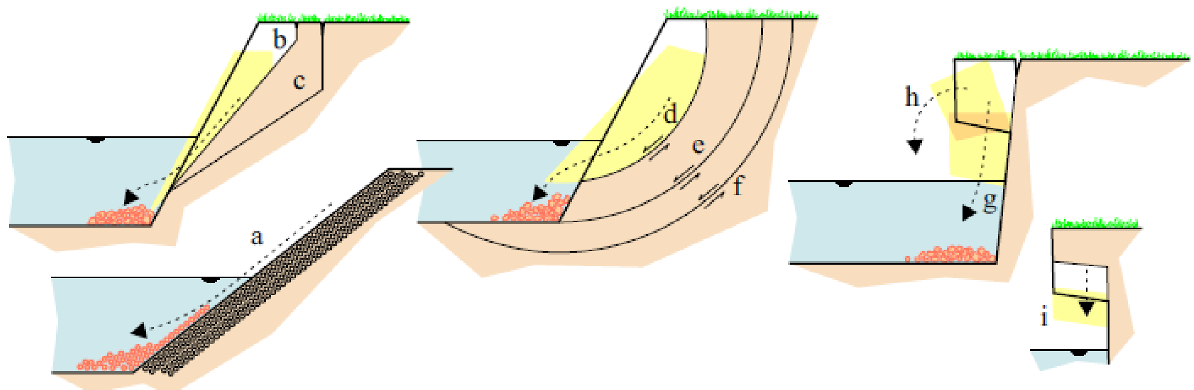

Figure 10: Different types of mass failure for river banks (Jagers, 2003). These are semi-continuous processes. The middle and left illustrations are types of shear failure. The most right illustrations occur in cohesive soils with undercutting.

Just like there are different mechanisms of bank erosion, there are many factors that can influence the bank erosion rate. Other factors that influence the bank erosion rate that have been identified in literature are (Coleman, 1969; Crosato, 2008; Robert, 2003;):

- Near bank flow strength
- The presence of riparian vegetation.
- Groundwater flow
- Pore water pressure/ moisture content of the bank
- The composition of bank material (e.g. cohesive, coarse/fine)
- Channel curvature or radii of curvature
- The angle of the bank (steeper banks are generally more like to erode)
- Rate of rise and fall of river level
- Formation and movement of large bedforms

2.2.3 Formation and abandonment of channels (bifurcations and confluences)

Especially in the case of large bars or islands, braided and anabranching rivers consist of a series of bifurcations and confluences. A bifurcation occurs when the channel splits into two or more channels. There exist different mechanics that lead to the formation of bifurcations in multithreaded river planforms. First of all, bar formation, due to accretion of sediment can be a reason that the flow bifurcates. Furthermore, avulsion, which is the incision of a new channel into the floodplain, is considered to be an important reason for the occurrence of anabranching river patterns (Kleinhans & Van den Berg, 2011)

Dynamics of bifurcations play an important role in how the channels develop over time, and whether and when a channel is abandoned. The distribution of the flow and sediment determines the evolution of the channels. Factors that influence these dynamics are gradient advantages, the bifurcation angle, the bed geometry and the mode of sediment transport (bed load/ suspended load) (Kleinhans et al., 2013). For example, a gradient advantage might increase the flow in one channel and cause abandonment of the other channel. As braided rivers are often highly dynamic and the geometry might change rapidly, the evolution of the individual channels is difficult to predict (Jagers, 2003).

2.2.4 Summary of large scale morphodynamics found in multithreaded rivers

A summary of the planform dynamics that were mentioned in the previous sections is given in Table 2.

Table 2: Summary of the large-scale river morphodynamics in multithreaded rivers

Phenomena	Main process	Explanation
Formation of mid-channel bars and islands	Stalling of bedload transport	Local reduction of flow speed, which reduces transport capacity.
	Avulsion	Local geometry cannot adjust fast enough to accommodate the flow.
Migration of mid-channel bars	Erosion at the head and deposition at the tail	Strong flow strength at the head and the wake behind bar favours deposition
Channel migration	Secondary flow	Additional factors of influence: - Radii of curvature - Bank strength
	Movement and formation of bars and large bedforms	Bars and other bedforms change flow direction which can impact channel migration.
Channel abandonment	Instability	Division of flow and sediment, mode of transport (suspended/ bed load), gradient, geometry
Channel formation	Avulsion	See formation of mid-channel bars and islands.
	Deposition of mid-channel bars	See formation of mid-channel bars and islands.

2.3 REMOTE SENSING OF SURFACE WATER

This section will mostly focus on the general topic of remote sensing with a focus on detecting surface water. It thereby serves as an introduction to the next section, in which there is specifically focused on the topic of detecting planform dynamics with satellite imagery. For studying planform dynamics surface water detection plays an important role, which is why it is elaborately discussed in this section.

2.3.1 Satellite sources

One of the uses of satellite imagery, that is of particular interest in this thesis is the analysis of large-scale surface water changes. For detecting surface water, different sources of satellite imagery can be used. The first distinction that can be made is the type of sensor. There exist two types of sensors that are mostly used for surface water detection: Microwave sensors and optical sensors. Microwave sensors can function under all weather conditions, function day and night and can penetrate clouds. They can detect the flat surface of surface water, which reflects a different signal than the surroundings. Schuman and Moller (2015), found Synthetic Aperture Radar (SAR), which is a type of microwave sensor, to be the most suitable for monitoring flood inundation. The other type of sensor is an optical sensor. Optical sensors have been widely used to map surface water changes. Water can be detected based on reflectance properties of the surface. A disadvantage of optical satellite imagery is that it is disturbed by cloud cover, and thus it is most useful in clear weather conditions. Despite this, it is still the preferred source for monitoring surface water, due to the straightforward interpretability (Bioresita et al., 2018). Furthermore, optical satellite imagery is more widely available and provides a long time series. For these reasons, the focus in the next sections will be on optical satellite imagery.

There are various sources of optical satellite imagery available. Satellite imagery can be categorized based on spatial resolution: Coarse (>200 m), medium (5-200) and high resolution (<5 m). (Huang et al., 2018). Coarse resolution satellite imagery, such as MODIS, is very effective in monitoring large areas of the earth's surface and has a high temporal resolution. However, due to the limited resolution this type of satellite imagery is mostly relevant for the analysis of large surface water bodies, and not to detect river changes. In the medium category, a popular source for surface water detection is Landsat imagery as it covers over 40 years. Most of this period the spatial resolution is 30 meters with a revisit time of once every 16 days. As the spatial resolution is relatively high, it provides the ability to detect the dynamics of most surface water bodies. Furthermore, due to its long availability, it is widely used in detecting surface water changes (Huang et al., 2018). More recently, in 2015, medium resolution Sentinel-2 imagery became available. Although it only has a limited survey length, it provides a 10 m resolution, which is thus able to detect smaller surface water changes. High-resolution satellite sources have become more common in the last decade. Examples are RapidEye, Ikonos and Quickbird. Due to the high resolution, these sources provide the ability to map smaller changes with higher accuracy. However, the (non-commercial) availability is limited. Furthermore, the revisit frequency and spatial extent are often limited (Huang et al., 2018). This limits the ability for large scale analysis with high-resolution imagery.

2.3.2 Mapping surface characteristics with satellite imagery

To be able to classify the earth's surface there exist different methods. Yang et al (2015) identified various methods to detect surface water, of which 4 different methods are:

1: Digitizing through visual interpretation

This is a manual technique and therefore a labour-intensive method. This makes this type of analysis difficult to perform on a large scale (Yang, et al., 2015). Nevertheless, it can be a very accurate method. For this reason, this kind of methodology is also applied for river applications. For example, Hossain et al. (2013) used digitizing to map the change of river banklines over time.

2*: Density-slicing of a single band*
The reflectance properties of a single band are used. Combined with a threshold, water can be detected. This is a very simple and efficient method. However, it only uses a single band which can give limited accuracy.

3: *Supervised or unsupervised classification*
Using reflectance properties of the surface in all bands, classes can be distinguished based on different reflectance properties. In supervised classification training pixels are defined, which are used to classify other pixels. The accuracy of supervised classification largely depends on the used training pixels and therefore on a priori expertise (Yang et al., 2015). In unsupervised classification, the process is done fully automatically, which can give limited accuracy in optically complex images (Donchyts et al., 2018; Yang et al., 2015).

4: Water indices
Water indices use a combination of two or more bands. By setting a threshold water is distinguished from its surroundings. This method has proven to be effective and convenient (Yang et al., 2015).

Especially the fourth category is very popular for water delineation (Fisher & Danahar, 2013), which is why it will be elaborated. The main principle of classification is distinguishing different reflection properties of the earth's surface. Indices are focused specifically on one subject, such as vegetation or water. A well-known index is the Normalized Difference Vegetation Index (NDVI), which can be used to map the vegetated surface. Also, indices were developed for the detection of surface water. One of the first is the Normalised Difference Water Index, or NDWI (McFeeters, 1996). Later this index was updated to the mNDWI (Xu, 2006) which is now widely considered as more stable and reliable (Huang et al., 2018). The mNDWI is given in equation 2.

$$mNDWI = \frac{Green - SWIR}{Green + SWIR} \tag{2}$$

Other examples of water indices that have been developed are the AWEI (Feyisa et al., 2014) and the WI 2015 (Fisher et al., 2016). Fisher et al. (2016) conducted a comparison between several popular water indices. They found that none of the indices performed the best, and the performance largely depends on local conditions.

Detecting water bodies with water indices requires the use of a threshold value. Thresholding is one of the most critical issues for using water indices (Huang et al., 2018). For water, a common threshold that is used is a value of 0. However, local adjustments to the threshold might provide better results. This can become problematic if the analysis is performed on a large scale, which means that manual adjustments of the threshold can be troublesome. This is the reason that automated thresholding techniques have been developed. Donchyts (2018) used an automated thresholding technique for the mNDWI to map global surface water changes. For mapping global surface water changes Donchyts (2018) used Otsu thresholding, which determines a threshold automatically based on a split in the reflectance values.

2.4 MAPPING PLANFORM DYNAMICS WITH SATELLITE IMAGERY

As satellite imagery shows large potential to map river morphodynamics over large areas and during relatively long time periods, it is not surprising that detecting river morphodynamics with satellite imagery has been studied extensively. The methodology and the extracted metrics of river morphodynamics, however, greatly vary over literature. The different methods of studying river morphodynamics will be treated in this section.

2.4.1 Method of classifying river surfaces

The methods for distinguishing surface water, i.e. water indices, digitizing and (un)-supervised classification are all commonly found in a satellite-based analysis of river morphodynamics**.** The most found method in the past is digitization. This is likely due to the involved complexity of using automated classification methods that was present in the past. Especially in complex multichannel rivers, it can be difficult to automatically detect banklines. This is why in these applications the usage of digitization is commonly found. Digitization is often performed in GIS software and by comparing banklines over time statistics of erosion and deposition can be generated. Examples in literature that applied these methods are Hossain et al. (2013) and Baki & Gan (2012), who both delineated the bank lines for a multithreaded river. The main metrics that can be extracted from these types of methods are bank migration metrics. A disadvantage of these approaches is that the spatial scale of the analysis is limited, due to the large processing time of digitization. Furthermore, digitization often means that the river morphodynamics can only be selectively detected. Due to long the long processing time, the time intervals between images are often relatively long (multiple years).

Besides the digitization approach, automated methods of classification have become more common. Satellite imagery has become more widely available over recent years, which makes the analysis of river planforms and their changes easier. The methods vary from simply determining a water index to get an indication of the banklines, which facilitates a combination of manual and semi-automated extraction of changes (e.g. Kong et al., 2020; Langat et al., 2019; Yang., et al., 2015) to the development complete tools in which most of the quantification of changes and processing of the satellite imagery is done automatically (e.g. Monegaglia et al., 2018; Rowland et al., 2016; Schwenk et al., 2017).

Generally, when automatic detection of the river surface is used to study river morphodynamics, careful consideration should be taken whether something is included in the river mask. Although automated methods for surface water detection have large advantages in terms of processing time, it has a large downside when it is applied to rivers. The water level largely affects the extent of the water surface, and in the case of rivers, the water level can vary to a large extent. Especially for braiding rivers and rivers where banks are gently sloped, the water level has a large effect on the extent of the water surface. Despite this disadvantage, automatic detection is still commonly applied, by carefully selecting what is included in the analysis. One method to consider the water level is to use measured water levels. An example is Yang et al. (2015) where images were selected within a certain water level range. Alternatively, a widely used approach is the detection of the vegetation boundary. Hereby, there is assumed that vegetated areas are not part of the active channel anymore (Rowland, et al., 2016). The active channel does include both unvegetated bars and the water surface. The assumption behind this is that in the active channel there is not enough time for vegetation to establish. Some uncertainties arise when this approach is used in arid regions with sparse vegetation and with seasonal variations in vegetation cover. Nevertheless, it is an approach that can consistently locate bank lines independent of river stage (Rowland et al., 2016)

2.4.2 Quantifying river morphodynamics with satellite imagery

Once the river surface has been identified the change between images in the time series can be quantified. The type of river change metrics that are being extracted varies in literature. A key difference between quantification methods is those who focus on single thread meandering rivers and multithreaded rivers. Rowland et al. (2016) give an overview of the methods that have been used in the past to quantify river morphodynamics. First of all, an important difference in methods for quantifying river morphodynamics is the use of calculations based on a raster, which is how satellite imagery is stored, or the use of vector operations. Secondly, depending on the studied river or river planform the focus lies on different metrics that describe the morphodynamics. In meandering rivers, mapping channel migration can be very relevant as it is a process that accounts for most of the planform dynamics. To map and visualise channel migration often centreline movement is tracked (e.g. Monegaglia et al., 2018; Schwenk et al., 2017). On the other hand, when studying braided or multithreaded rivers, the main interest is generally in quantifying bank migration independent from channel migration. This is mostly because in multithreaded channels the planform dynamics are often not directly related to channel migration (Rowland et al., 2016).

2.4.3 Accuracy of river change metrics measured with satellite imagery

An important aspect that is affecting the accuracy of detecting the morphological change from satellite imagery is the effect of the river stage. This is mostly the case when solely the water surface is detected. Especially in wide and shallow channels, the river stage has a large effect on the water surface extent. When comparing satellite images over time this means that to accurately detect morphological changes, roughly the same river stage must be used (Hossain et al., 2013).

For automated detection on satellite imagery, classification errors might arise from incorrect training pixels or in selecting thresholds for the different indices (Rowland, et al., 2016). Furthermore, there can be mixed pixels along banks where both land and water are mixed, which is an important source of error in automated detection of surface water (Donchyts et al., 2016). Also, independent of the classification method (automated or manual), seasonal changes in vegetation or overhanging vegetation can lead to errors in extracting river bank lines (Rowland et al., 2016). Quantifying these measurement errors, for example for bank line extraction, is not straightforward. Validation data on the river bank locations is generally not available. Sometimes, to get an idea of the error of automated methods, manual delineation techniques are compared with automated techniques (e.g. Rowland et al., 2016). Whether errors are significant depends on the resolution of images, the size of the river, the rate of channel change and the time interval between images. For example, coarse resolution imagery can be used, as long as shifts occur that are greater than the maximum error in delineating bank lines (Rowland et al., 2016)

2.4.4 Existing automated tools for extracting river metrics

As satellite imagery has become more available over recent years, analysis of river planforms and their metrics has become more common. To automate and generalize the methods for deriving metrics from satellite imagery several tools have been developed. Some of the more complete tools are Changeom (Fisher et al., 2013), SCREAM (Rowland et al., 2016), Rivmap (Schwenk et al., 2017) and PyRis (Monegaglia et al., 2018). Depending on the used tools different metrics can be generated, amongst those are the channel sinuosity, the migration rate, radii of curvature, the width, the length of the channel, bank changes and areas of erosion and accretion. Although these tools are quite advanced and have successfully been able to derive planform dynamics, many of these tools are mainly designed for metrics for (single-thread) meandering rivers, such as PyRis, RivMap and Changeom. The analysis is often centreline based, in this way channel migration of meandering rivers can be mapped. Extracting centrelines from multichannel rivers can be complicated (Monegaglia et al., 2018). Furthermore, as Rowland et al. (2016) mention, bankline change, independent of centreline migration, often provides a more valuable metric than centreline-based migration rates that are often used for single-thread rivers.

2.5 Concluding remarks

The first section focussed on channel patterns and their controls. The controlling factors of the reach scale geometry and channel pattern are related to the hydrologic regime, sediment regime and valley characteristics. Large scale changes of river geometry take place on time scales of years to decades. These changes are often related to long term changes in the discharge and sediment regime, as they are the most susceptible to change. Changes in the discharge and sediment regime can, for example, be caused by human interventions or climate change. The second section focussed on local planform dynamics such as the formation of bars and islands, channel avulsion and channel migration. If these dynamics are investigated on small spatial scales, explaining these dynamics requires knowledge about complex interactions between local flow and sediment transport. Furthermore, local details about bank composition are often required to explain channel migration. This limits the possibilities to study and explain these local dynamics in remote sensing studies, without the availability of detailed additional data sources about local flow and transport dynamics. Nevertheless, these local dynamics can be contextualised on a broader scale (river reach). In this way, they can be related to more broad concepts such as the discharge and its variability (Carling et al., 2014). For example, avulsions and bank erosion are found to be strongly related to flood season intensity. Furthermore, the yearly and seasonal variability in flood discharges are commonly linked to the formation and stabilisation of islands, which are key in the formation of multithreaded planforms. The combination of the different planform dynamics eventually give rise to the channel pattern. Therefore, understanding their drivers in a broader context is also relevant to improve the understanding of the controls of channel patterns. For this study, which uses satellite images to study planform dynamics, these findings have important implications. Large reach scale changes in the channel geometry and channel pattern take place on time scales of years to decades. To find reach scale changes in the river geometry and channel pattern multi-year or decadal intervals would suffice. However, to truly characterize reach scale planform dynamics and to investigate their drivers with satellite images, a high temporal resolution is required (Schwenk et al., 2017). This, for example, allows to identify the impacts of flood events and the impact of the yearly variability in flood discharge on planforms dynamics such as avulsion and island formation.

From a remote sensing perspective, it becomes clear that there are some challenges for detecting and quantifying river morphodynamics. There have been several investigations on river morphodynamics for multithreaded rivers with manual digitization. However, they often focussed on relatively small sections and/or long time intervals due to manual delineation of river boundaries. This prevents to study key drivers of reach scale planform dynamics. Furthermore, when studying multiyear periods, it can obscure important temporal details, such as yearly variability in flood discharge. (Semi)-Automated classification methods have large advantages in terms of processing time, which allows studying reach scales at small time intervals. An important challenge with automated detection techniques is to consistently compare the river surface over time. This is due to a large effect of water levels on the extent of the water surface. Besides, for semi-automated approaches, a lot of studies focussed on single thread meandering rivers. The techniques to derive planform dynamics for single-threaded rivers are generally not transferable to multithreaded rivers. Thus, the challenge that has to be tackled in this study is to develop an automated method, that can deal with a multithreaded channel planform, whilst at the same time being able to study large spatial scales for small time intervals.

3 METHODS

In this chapter, the method of automated detection of planform dynamics with satellite imagery is discussed. The developed method for detecting planform dynamics with satellite images is optimised for the case study of the Ayeyarwady river. The main focus in this chapter is therefore on using the method for the Ayeyarwady river. However, it was also developed with applicability outside the case study in mind.

The method is composed of several steps (see Figure 11). The first step is selecting the satellite images for the analysis. After this, the images are classified to detect the river bodies over time. The third part of the method is to quantify the observed rivers morphodynamics and to derive metrics of planform dynamics. Finally, the results are analysed to find possible explanations for differences in time and space. The four parts of the method will be discussed in the next sections. All steps are performed by a combination of a Python script and the Earth Engine Python API. An example script is given in Appendix F.

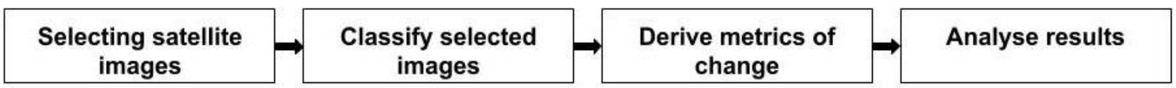

Figure 11: The four different steps that are taken in the method

3.1 SELECTING SATELLITE IMAGES

3.1.1 Landsat imagery

Due to its easier interpretability and wider availability, optical satellite imagery is used, more specifically Landsat imagery. Landsat imagery is the only non-commercially available source that can provide a long time series of more than 30 years. An overview of the different available Landsat missions is given in Table 3. The first Landsat missions (1, 2, 3 MSS) only provide a limited resolution of 60 m. Besides, they only have a small range of bands. Therefore, they are not included in the analysis. The Landsat images, excluding the first three Landsat missions, cover 1984 to present. The study area is covered by path 133 with rows 47 and 48 (see Figure 12). Because the study area is covered by a single path, an image of the entire study area is available on the same day.

Landsat images have different products: Raw, Top of Atmosphere reflectance (TOA), and Surface Reflectance (SR). There was opted to use top of atmosphere (TOA) satellite images, for which there are several reasons. First of all, correcting satellite images for atmospheric distortions is a complex procedure and can lead to errors (Donchyts, 2018). Besides, multiple sources mention limited differences between TOA or SR images in the classification of surface water (Fisher et al., 2016; Huang et al., 2018). Furthermore, an often-mentioned downside of the use of TOA reflections for change analysis is that the atmospheric properties affect the measured reflections. Therefore, the reflective properties of for example rivers can vary over time. For accurate representations of the surface water boundaries, automated classification methods should take into account these changing conditions errors (Donchyts, 2018). On the other hand, changing conditions also affect surface reflectance (SR) images. For example, rivers can carry different concentrations of sediment which alters the reflectance properties. Furthermore, SR images are still affected by high concentrations of haze and fog (Donchyts, 2018). Therefore, similar problems arise independently of the use of TOA of SR imagery, which resulted in the use of TOA imagery.

Table 3: Overview of Landsat missions

Landsat mission	Time period[1]	Bands[2]	Resolution[3]
Landsat 1 MSS	July 1972- January 1978	4	60
Landsat 2 MSS	January 1975-July 1983	4	60
Landsat 3 MSS	March 1978- September 1983	4	60
Landsat 4 TM	July 1984- December 1993	7	30
Landsat 5 TM	March 1984- January 2013	7	30
Landsat 7 ETM	April 1999- May 2003[4]	8	30
Landsat 8 OLI	February 2013- Present	11	30

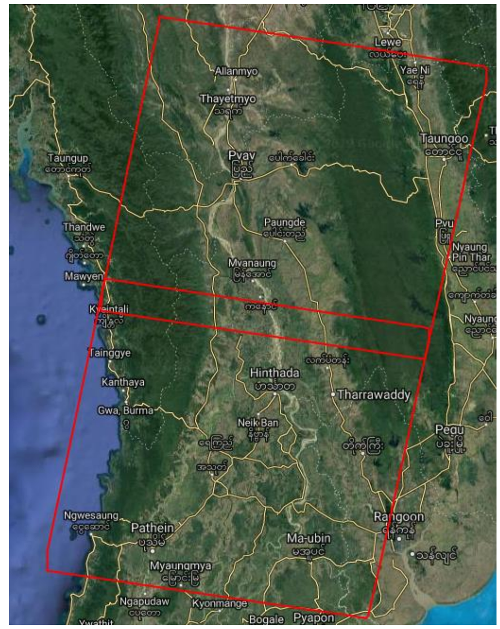

Figure 12: Landsat path 133 and row 47+48

3.1.2 Time-interval in between images

The time-interval between images is an important factor for studying river morphodynamics. For the Ayeyarwady river, there is a clear wet season with high discharges and a dry season with low discharges. Large changes of river geometry occur during the wet season, which are easily detectable with the resolution of Landsat images. However, during wet seasons the vast majority of the images are heavily impacted by cloud cover, which limits the availability of suitable images. Therefore, the smallest scale where reliably images are available is a yearly scale, in which images are selected in dry seasons with limited cloud cover. The dry season/low stage period for the Ayeyarwady river is generally around the months of January- April (see Figure 13).

A problem with a relatively small interval of one year is that errors in detection cause a relatively large uncertainty in the detected morphodynamics. With larger time intervals of multiple years, noise in the detection has a smaller contribution in the quantification of morphodynamics, as overall more changes (erosion and deposition) have occurred during the interval. At the same time, for multi-year intervals, it holds that some of the morphodynamics are possibly not detected (Rowland et al., 2016). For example, a channel can migrate one way and in the same time interval migrate back again to the same position. The result is that no change is detected, whilst the river migrated. Another argument for a yearly interval to measure river morphodynamics is that yearly changes in hydrological regime, such as the flood season intensity are often mentioned as a key driver of multithreaded anabranching river planforms (see section 2.1). For both reasons, there was opted for a yearly time scale where change is detected over each hydrological year.

---

[1] Source: https://www.usgs.gov/land-resources/nli/landsat/landsat-satellite-missions?qt-science_support_page_related_con=2#qt-science_support_page_related_con

[2] Source: https://www.usgs.gov/faqs/what-landsat-7-etm-slc-data?qt-news_science_products=0#qt-news_science_products

[3] Source: https://www.usgs.gov/faqs/what-landsat-7-etm-slc-data?qt-news_science_products=0#qt-news_science_products

[4] Scan line corrector failure since May 2003. Since May 2003 images have gaps, which renders them not useful for this study. Source: https://www.usgs.gov/faqs/what-landsat-7-etm-slc-data?qt-news_science_products=0#qt-news_science_products

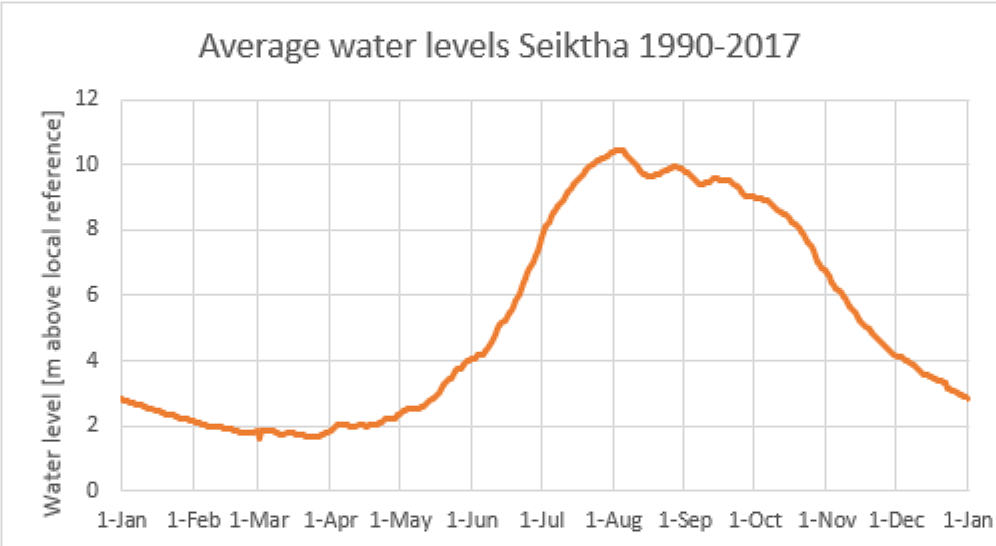

Figure 13: Overview of water levels Lower Ayeyarwady measured at Seiktha (Steijn, et al., 2019).

3.1.3 Dealing with uncertainty in the classification

Once the images for the river change analysis are selected a choice has to be made on how to process the images. Due to the use of yearly time-interval, the number of images to process is relatively large. Combined with the complex geometry of the Ayeyarwady and the use of automated change detection, the classification requires careful consideration.

There are different procedures to deal with cloud cover of satellite images. One is to select a single image where cloud cover is limited, which is most common in dry seasons. This is also commonly applied for studying river change (e.g. Baki & Gan, 2013). However, especially when automated classification is used for a single image, local conditions such as shadows, fog and clouds can lead to errors in classification. For example, for applications where the river is relatively complex consisting of multiple small channels, using a single image might miss a small channel in one image, whilst it is detected in the image one interval later. The use of a single image gives limited insight into this uncertainty in detection. Part of this uncertainty is often compensated by manually cleaning the detected river bodies (e.g. Rowland et al., 2016; Schwenk et al., 2017)

A way to reduce uncertainty is to use composite images. Composite images use the reflectance properties of multiple images to create a single classified image. This method is frequently used to deal with cloud cover. A method to prevent river change within the compositing interval is using images from dry seasons. During low river stages, one can assume that almost no river morphodynamics take place (Schwenk et al., 2017). At the same time, in the case study of the Ayeyarwady river for many years in the analysis only one or a couple of images are available in the dry season that are of sufficient quality (e.g. low cloud cover). This makes a compositing procedure difficult to perform, as noise is harder to identify. This was also identified by Schwenk et al. (2017) where composites needed some additional cleaning to remove noise. A disadvantage of manual cleaning it that it partly reduces the transferability to other cases. Furthermore, by using single composite images no idea of the uncertainty in the classification is generated, which makes it hard to quantify the performance and consistency of the classification algorithms. Therefore, a different method was developed to deal with the uncertainty in the classification. Instead of using a single (composite) image from one dry season which is compared with a single (composite) image from the next, all images that fulfil the selection criteria are classified. By detecting change between all classified images in the two dry seasons, this gives a range in the quantification of river change instead of a single value. Poor image quality or misdetections can be identified by a large uncertainty range. In the uncertainty range, misclassifications and uncertainty in thresholding are included.

3.1.4 Overview of all filtering steps and resulting images

Despite using a method that indicates an uncertainty range, strict selection criteria were used to minimise the uncertainty range where possible. An overview of the different filtering steps is given in Figure 14. A more detailed description of the different filtering steps is given in Appendix B.

First of all, the area affected by cloud cover in the surroundings of the river was minimised. Cloud cover can affect the performance in water detection severely (Huang et al., 2018). Next, to set up yearly intervals, images from the dry season are used (January-April, see Figure 13). This means that to detect change over a hydrological year (dry season – dry season), images from two calendar years need to be used. Using solely dry season images, where discharge is low, makes sure that there can be assumed that the banklines are nearly stational (Schwenk et al., 2017). Therefore, for all images in the same dry season roughly the same location of the river banklines should be detected. Both the dry season criteria and the cloud cover criteria resulted in some dry seasons where no images were available, which means it is not possible to quantify planform dynamics in these years. Furthermore, during some years only a single image was available in the dry season. With a single image in a dry season, the uncertainty in the detection cannot be identified. Therefore, these years were discarded.

In the end, in the period of 1988- 2019, the planform dynamics in 19 different hydrological years can be quantified (see Table 4). There are several gaps where planform dynamics cannot be quantified, which are: 1989-1994, 1996-1997, 2010-2013. In these years there were not sufficient images available to be able to quantify the river morphodynamics on a yearly scale. Table 4 also lists the total amount of possible samples for the quantification of planform changes. For example, for the wet season of 1988 in the preceding dry season (1988 Jan.-April) two images are available while for the proceeding dry season (1989 Jan.-April) 4 images are available. This means that 2 x 4 combinations of images can be generated which result in 8 possible samples that can be used to detect river change.

Even though, for investigating trends in planform dynamics a continuous time series of 30 years with yearly intervals is preferable, it was not found to be achievable for the case study. Nevertheless, in the end, most of the period of 1988-2019 is covered. Also, an important goal of the method is to identify key drivers and to create a better understanding of planform dynamics, which does not necessitate a continuous series. Therefore, there was opted to prefer a good performance of the algorithm and a reduction of uncertainty rather than creating a continuous time series.

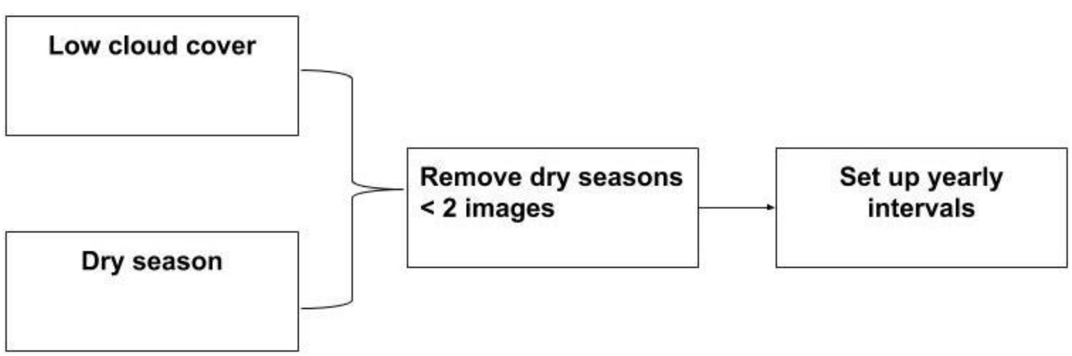

Figure 14: The general filtering steps to select images for the analysis

Table 4: Image selection. The black lines denote gaps in the analysis. Note that to get statistics over a hydrological year (~March to March) images from two dry seasons in different calendar years are used. For example, the hydrological year lasts from March 1988 to March 1989. To describe the hydrological years, images from two dry seasons are taken. The first is Jan.-April 1988 and the second Jan-April 1989. The wet season takes place from June-October and thus takes place in 1988. The accompanying Landsat image ID's are given in Appendix C.

	Wet season	Dry season year 1	Nr of images dry season 1	Dry season year 2	Nr of images dry season 2	Total samples
1	1988	1988	2	1989	4	8
2	1995	1995	2	1996	2	4
3	1998	1998	3	1999	2	6
4	1999	1999	2	2000	3	6
5	2000	2000	3	2001	3	9
6	2001	2001	3	2002	4	12
7	2002	2002	4	2003	3	12
8	2003	2003	3	2004	2	6
9	2004	2004	2	2005	3	6
10	2005	2005	3	2006	2	6
11	2006	2006	2	2007	5	10
12	2007	2007	5	2008	2	10
13	2008	2008	2	2009	4	8
14	2009	2009	4	2010	3	12
15	2014	2014	3	2015	3	9
16	2015	2015	3	2016	3	9
17	2016	2016	3	2017	4	12
18	2017	2017	4	2018	3	12
19	2018	2018	3	2019	2	6

3.2 CLASSIFICATION METHODS

Water indices, (un)- supervised classification and digitization are all commonly used to study river changes, or, more generally, surface water changes. Due to the spatial scale of the analysis and the use of a yearly time interval, automated detection methods are used.

Independent of the exact automated classification method, studying river planform dynamics with satellite imagery requires careful consideration. As was already mentioned in Chapter 2.4 the water level can affect the analysis of river morphodynamics. This is mainly the case if only the water surface is detected, which is compared over time. The water level affects the extent of the water surface and will therefore affect the measured river morphodynamics. To take into account the effect of the water level two different methods are used, which detect different changes.

The first method is detecting vegetation boundary instead of solely the water surface, which is a common approach in the analysis of river morphodynamics with satellite images (e.g. Monegaglia et al. 2018; Schwenk et al., 2017 and Rowland et al., 2016). This method assumes that the vegetation boundary is equal to the river bankline under bankfull conditions. The main metric that can be extracted from this method is the migration of banklines.

The second method uses water level measurements to make sure a similar water level is measured in each image. A problem with the vegetation boundary method is that only bankline change can be studied. A key characteristic of the morphodynamics of many multithreaded rivers is the formation and migration of bars, which are generally not vegetated. Part of the in-channel morphodynamics are therefore not possible to detect when bankline migration is studied. By controlling the water level, also river dynamics of exposed bars can be tracked. As dry season images are used, the location of the low stage channel can be tracked over time, including migration of exposed unvegetated bars.

To conclude, two different methods will be applied that detect different changes. By comparing the water surface over time, many of the in-channel and bar dynamics are exposed, whilst by comparing the vegetation boundary mainly the dynamics of the bankfull channel are detected. More details of both methods will be given in the next sections.

3.3 CLASSIFICATION METHOD 1: DETECTING CHANGES IN THE VEGETATION BOUNDARY

For detecting the vegetation boundary both bare sediment and the water surface are detected. This creates two separate masks of sediment bars and a water surface, which are combined to a single river mask. The steps of detecting the vegetation boundary are visualised in Figure 15.

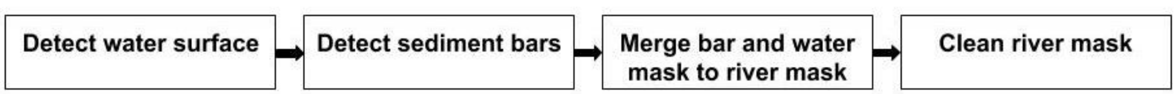

Figure 15: Steps of detecting the vegetation boundary

To detect the vegetation boundary a combination of the Normalised Difference Water Index (NDWI) and the Short-Wave Infrared (SWIR) Band is used. The NDWI is used to detect the water surface, whilst the SWIR band is used to detect unvegetated bars. The method uses the assumption that bare sediment and water are part of the active channel, whilst vegetation is not. Rowland et al. (2016), Schwenk et al. (2017) and Monegaglia et al (2018) all used similar approaches where bare sediment and the water surface are considered part of the active channel. However, Schwenk et al. (2017) and Rowland et al. (2016) used supervised classification to identify bare sediment and the water surface. The main reason for using a water index as opposed to supervised classification in the applied method is that water indices can easily take into account changing conditions. This can be done by automating the thresholding procedure with for example Otsu thresholding (e.g. Donchyts, 2018)

The used method is partly based on the method is of Monegaglia et al. (2018), who used the MNDWI, NDVI and SWIR band to detect water, vegetation and exposed sediment respectively. Furthermore, they also applied Otsu thresholding to take into account changing conditions. The method of this study has two key differences with the method of Monegaglia et al (2018). The first is that the vegetated surface is not detected in the method used in this study. Monegaglia et al. (2018) excluded the vegetation layer detected with the NDVI from the river mask. There was opted to not include the NDVI as the performance of the detection of the river boundaries was generally not improved. Furthermore, due to dry vegetation and sometimes more barren areas surrounding the Ayeyarwady river in the dry seasons, the detection of vegetation was troublesome which is an additional reason for not including the NDVI. The second difference is that for the detection of the water surface there was opted for the NDWI instead of the used mNDWI by Monegaglia et al. (2018). The detection of the water surface will be more elaborately discussed in the next subsection.

3.3.1 Detection of surface water

There has been extensive research on the applicability of water indices, and often there is concluded that none of them perform best and the performance of the indices mainly depends on local conditions (Fisher et al., 2016). Two well-known indices are the MNDWI and the NDWI. Generally, the MNDWI is considered to be more stable and less affected by sediment concentrations in the river (Huang et al., 2018). However, it is more sensitive to clouds and (hill) shadows. To decide which index performs best for the case study both the MNDWI and NDWI were applied and their performance was compared. It was found that the MNDWI is indeed more stable and therefore more suitable to clearly distinguish a land and a water class. Nevertheless, the detected water surfaces were fairly similar between the NDWI and MNDWI. In the end, there was opted to use the NDWI, as it was found to be more suitable for the case of the Ayeyarwady river. The better performance especially became clear for the detection of surface water around sediment bars. More information about the differences between the NDWI and the MNDWI for the case study and the cause of the differences in the classification is given in Appendix B.

Otsu thresholding is used which makes sure the threshold is adjusted to changing conditions of the water surface and the atmosphere. Otsu thresholding is a well-known algorithm to automatically optimise thresholds (Otsu, 1975). Both Monegaglia et al. (2018) and Donchyts (2018) applied Otsu thresholding in combination with water indices to detect surface water changes. For the Otsu thresholding algorithm to perform optimally, careful consideration should be given towards the input. Otsu thresholding does not work optimally when in the region of interest, the fraction of water pixels is small (Donchyts, 2018). Selecting a large fraction of water pixels is complicated as the river migrates which means it is not evident to select water pixels in each image. To optimise the input for the thresholding procedure Donchyts (2018) developed a method to automatically detect the surface water edges. The surface water edges are the most critical for thresholding, as it represents the boundary between land and water. A similar approach is used in this study, but it was modified and simplified to apply it for the Ayeyarwady river. More information on the Otsu thresholding procedure is given in Appendix B.

3.3.2 Detection of sediment bars

For the detection of unvegetated bars the SWIR band is used, which can be used to detect mineral deposits (Monegaglia et al., 2018). Due to the use of a single band, distinguishing the image into two classes, so a sediment bar class and a non-sediment bars class, is more complicated than with indices that use a combination of bands. Furthermore, the dynamic character of bars, and the relatively small surface area bars represent in the river surface, provide additional complexity. These aspects prevented to select adequate input for Otsu thresholding. Similar problems with Otsu thresholding were mentioned by Monegaglia et al. (2018). To account for these problems there was opted to use a manually optimized threshold that is kept constant over time. The threshold is based on studying the reflectance properties of bars for the Ayeyarwady river. The constant threshold was found to provide sufficient results under varying conditions. This can partly be explained due to the use of the SWIR band. The near-infrared and infrared bands are only slightly affected by atmospheric distortions (Donchyts, 2018). Furthermore, the reflective properties of bars were found to not change over time. More information on the manual selection of the threshold is given in Appendix B.

3.3.3 Generating river mask and noise removal

Once the individual layers are classified a couple of operations are performed to remove noise and optimize the river masks. First of all, both the sediment bars layer and the water layer are combined (see Figure 16 b, c, d). At this point, the masks still include noise from for example clouds, hill shadows and disconnected water bodies. This noise is removed based on connectivity with the main river body. Detecting the main river body relies on a Global River Width from Landsat (GRWL) dataset (Allen & Pavelsky, 2018), which includes centrelines of rivers wider than 30 meters globally. Based on connectivity with the centreline of the Ayeyarwady river, the river body can be identified, and disconnected noise can be removed. This method is based on Yang et al. (2019), who focussed on determining river widths with optical satellite imagery. The effect of this step is illustrated in Figure 16 e. Finally, merging the bars and water mask leaves some gaps in between the masks, which is due to the presence of mixed pixels. A commonly applied algorithm in computer vision to close gaps is binary closing (Serra, 1983). Binary closing is applied with a kernel of the size of 2 pixels (+/- 60 meters for Landsat), which is small enough to make sure only the small gaps between sediment bars and the water surface are filled in. Larger gaps in the binary image such as vegetated islands are left untouched. The effect of this step is illustrated in Figure 16 f.

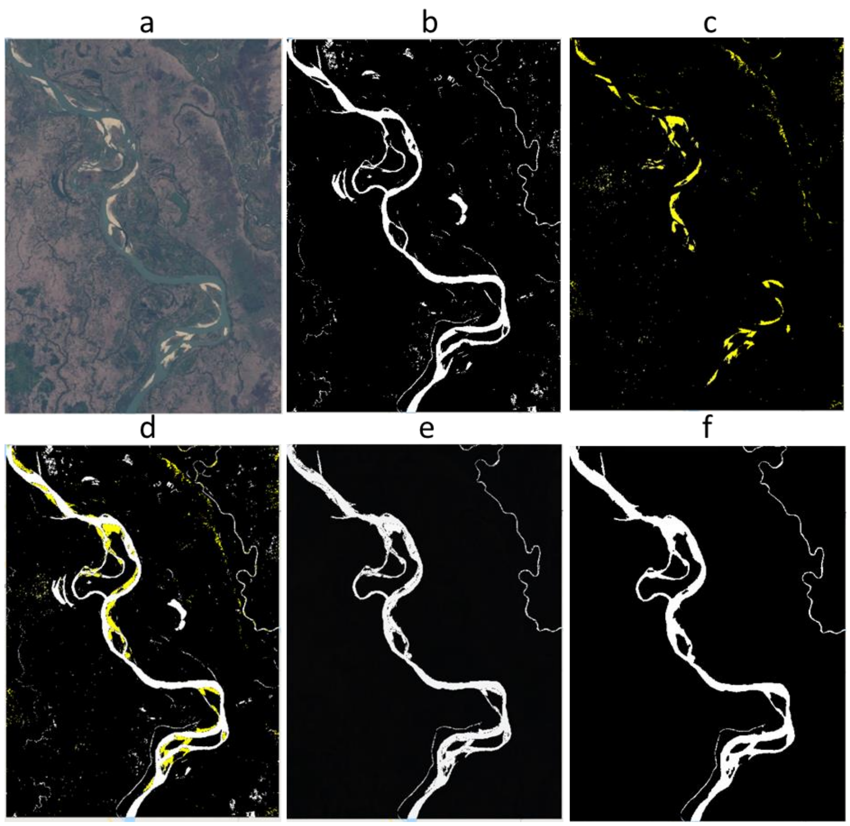

Figure 16: a) The Landsat image. b) The detection of surface water. c) The detection of sediment bars. d) Merging the water and bars mask. e) After merging a single river mask is generated (white). From this river mask noise is removed based on connectivity with the river centerline. f) closing gaps in the river mask between the bar layer and water layer with binary closing.

3.4 Classification method 2: Detecting changes in the water surface

Studying the change of the water surface only requires the use of a water index. The method of detecting surface water is described in section 3.3.1. Noise due to for example cut-off lakes, clouds and shadows and temporarily abandoned channels, that are not connected to the low stage channel are removed using the centerline method that is described in section 3.3.3.

The difficulty with solely relying on the surface water detection is that the extent of the water surface changes with varying water levels. Furthermore, by how far the bars are exposed and how many channels are active in the river planform largely depends on the river stage. Therefore, the water level differences over time are minimised by setting a water level range. Again, for similar reasons as mentioned in section 3.1, also in this classification method images from the dry season are used. By solely using images where low stages are measured, ultimately what is detected over time is the location of the low stage channel(s). This gives a different idea of locations where deposition occurred compared to last year's low stage channel and does not depend on vegetation growth before deposition is found. An illustration of the change detection is given in Figure 17.

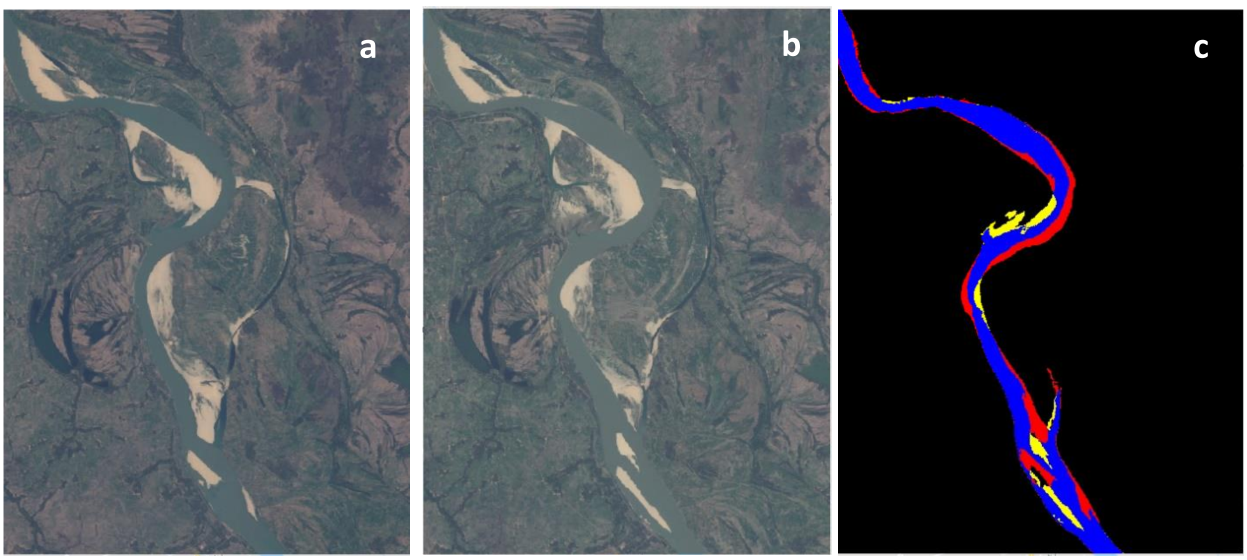

Figure 17: Illustration of the movement of the low stage channel between the dry season of 1991(a) and 1992(b) and the detected differences (c). Red = erosion, yellow = deposition and blue = no change. Note that both the formation and erosion of bars are included in the quantification of the differences.

3.4.1 Water level data and additional criteria for selecting satellite images

To be able to make accurate comparisons over time, a similar water level must be present in each image. To select images based on the measured water levels, water level data from 4 measurement locations is available from 1990-2019 (see Figure 18). More information on the water level data is given in Appendix A.

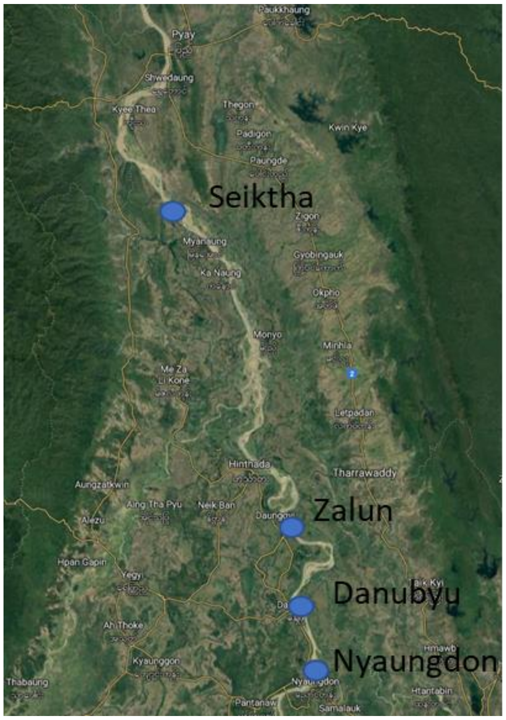

Figure 18: Water level measurement locations. Satellite image from Google Earth (2019)

Studying the water level data reveals that the spatial correlation between the measurement locations over the 30-year period is relatively low. There can be many reasons for low spatial correlation, including delayed arrival of discharge peaks and tidal range due to proximity to the delta. However, Figure 19 reveals that during some dry seasons the water level at some measurement locations can strongly vary (> 2m difference) from other years and other measurement locations. The hypothesis for the low spatial correlation is therefore that geometric changes of the river (cut-off, depth, width) changes the relation between two measurement locations over time.

This has some important implications for the detection of river change. First of all, a single measurement location does not represent the water levels over a large area. So preferably a combination of multiple locations is used to select images with similar water levels in the study area. Secondly, there can be relatively large water level differences on small spatial scales. Furthermore, the multithreaded planform of the Ayeyarwady has gently sloped banks. The large water levels differences and gently sloped banks indicate that river change detection on small spatial scales is highly uncertain. Local differences in water levels over time can have a large impact on the extent of the water surface.

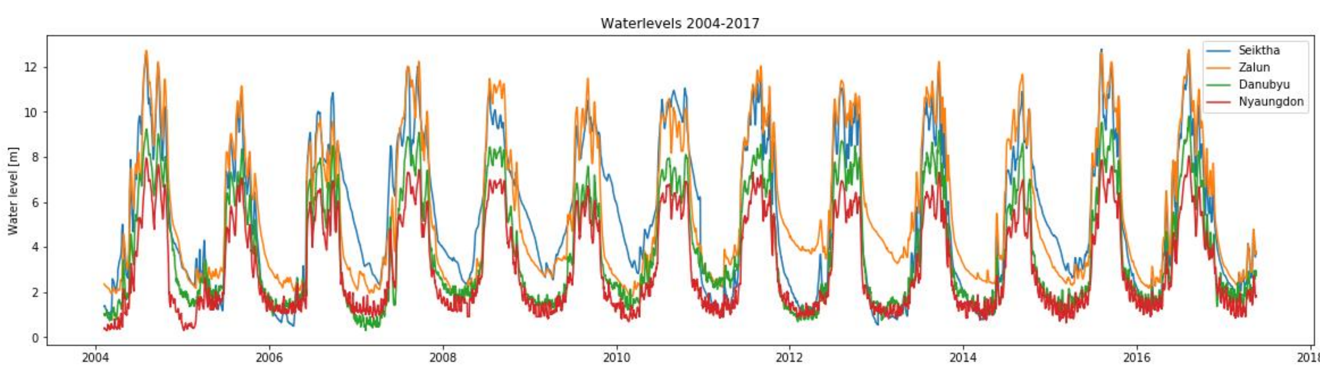

Figure 19: Water levels from the 4 measurement locations acquired by Steijn et al. (2019). It becomes clear that during some dry seasons the measured water levels strongly deviate from other years, but also from other measurement locations.

Compared to the method that detects the vegetation boundary described in the previous section, this method requires an additional criterium of the water level. An overview of the filtering steps is given in Figure 20. To reduce the spread in the quantification of river morphodynamics, a water level range is used. Furthermore, as a single measurement location does not represent the water level of long river stretch there was opted to use the combination of the measurement locations in Figure 18. A maximum allowed range of 1 meter is used, which was found to be optimal to reduce the spread in the quantification whilst retaining sufficient samples. The exact procedure of the selection based on water levels is elaborated in Appendix B.

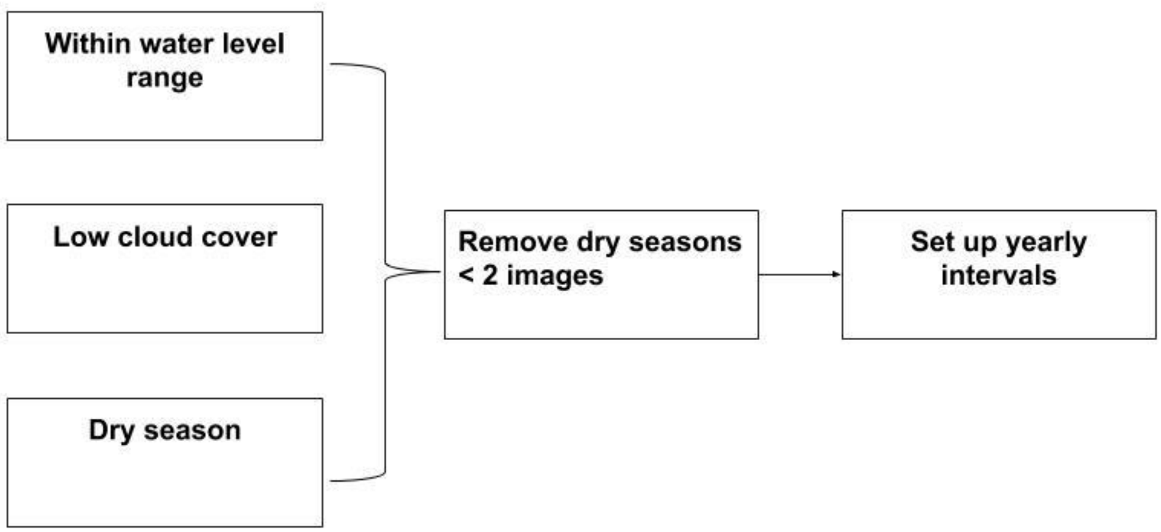

Figure 20: Selection criteria for method 2 of change detection

As a result of the strongly fluctuating water levels in the dry seasons, only limited images fulfilled the selection criteria. In total, the planform dynamics measured in 7 different hydrological years can be quantified (see Table 5).

Table 5: Resulting images after using the selection criteria, including the additional selection criteria of the water level range that is used for method 2. The accompanying Landsat image ID's are given in Appendix C.

	Wet season	Dry season year 1	Nr of images dry season 1	Dry season year 2	Nr of images dry season 2	Total samples
1	1995	1995	2	1996	2	4
2	1996	1996	2	1997	2	4
3	1999	1999	2	2000	2	4
4	2000	2000	2	2001	2	4
5	2001	2001	2	2002	4	8
6	2002	2002	4	2003	4	16
7	2003	2003	4	2004	3	12

3.5 DERIVING METRICS OF PLANFORM CHANGES

For deriving metrics of change, it is important that the planform dynamics can reliably be quantified on reach scales. Multiple studies show the potential for automatic extraction of metrics related to river change, such as river widths, sinuosity, linear rates of change and area-based changes (e.g. Monegaglia et al., 2018; Schwenk et al., 2016; Yang et al., 2019). An overview of some of the different metrics that have been studied before with satellite images is given in Rowland et al. (2016). However, in many occasions, there is focussed on either meandering rivers, or simplified shapes of multithreaded rivers are used. An example of a simplified shape is only selecting the outer bank lines, thereby removing islands or by only selecting the main channel. This removes a large part of the in-channel morphodynamics, which are an essential part of multithreaded river planforms. Furthermore, in the study of planform dynamics with satellite imagery, a common approach for meandering rivers is to determine linear rates of change. These metrics map channel migration and are very intuitive. They can be expressed in easy to interpret units such as the amount of migration in meter per year. For many complex multithreaded rivers, such as the Ayeyarwady, a common occurrence is the formation of new channels and abandonment of old channels. These fast changes are hard to describe in linear rates of change, which makes it hard to quantify reach scale dynamics. This is different in more continuously migrating channels that often occur in meandering rivers.

To account for the complexity of many multithreaded rivers the metrics are all area-based. Extracting these metrics can be done based on channel mask differencing. An example is given in Figure 21. Planform dynamics such as erosion and deposition are expressed as eroded and deposited areas. Area-based change measurements have the benefit that all changes can be measured, as opposed to linear rates of change. This makes these measurements very suitable for complex multithreaded rivers. This is also a downside, as all change is directly measured which includes classification errors. Therefore, these types of metrics are relatively sensitive to uncertainties in classification (Schwenk et al., 2017). Furthermore, if a channel migrates more than a channel's width within the selected time interval it underpredicts erosion or accretion (Rowland et al., 2016). This can be seen in Figure 21. In some locations the channel has significantly migrated between 1988-2019. However, only the new positions of the channel in 2019 are marked as eroded areas, whilst a much larger area might be eroded when the channel slowly migrates over time. To counter these problems first of all the time intervals were set to 1 year (see section 3.1.2) as migration is relatively limited in yearly intervals. Secondly, the uncertainty in classification is directly included in the analysis (see section 3.1.3), which allows taking into account the sensitivity of area-based measurements.

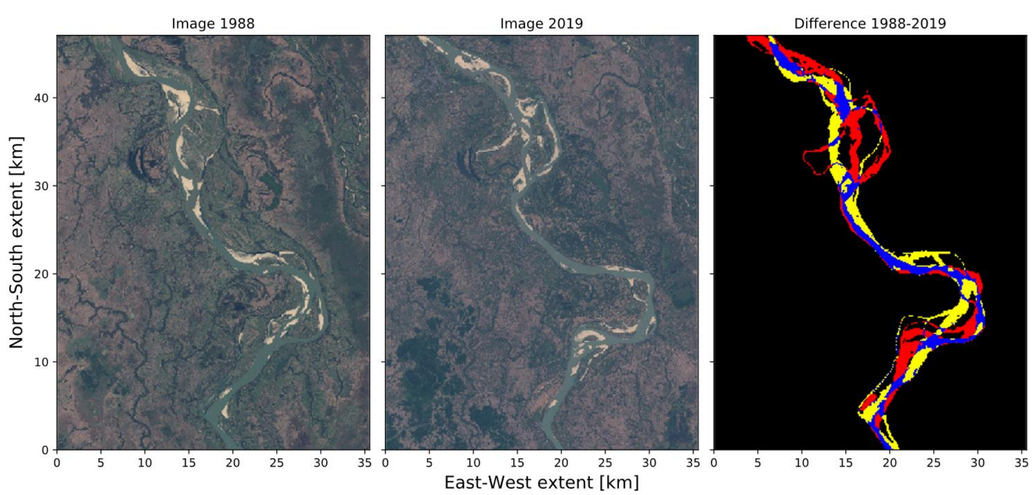

Figure 21: Example of mask differencing approach. Red shows eroded areas, yellow shows deposited areas and finally blue shows areas with no change.

For an expression of the river geometry, the total surface area of the river is taken which expresses the combination of river length and width. Both the river length and width are trivial to determine automatically on reach scales for multithreaded river planform due to their complex geometry. The surface area, however, still allows to express the river geometry of the planform on reach scales. On a yearly time scale, the changes in active channel area are measured.

Furthermore, to be able to normalize the morphological change, or to allow for comparison over the river length, the morphological change is normalized with the channel area. This type of metric is commonly seen in the study of planform dynamics (Mertes et al., 1996; Poxeito et al., 2009; Rowland et al., 2016). To make up for different time intervals in the analysis, the morphological change can be divided by the time interval between images. The result is a morphological change rate parameter (see equation 3). It also includes the total migration of the channel relative to the original channel size (Poxeito et al., 2009). Both erosion and deposition are measured as change between two images (t1-t2). The channel area that is used is the channel area measured at t1, so it is the reference channel area.

$$Migration\,rate\;[yr^{-1}] = \frac{A_{deposition}\;[km^2] + A_{erosion}[km^2]}{A_{channel}\;[km^2] * T_{interval}\;[yr]} \quad (3)$$

To summarize to describe planform dynamics the metrics that are derived on a yearly timescale are: Eroded areas, deposited areas, and migration rate. To track the geometry of the river the change in active channel area is measured, which is the net difference between erosion and deposition.

For studying spatial differences in planform dynamics measured in the study area, it was divided into different sections. Subdivision in small areas enlarges the effect of local outliers and misdetections in the morphodynamics metrics. In the end, there was opted to divide the studied river length of 250 km into 15 sections of roughly 17 km (see Figure 22). The subdivision into 15 areas is small enough to spot significant differences over the river length, whilst at the same time limiting the effect of local outliers. To select 15 different river sections, first of all the river shape was extracted from the classified river masks, which was then subdivided with orthogonal cross-sections. The exact procedure is elaborated in Appendix B.

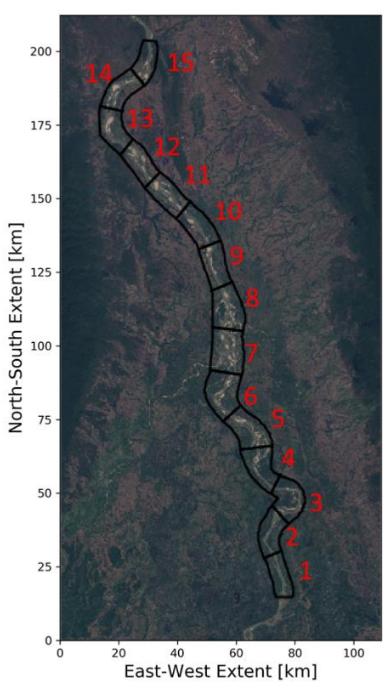

Figure 22: Subdivision of the study area

3.6 Analysing the results

To find possible explanations for differences in time and space, the main focus will be on the hydrologic regime as it is known as an important driver of reach scale planform dynamics (see section 2.5). As a representation of the hydrologic regime river stage data is used. Water levels are an imperfect representation of discharge, due to the dependency on the geometry. The geometry of the Ayeyarwady river is strongly variable over time. To somewhat compensate for the changing geometry, the water level measurement location of Danubyu is used (see Figure 18), as relatively little geometric changes on the surface occur over the 30 year period of interest. A benefit of using data on the hydrologic regime is that it is commonly available for most large rivers of the world.

The variability on both seasonal and yearly scales are believed to have an important influence on planform dynamics, such as the formation of bars and islands (see section 2.1). By calculating the water level statistics during the same year as the measured planform dynamics they can be quantitively linked. To investigate key drivers of planform changes, the water levels statistics are investigated on different time scales. Time scales of particular interest are the peak water levels and the average flood season intensity. For example, peak water levels/ peak discharges are known to create avulsions, which is often characterised as a key dynamic for anabranching river planforms (see section 2.1.4). Besides, an interesting question is whether the average flood season intensity or the peak flow conditions are dominant for planform changes.

As flood seasons have different characteristics each year, such as varying starts and ends, the average intensity of a flood season is hard to consistently determine. To account for this a moving average is taken (see equation 4).

$$\bar{h}_t = \frac{1}{n}\sum_{i=0}^{n-1} h_{t-i} \tag{4}$$

In which:
$\bar{h}_t$= is the average water level at time t, in which t is in days
n= window size (days)

After calculating the moving average for all the samples in a year, this creates a total of 365- n (window size) samples. As the interest lies in the maximum intensity, which for example describes the flood season intensity, the maximum of all the moving average samples for a year is taken (see equation 5).

$$\max\left(\left[\bar{h}_1, \ldots., \bar{h}_{365-n}\right]\right) \tag{5}$$

Different window sizes were taken to account for intensity on different time scales (see Table 6). By taking averages on different time scales, both the effect of magnitude and duration can be investigated. An example of the different statistics derived for one of the years in the analysis is visualised in Figure 23.

Table 6: Derived statistics of water level measurements

Statistic of interest	Window size
Peak water level	7 days
Max flood wave intensity	30 days
Average flood season intensity	4 months (≈ 120 days)
Average intensity excluding dry season	6 months (≈ 180 days)
Average yearly intensity	No need for a window

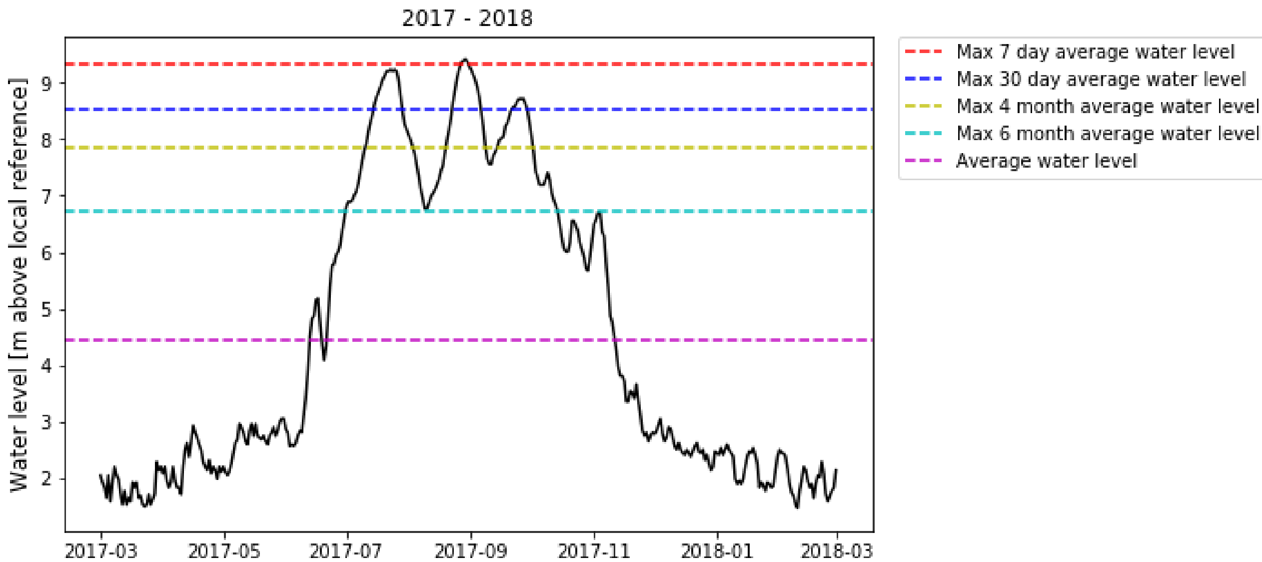

Figure 23: Example of the different statistics derived from water level measurements for one of the years in the analysis (2017-2018)

3.7 OVERVIEW OF THE DIFFERENT STEPS AND METHODS

A recap of all different steps and methods that are applied is given in Figure 24.

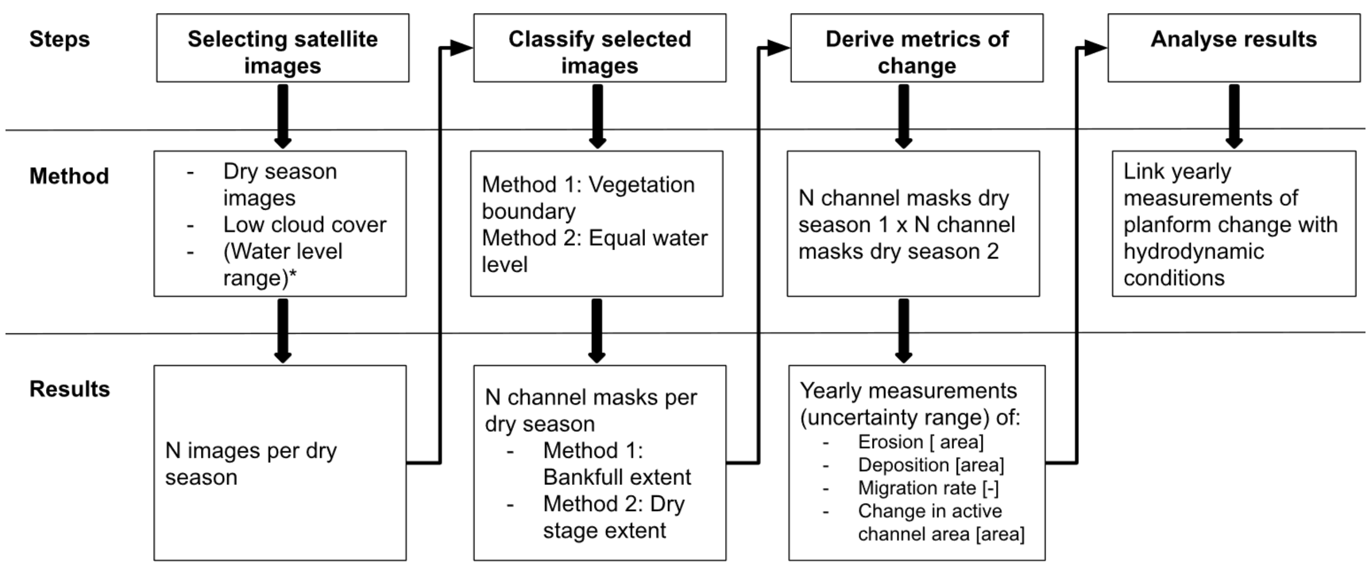

*** Water level ranges to select images are only used for classification method 2**

Figure 24: Overview of different steps and methods used in the method.

4 CASE STUDY: PLANFORM DYNAMICS OF THE AYEYARWADY RIVER

This chapter has 7 sections. The first section discusses the general characteristics of the Ayeyarwady river related to the river planform and its dynamics. The second section discusses the observed planform dynamics between 1988-2019. The third section describes the quantification of bankfull channel changes (method 1 of classification). In the fourth section the quantification of low stage channel dynamics is discussed (method 2 of classification). Next, the two methods are compared in section 5. The second to last section discusses the uncertainty in the detection methods. Finally, a recap of this chapter is given in the last section.

4.1 CHARACTERISATION OF AYEYARWADY RIVER

4.1.1 Characterization of the river planform and related properties

Over the length of the Ayeyarwady river the presence of relatively stable vegetated islands is common, which indicates that anabranching is a good characterisation of the planform. Also in the study area, the presence of islands is common, although the planform has some different characteristics over the river length within the study area (see Figure 25). Following the scheme from Figure 5, the characteristics in the categories of flow and hydrologic regime, sediment transport and supply and geometric properties are discussed as they are often mentioned to be the controls of the channel pattern.

The hydrological regime shows strong seasonal variability. The Ayeyarwady river is one of the last long free-flowing rivers in Asia (WWF, 2019), which means the natural variability is still present. The discharge of the Ayeyarwady is strongly seasonal with typical discharges up to 30000 m^3/s in the wet season and discharges lower than 5000 m^3/s in the dry season (Ligthart, 2017).

The sediment transport and sediment supply are generally characterised by sandy material. The river banks are often sandy with different intensities of vegetation growth (Van Duijn, 2018). The median grain in the river of bedload transport is 0.3 mm, which means the river mostly transports medium-sized sand (Van der Velden, 2015). Besides, there have been reports of a large load of suspended sand (63 % of the total suspended load) (Park et al., 2017), which is also commonly mentioned for other large anabranching planforms (Latrubesse, 2008).

Some of the geometric properties that are often described as influential on channel planform are the channel slope and the floodplain width. An estimate of the water surface slope can be generated through SRTM elevation data (LeFavour & Alsdorf, 2005). In the study area the average slope is around 7 cm/km (see Figure 26). The study by Park et al. (2017) mentions similar slopes for the more upstream sections. Latrubresse (2008) mentions that the slope of anabranching rivers is typically around 7 cm/km or less, which means also the Ayeyarwady river fits in this description. Besides an often mentioned geometric property that favours the formation of anabranching planforms instead of braiding planforms is the floodplain width. Based on the HAND map, or height above nearest drainage (see Nobre et al. (2010) for a description), which is generated from SRTM elevation data, an estimation of the floodplain width can be generated. The floodplain is wide in the study area which is the start of the delta. The exception is northern the northern part of the study area, which is hillier compared to the more downstream sections (see Figure 27c). If the entire river is inspected, it becomes clear that the presence of vegetated islands is common along the entire river length, although in some sections the number of islands is much larger than in others. Interestingly, especially where the floodplain is wider, identified by the HAND map (see Figure 27), both the size and the numbers of islands seem to increase. This fits the theory mentioned by Moron et al. (2017) where the floodplain width is considered to be an important driver in the anabranching planform.

4.1.2 Human interventions in the study area

A complicating factor in parts of the study area is the presence of dikes that restrict the floodplain width (see Figure 28). As the study area is the start of the delta of the Ayeyarwady river, dikes are in place to prevent flooding in the surrounding low-lying areas. Most of the embankments have been in place since the late 19th century (Ivars & Venot, 2019), which means floodplain width did not change in the study period. Furthermore, the river can generally move freely in the non-constricted part of the floodplain. Although not widespread sometimes human interventions took place in small sections to prevent unwanted effects of river morphodynamics. Examples are bank protection and the placement of groins. An intervention that is clearly visible in the satellite imagery is the creation of a cut-off which occurred in the south of the study area (see Figure 29).

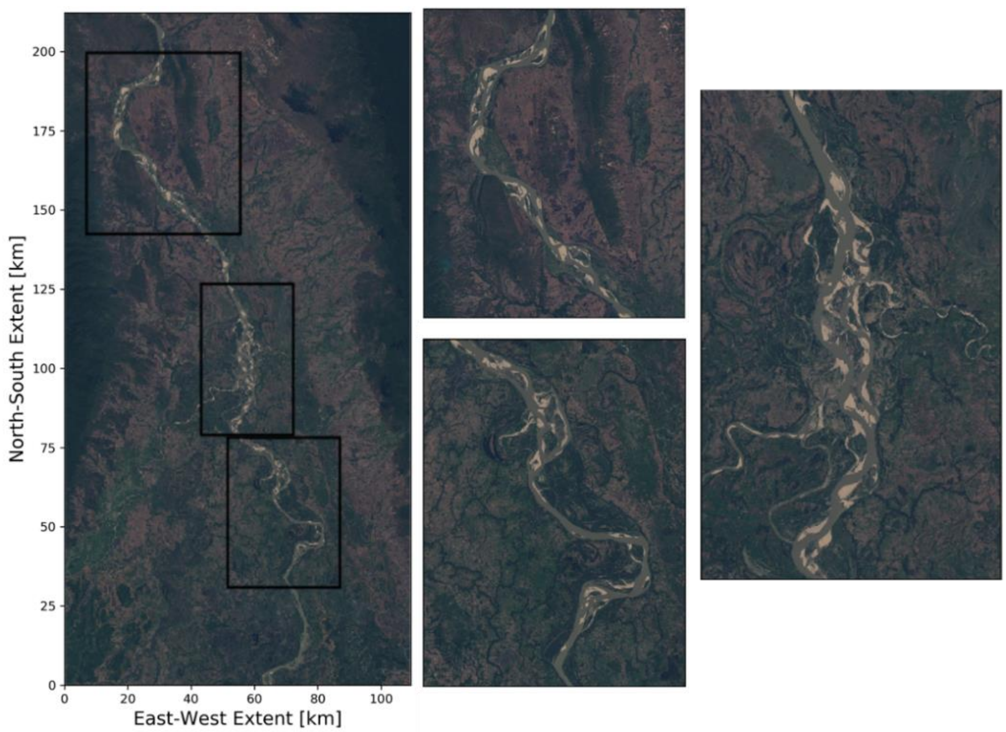

Figure 25: The study area with some of the distinct regions. The northern region has some islands but is also partly single-threaded. The middle region is very dynamic and has multiple channels. The southern region shows some signs of meandering.

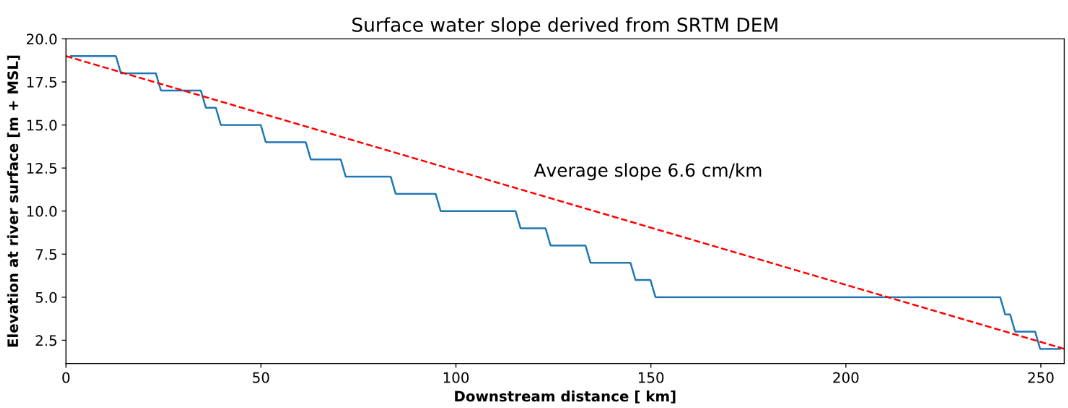

Figure 26: Estimation of the surface water slope in the study area based on the SRTM data from 2000. On average a 6.6 cm/km slope is found. The lower sections of the study area have a considerably lower slope than the upper parts of the study area. More information on the procedure to derive the slope is given in Appendix D.

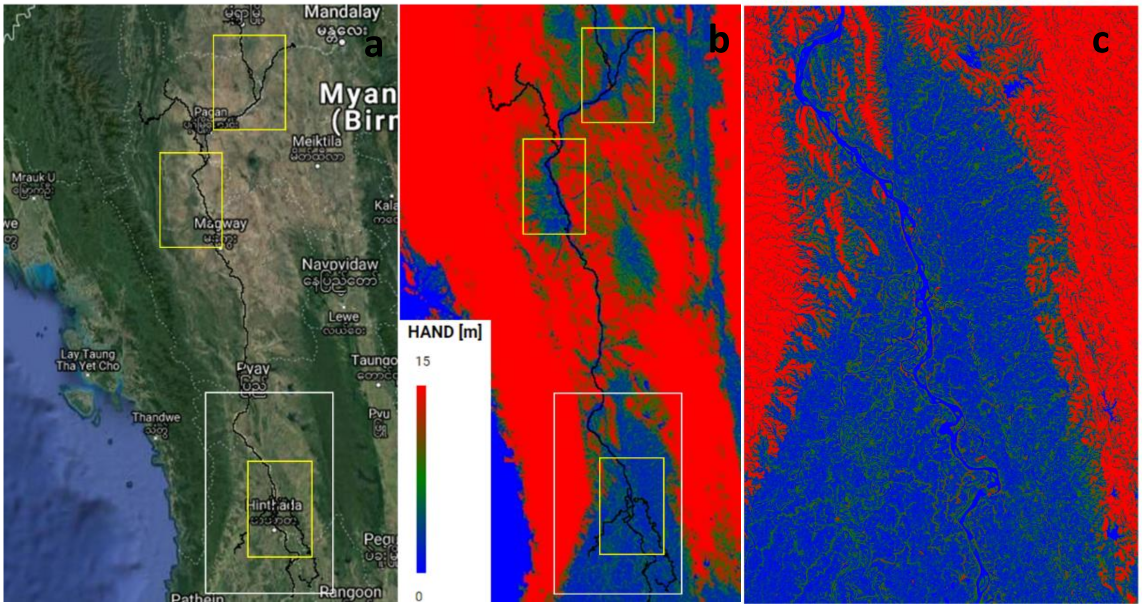

Figure 27: a) Overview of the Ayeyarwady river and the study area. In yellow the sections with more intense braiding are marked. The white rectangle marks the study area. b) The elevation, expressed in height above nearest drainage, shows that the sections with more intense braiding generally occur where there is a wide floodplain. c) A zoom of the HAND map in the study area

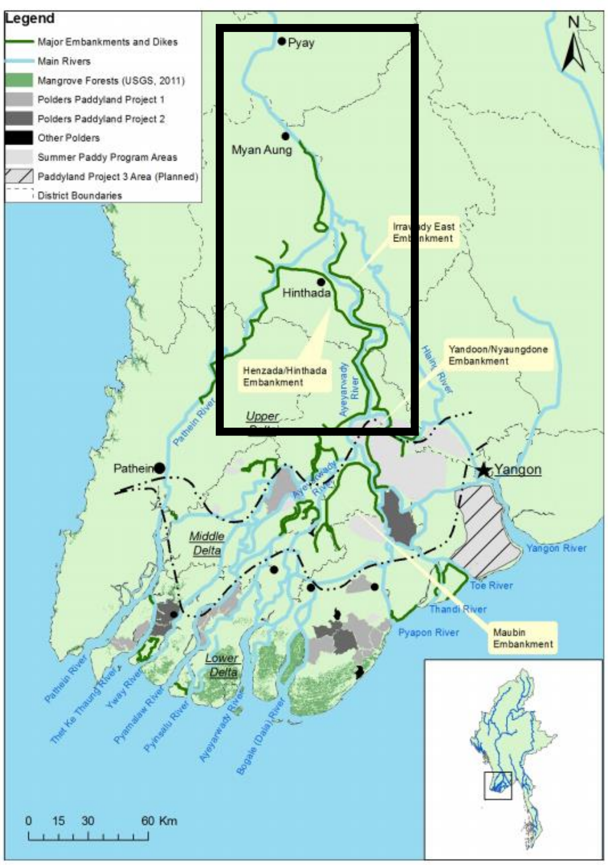

Figure 28: Embankments that are present in the lower Ayeyarwady river (Ivars & Venot, 2019). The black rectangle marks the study area.

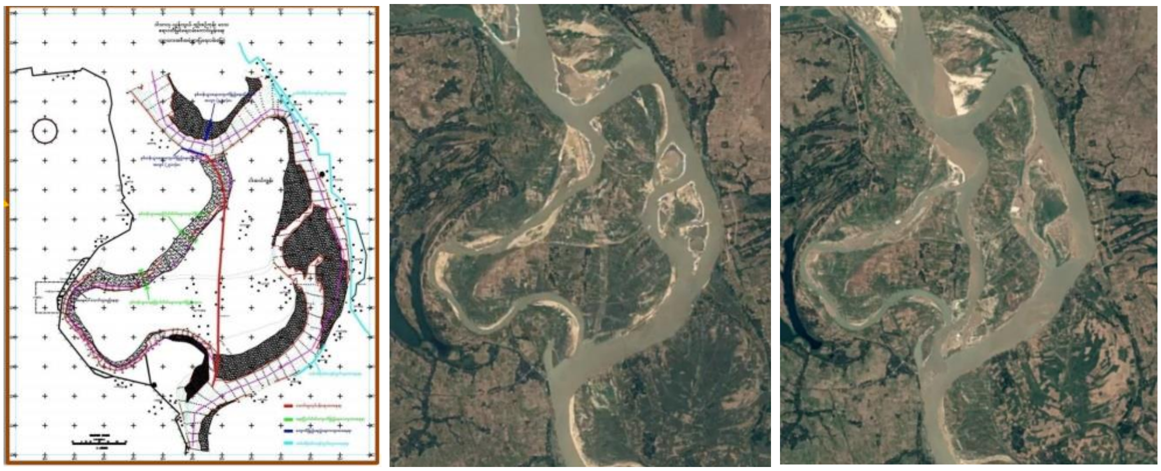

Figure 29: The artificial cut-off that was created in 2016 in the south of the study area. The left tile shows a drawing of the planned intervention (DRR, 2015). The middle tile shows the situation in early 2016, whilst the right tile clearly shows the effect of the intervention in late 2016.

4.2 Visual inspection of the planform dynamics between 1988-2019

Visual inspection of the river change reveals the dominant planform dynamics with-in the Ayeyarwady river planform. Most of the planform dynamics within multithreaded planforms mentioned in Chapter 2.2 are also found within the channel planform of the Ayeyarwady river. As the study area has different characteristics in terms of river morphodynamics it was subdivided into three different regions (see Figure 25). For the visualisation of the river morphodynamics method 1 of detection has been used. This means that changes in the vegetation boundary, which describes the active channel under bankfull conditions, are mapped in Figure 30 - Figure 35. The main reason for visualising this method is that it covers most of the period of 1988-2019.

4.2.1 Northern region

The planform dynamics of the northern region throughout 1988-2019 are illustrated in Figure 30 and Figure 31. The northern region is largely single-threaded, except for some sections in which islands are present. It is the least dynamic region in the study area in terms of bankline migration. Its surroundings are hillier compared to the other river sections (see Figure 27), which indicates the river floodplain is more constricted. This partly explains the relatively low lateral migration of the outer banks of the river in this region. The largest part of the morphodynamics in this area take place due to the formation, erosion and migration of bars and islands. Although over the entire section the outer banks migrate relatively little compared to other sections, locally there can be large erosion rates. The interplay of bar and island formation and changing flow direction/secondary circulation seems to play an important role. Based on visually inspecting the morphodynamics over the 30-year period, the mechanism responsible here for the multithreaded river planform is the stabilisation of deposits rather than avulsion into the floodplain. The yellow areas in Figure 31 within the channel boundaries indicate areas where vegetation has grown, and deposits are stabilised.

4.2.2 Middle region

The morphodynamics of the middle region over the period of 1988-2019 are illustrated in Figure 32 and in Figure 33. The middle region is characterised by intense changes in the river planform. Compared to the hillier northern region the floodplain widens, even though it is partly restricted by dikes (see Figure 28). Throughout the entire period 1988-2019, the river has been largely multithreaded.

Different mechanisms seem to be responsible for the formation of new channels and islands. First of all, the yellow areas in the middle of the channel show where vegetation has grown in the time period and thus mid-channel deposits were stabilized. Besides, the formation of a new channel by cutting into the floodplain and abandonment of old channels is playing a key role in the planform changes. For example, the green rectangle in Figure 33 shows that a new channel is formed by eroding an existing island. An important role in the morphodynamics in this region is likely attributed to the bifurcation of the Pathein river and Hliang river from the Ayeyarwady river. The connection between the bifurcations and the Ayeyarwady river has changed frequently (see Figure 32). Furthermore, the bifurcations cause a redistribution of water and sediment, which can be a reason for large scale deposits and planform changes.

4.2.3 Southern region

The morphodynamics of the southern region throughout 1988-2019 are illustrated in Figure 34 and Figure 35. The southern region is partly single-threaded again. Nevertheless, it shows very dynamic behaviour. The channel is relatively sinuous. An interesting aspect is that the water surface slope also reduced in this region (see Figure 26). A hypothesis for the sudden change in planform shape is that human intervention keeps the meandering shape in place. The presence of dikes (see Figure 28) prevents the formation of new channels and restricts the floodplain. Furthermore, the large meander bend in the south of this region has barely migrated eastward between 1988 – 2019 whilst is it is expected based on the geometry (see Figure 34). Again, human interventions might play a role in this as a dike is located just outside this meander bend (see Figure 28).

In terms of planform changes the northern part of this region is the most dynamic (see Figure 34). An avulsion created a planform with two channels separated by a large island (see Figure 35 between 1988-2000). After this secondary flow is likely responsible for migrating both channels outward. Eventually, human interventions took place as was mentioned before (see Figure 29). This is the reason the unusual cut-off in the large island is visible between 2015-2019. Even though an avulsion created a multichannel planform in the north of this region, generally the mechanism that is responsible for the multithreaded planform is the stabilisation of deposits. This is especially clear in the south of this region, indicated by the large yellow areas in the middle of the channel (see Figure 35). Besides the interplay of bar/island formation and migration and changing flow directions seems to play an important reason for local erosion of banklines.

4.2.4 Concluding remarks

From visual inspection of the river morphodynamics several in the different regions several processes and dynamics became clear. First of all, migration of the main channel seems to be present but it often not continuous. Secondly, both avulsions, as well as stabilised deposits, create new islands and channels. Referring to Chapter 2.1, both avulsion as stabilisation of deposits are mentioned as key planform dynamics in the anabranching river planform. Based on the visual inspection the most common phenomena that create a multithreaded anabranching planform is the stabilisation of deposits rather than avulsion into the floodplain.

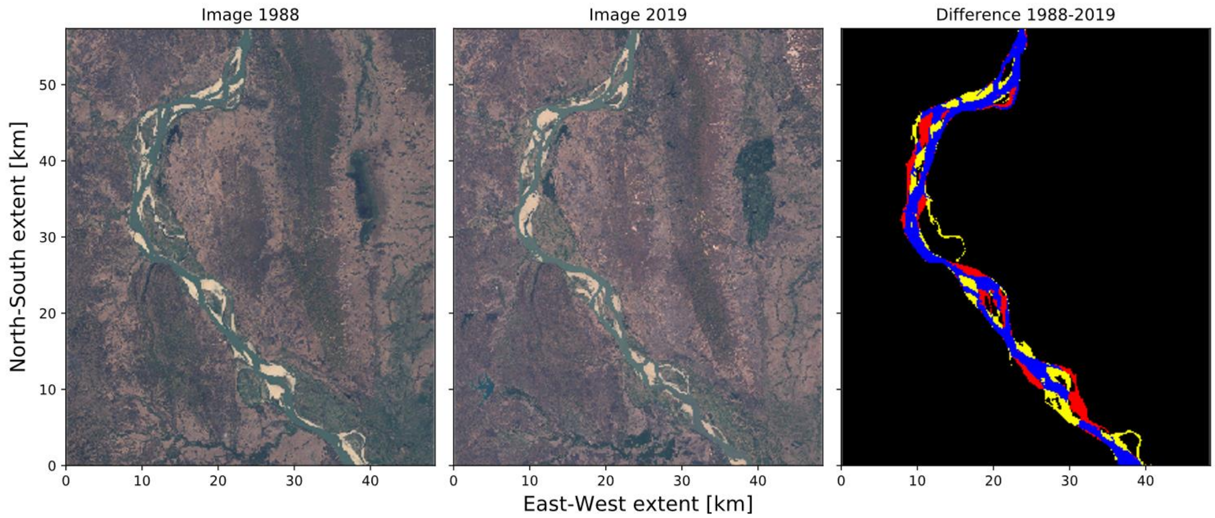

Figure 30: Total migration of the banklines in the northern region between 1988-2019 The rectangles indicate local constrictions of the river. Red = erosion, yellow = deposition, blue= no change.

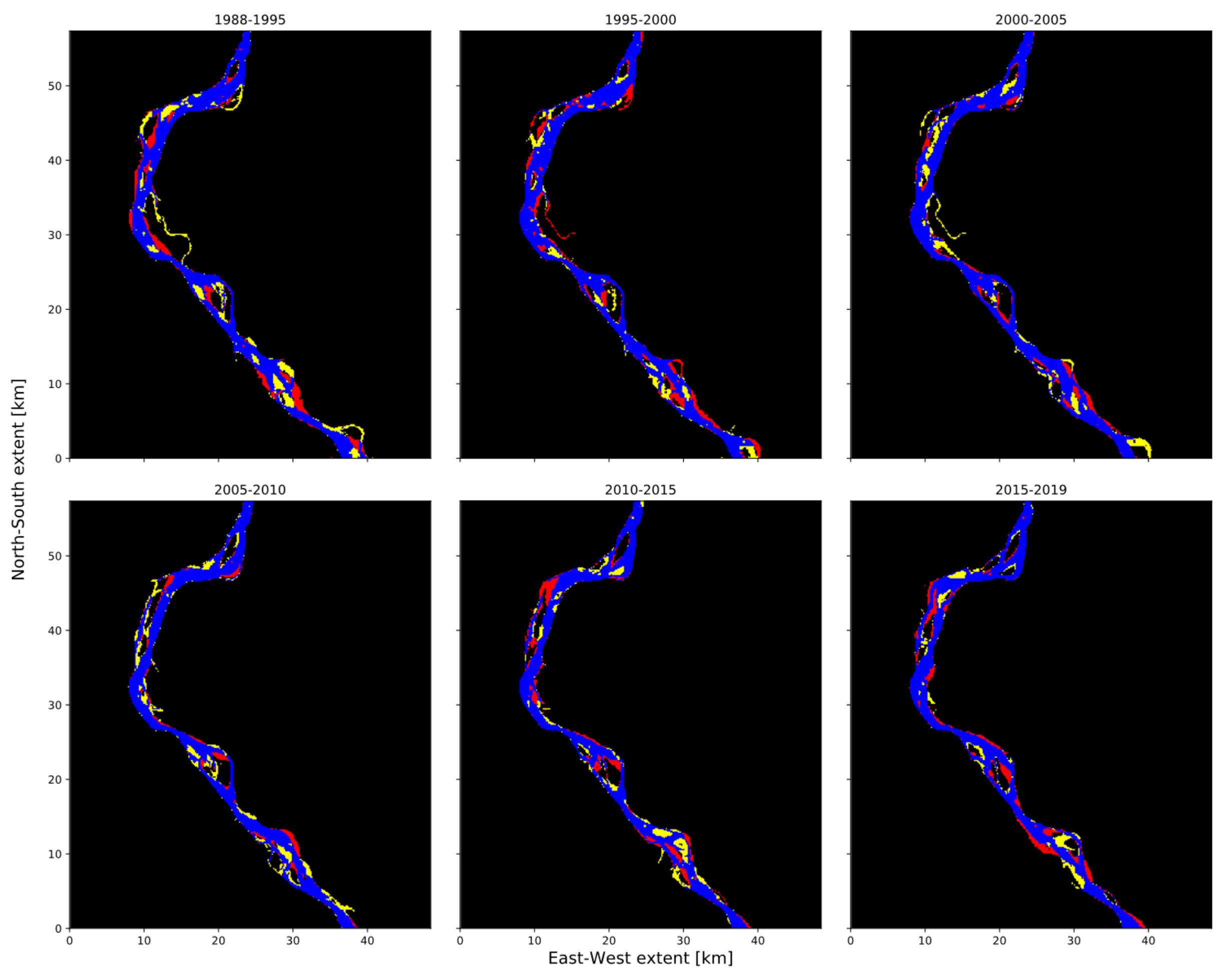

Figure 31: Migration of the banklines in the northern region over time. Red = erosion, yellow = deposition, blue= no change

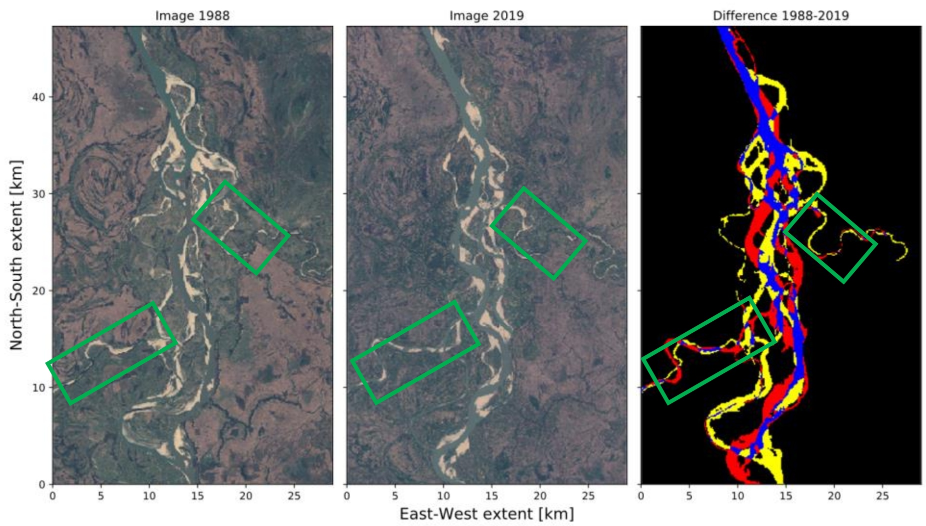

Figure 32: Total migration of the banklines in the middle region between 1988-2019. The rectangles indicate the bifurcations that are discussed in text.. Red = erosion, yellow = deposition, blue= no change.

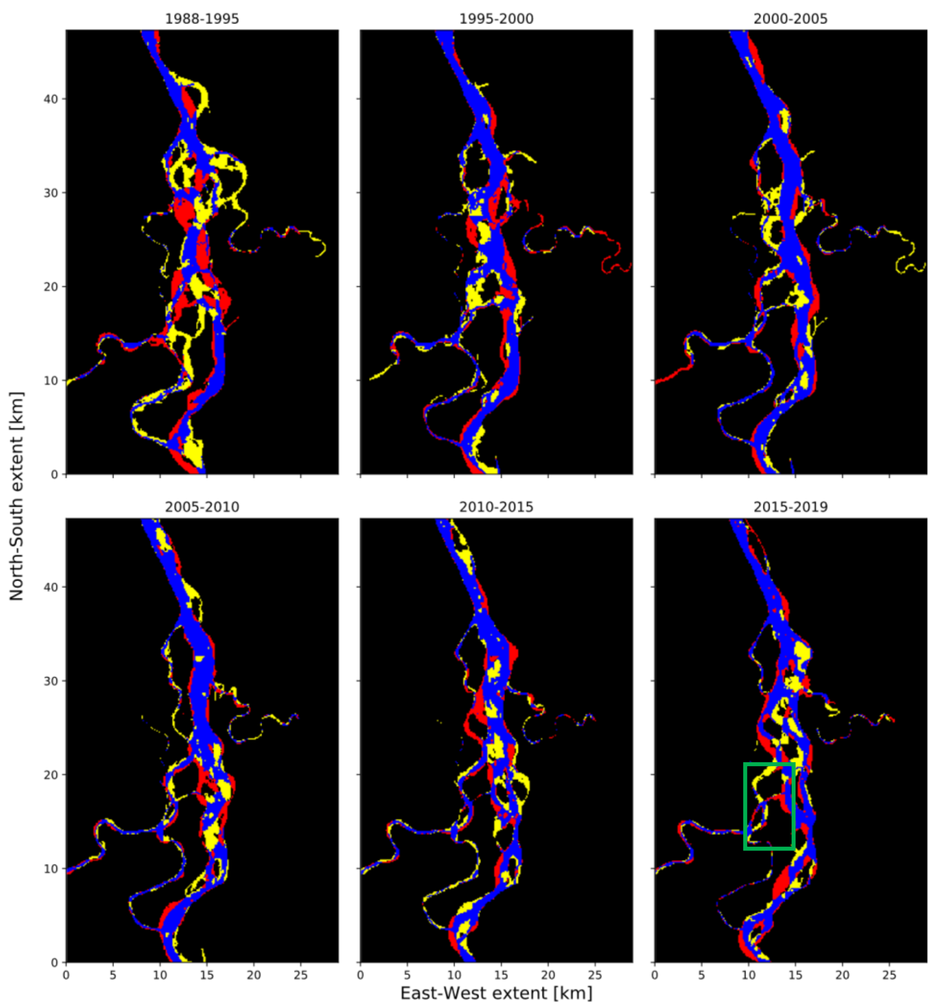

Figure 33: Migration of banklines middle region over time. Red = erosion, yellow = deposition, blue= no change. The green rectangle indicates the formation of a new channel by avulsion and the abandonment of the old channel.

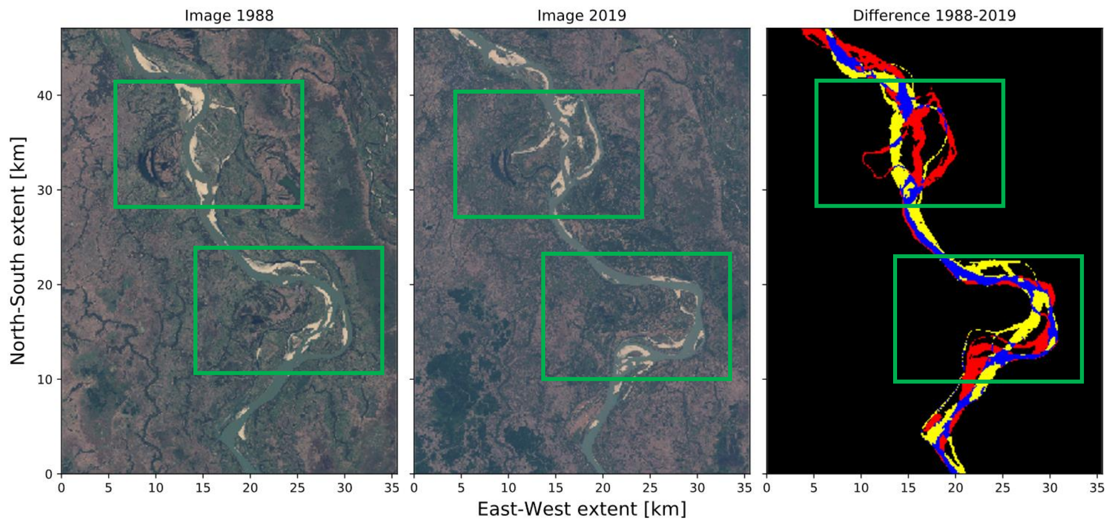

Figure 34: Total migration of the banklines in the southern region between 1988-2019. The rectangles indicate the most dynamic areas that are discussed in the text. Red = erosion, yellow = deposition, blue= no change

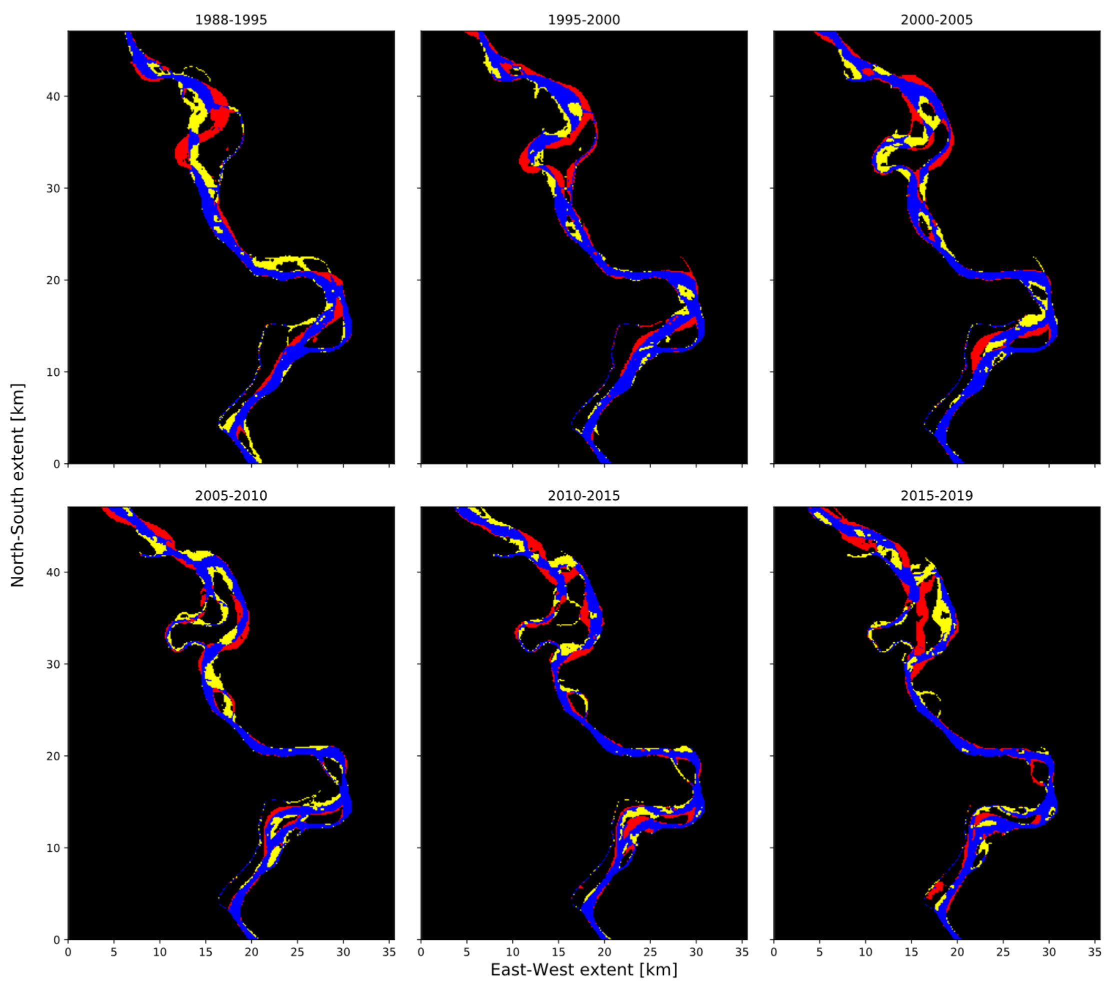

Figure 35: Migration of banklines in southern region over time. Red = erosion, yellow = deposition, blue= no change

4.3 QUANTIFICATION OF BANKFULL CHANNEL DYNAMICS (CLASSIFICATION METHOD 1)

In this section, the quantified planform dynamics that are derived by detecting the vegetation boundary, or bankfull channel, are discussed. Both differences over time and spatial differences are investigated. After this, possible controls of the measured planform dynamics are discussed.

4.3.1 Differences over time in the entire study area

Figure 36- Figure 40 show the differences in erosion, deposition, migration, change in channel area and total channel area over time. The metrics are measured over the entire river section of roughly 250 km. Furthermore, the figures show the uncertainty ranges in the quantification. The red numbers show the number of samples the metric is based on. Note that the samples differ from those in Table 4, which shows the total number of possible samples. Due to limitations in useable memory in Google Earth Engine only a limited number of computations were performed, which means sometimes the number of samples is lower than the maximum achievable samples mentioned in Table 4.

With this method of classification, erosion of the vegetated floodplain is measured. Over the 19 different wet seasons that were in the samples, large differences in erosion over time are measured. Some years show a factor 3 the amount of measured erosion than others. Deposition mostly shows the opposite behaviour as erosion. Years with large erosion generally show little deposition. At the same time, the differences over time in deposition are less pronounced. The different behaviour of deposition can be explained by the way the metric of deposition is measured. Within this method the advance of the vegetation boundary is detected which is not necessarily related to depositional processes. Also other factors can influence the growth of vegetation, which are not necessarily related to river morphodynamics.

Due to the partly counteracting behaviour of erosion and deposition the migration rate is relatively constant. Some outliers are years that are characterised by a lot of floodplain erosion such as 1988, 1995, 2004, 2007, 2015-2019. The average migration rate of the lower Ayeyarwady is 0.15 yr^{-1} during the period of 1988-2019. This means that on average each year the lower Ayeyarwady river migrates 15% of its active river surface at bankfull stage.

For the change active channel area metric, it becomes clear that a strong expansion in channel area generally occurs during single years, which is followed by a couple of years of continuous reduction in active channel area (see Figure 39). The total channel area has reduced over the last 30 years (see Figure 40). However, compared to 1988 the active channel area has only reduced by 6 % in 2019. On the other hand, compared to the maximum active channel area that was measured in 1998 the active channel is reduced by 12% in 2019.

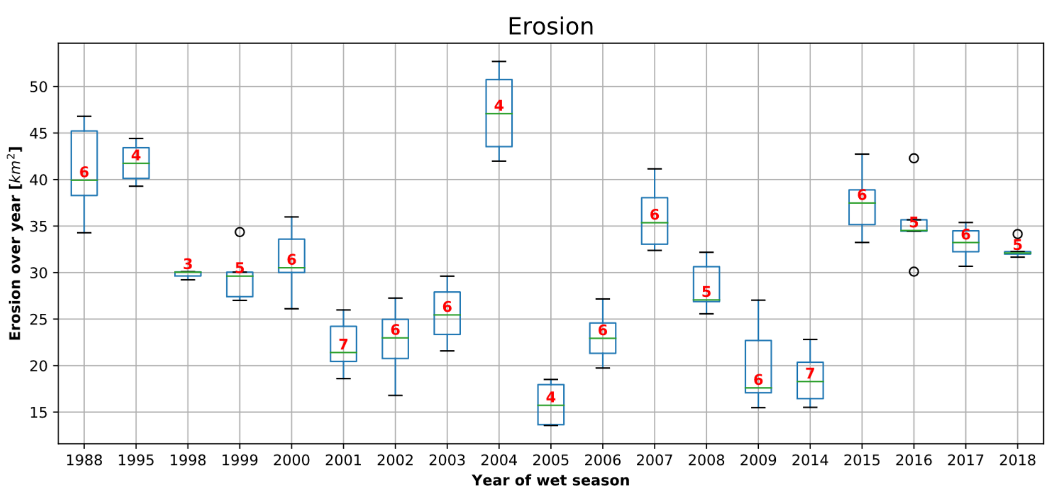

Figure 36: Boxplot of the differences in erosion measured in the entire study area. In red the number of samples.

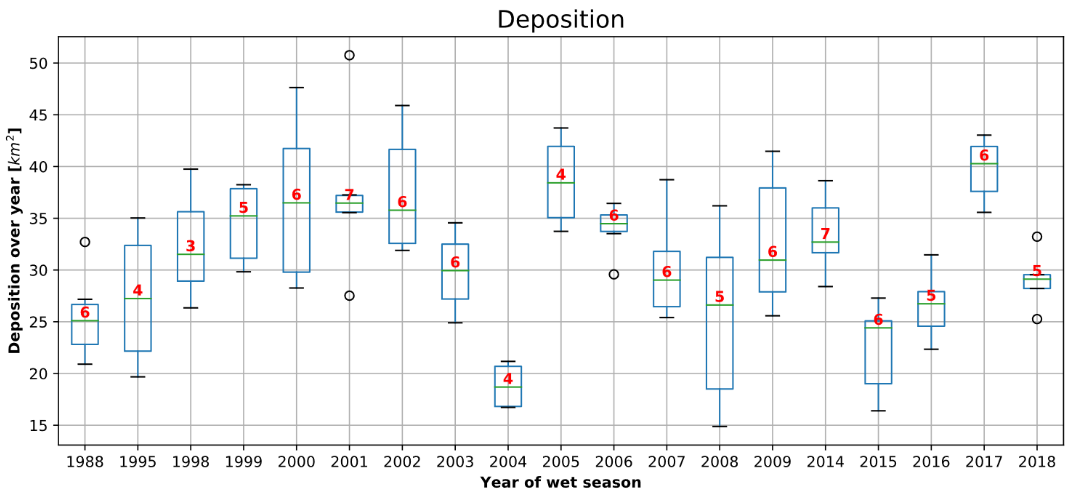

Figure 37: Boxplot of the differences in deposition measured in the entire study area. In red the number of samples.

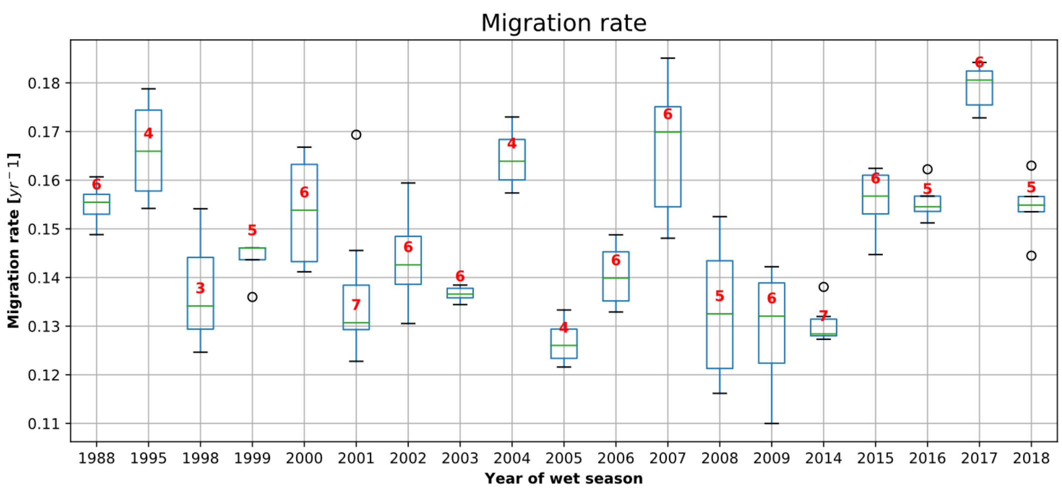

Figure 38: Boxplot of the differences in migration rates measured in the entire study area. In red the number of samples

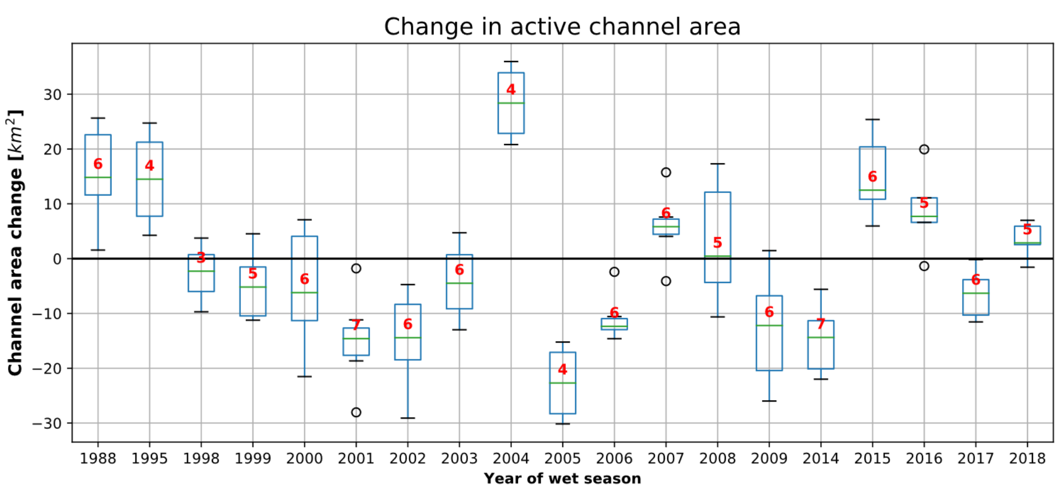

Figure 39: Boxplot of the change in active channel area, or the difference between erosion and deposition. In red the number of samples

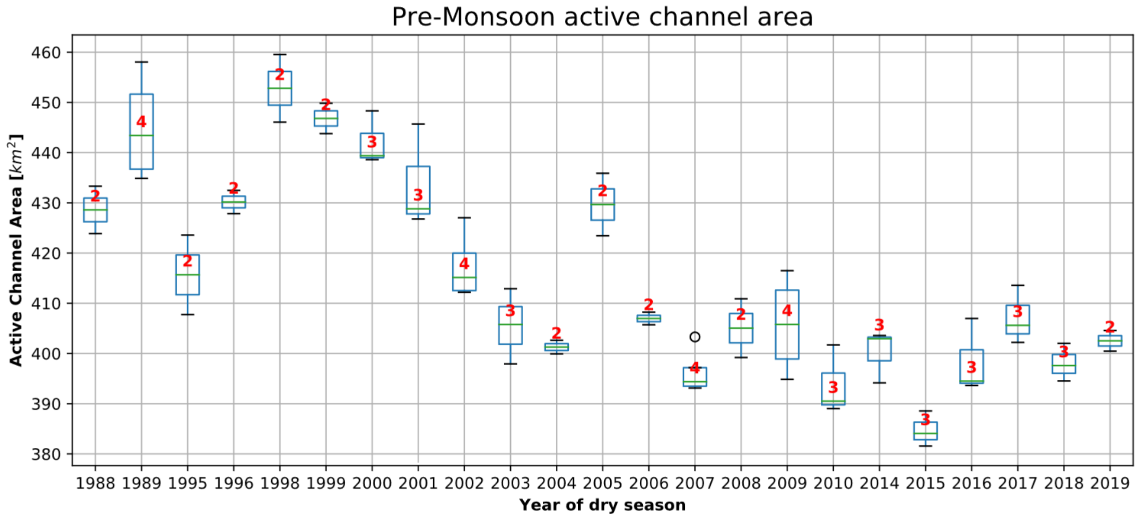

Figure 40: Boxplot of the active channel area over time. As the active channel area is measured by images from a single year, as opposed to measuring planform change where the combination of two years are used, the samples differ from Figure 36 to Figure 39. This figure and Figure 39 are strongly related. Figure 39 shows that over the year 1988 the channel area expanded, which is measured in this figure in the dry season of 1989.

4.3.2 The spatial differences in planform changes

As explained in Chapter 3.6 the study area was divided into 15 polygons (see Figure 41). For spatial differences in river planform dynamics, there is focused on migration rates, which is the combination of eroded and deposited areas divided by the channel area. This removes the dependence on width and length of the river section, which makes the planform dynamics more comparable. For geometric changes, the change in the active channel area is plotted over time.

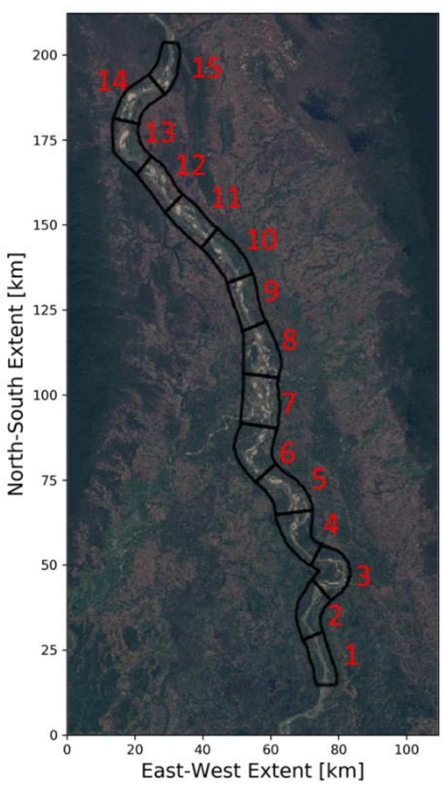

Figure 41: Division of the study area in subsections

Figure 42 shows the average migration rate over the number of samples in each polygon and does not show the uncertainty ranges. The individual areas all show relatively similar behaviour, so the general pattern over the entire study area with a single year with large migration(e.g. 88, 95, 04, 07), followed by multiple years of low migration rates (see Figure 38) is also visible on smaller spatial scales. It should be noted that due to small-scale outliers and misdetections can have large influences on small spatial scales, which sometimes explains large migration rates or single outliers. Nevertheless, an interesting pattern that is revealed is the large migration rates in polygons 4-6 from 2016-2018. Compared to other areas over the river length it becomes clear that the migration rates are relatively high. These high migration rates are likely related to the large human interventions in polygon 4 and 5 (see Figure 29). The creation of a cut-off can have both downstream as upstream impacts on flow and sediment transport dynamics.

The average migration rate over time shows that the middle section (7) is the most dynamic (see the right tile of Figure 42). This also became clear from the visual inspection. Nevertheless, normalised to the channel area, so accounting for differences in length and width, the migration rates are relatively comparable over the river length. Other dynamic areas are area 4 and 5, which are located in the southern region and is the location where the river shows relatively large lateral migration. Besides an explanation for the high average migration rates can be the human intervention that took place in 2016.

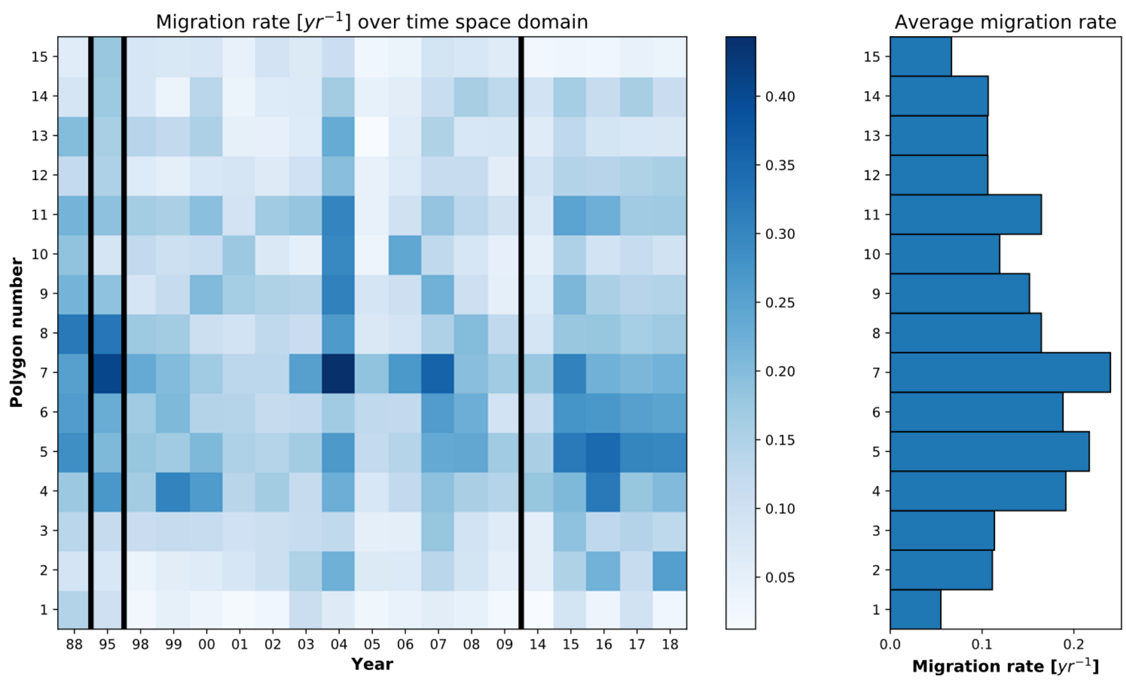

Figure 42: Differences in migration rates over the time-space domain (left) and the average migration rate (right). The black lines denote gaps in the analysis of yearly intervals. Note that the average migration rate is calculated by averaging the samples over time.

The change in the active channel area over the time-space domain is given in Figure 43. Again, it should be noted that small-scale outliers and misdetections can have large influences on small spatial scales, which sometimes explains single outliers. Similar to migration, a pattern reveals in which some years show large expansion in channel area, which is followed by a couple of years of reduction in the channel area. This response is observed along the entire river length. An example of a single year of net erosion that clearly stands out is 2004, which is likely related to intense flood season with prolonged high-water levels, combined with a tropical cyclone (IFRC, 2004). The effect of the human intervention, which introduced an artificial cut-off (see Figure 29), is also visible in the left tile of Figure 43. The temporary increase in the active channel area in polygon 4 and 5 in 2016, followed by a strong reduction the year after, shows the effect of the intervention.

Earlier it was already noted that the active channel area decreased over the period of 1988 to 2019 (see Figure 40). Most polygons show a decrease in the active channel area (see the right tile of Figure 43). Polygons 5 and 7 are the only clear exceptions and show an increase in the active channel area. On the other hand, the largest decrease in channel area is found in polygons 8 and 10. This region is visualised in Figure 44. From the visualisation, it becomes clear that the planform in this region changed from a wide multithreaded planform at bankfull stage, with vegetated islands, to a narrower single-threaded planform at bankfull stage. The development of the active channel area with respect to the reference year of 1988 is given in Figure 45. Most polygons show a reduction in the active channel area between 1998 and 2010. This figure also shows that a large part of the increase in active channel area in the polygon 5 and 7 that is measured in 2019 already occurred between 1988 and 1998.

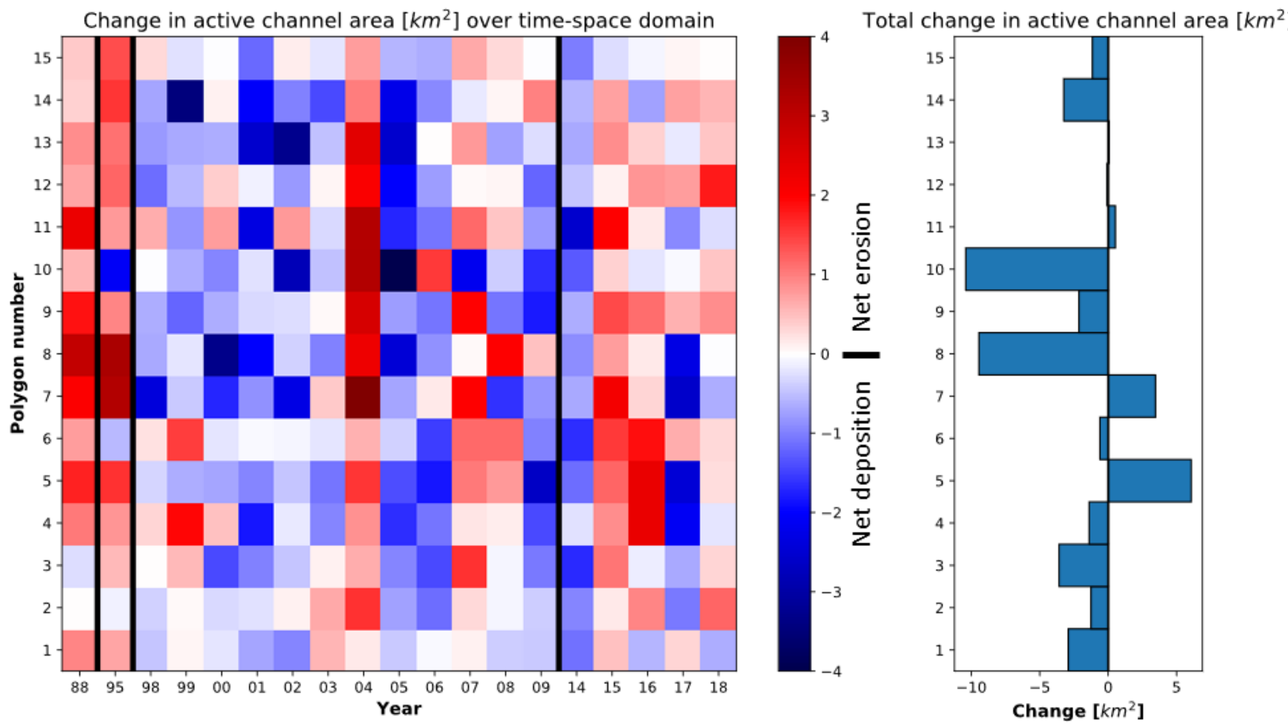

Figure 43: Change in active channel area over the time space domain (left) and total change in active channel area (right). The black lines denote gaps in the analysis of yearly intervals. Note that the total change of active channel area is calculated by taking the difference in active channel area between 1988 and 2019.

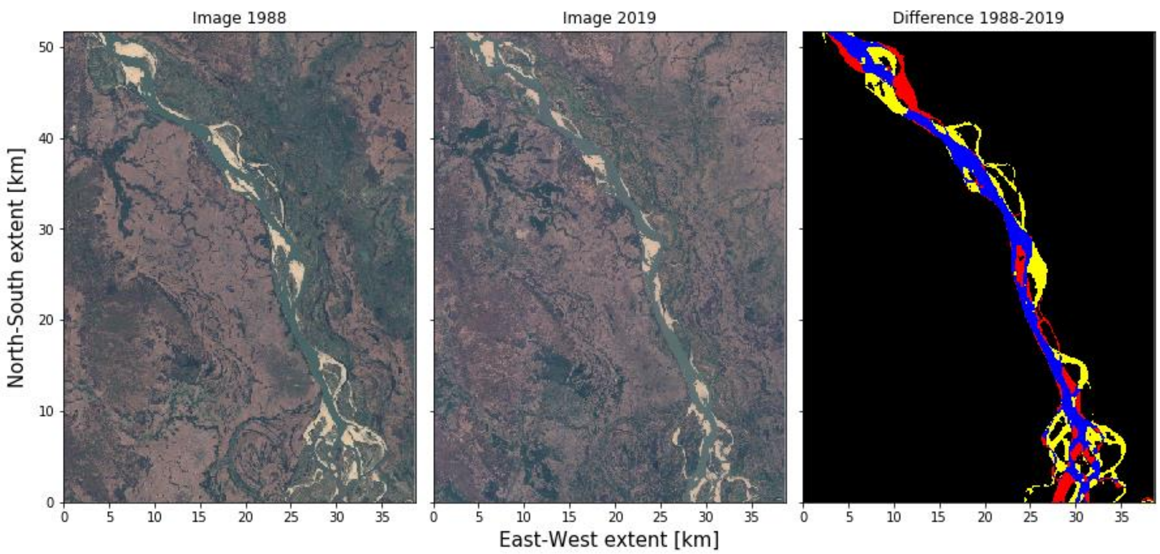

Figure 44: Change in active channel area visualized in the region with the largest reduction in active channel area (polygon 8-10)

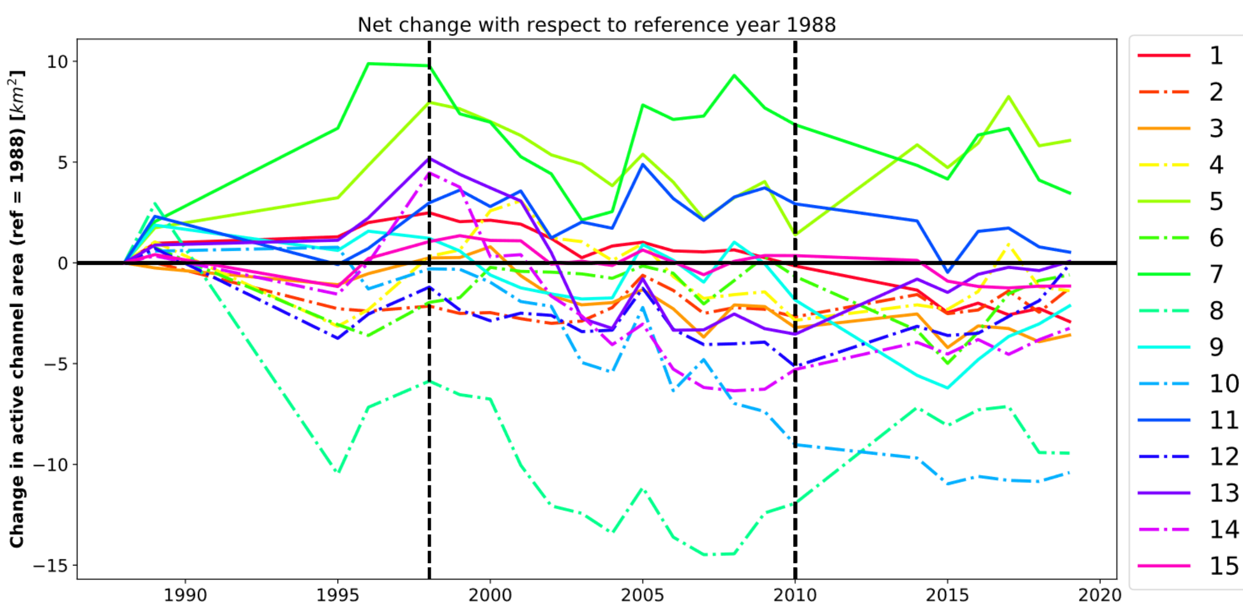

Figure 45: The change in active channel area with respect to the reference year of 1988 in the 15 different river sections. In Figure 40 the active channel area is plotted over the entire study area. The largest total reduction in active channel area is found between 1998 and 2010. This period is illustrated in this figure by the vertical dotted lines. Most polygons show a reduction in active channel area in this period.

4.3.3 The relation between the hydrologic regime and planform dynamics

The main reason for linking stage statistics with river morphodynamics is to detect key drivers of reach scale planform dynamics. Therefore, the planform dynamics measured over the entire study area are used. The statistics of erosion, deposition, migration and change in active channel area (see Figure 36-Figure 39) are averaged over the samples. This gives a single value of these metrics for each year, which can be linked to the hydrodynamic conditions.

The relation between the different channel stage statistics and measured morphodynamic changes in the same year is given in Table 7. The calculation of the water level statistics is described more elaborately in section 3.6. Generally, it becomes clear that there is a strong relation between the channel stage statistics and planform changes. Besides, almost all relations, except for some related to deposition, are statistically different from zero based on a two-tailed t-test ($\alpha = 0.05$, see Appendix E for calculations). The highest correlations are generally found for the average intensity over a 4-month period, which can be seen as a description of the average flood season intensity. The relation between the maximum 4-month average stage to the different planform change metrics is illustrated in Figure 46.

Erosion and the stage statistics show the strongest relations. This can be easily interpreted as more intense hydrodynamics favours erosion of floodplains. On the other hand, deposition shows the weakest relations. Deposition is measured by an advance in the vegetation boundary, which is thus less straightforward to interpret. The relation between deposition and stage is negative and is weaker. The highest correlation is found for the 30-day average (see Table 7), which suggests that especially the absence of relatively intense floods might be beneficial for vegetation development. The negative relation can be explained. Even though in years with intense flood seasons the sediment transport and the amount of deposition of sediment are large, vegetation can generally form when hydrodynamic conditions allow it. This process is further illustrated by the fact that only during years with low average flood season intensity the active channel area decreases (see Figure 46), and thus vegetation can develop. A weaker relation can be explained as vegetation development is likely to be influenced by other factors, besides hydrodynamic conditions in the river.

Despite the relative weak relation between deposition and the different stage statistics, both migration and change in active channel area have relatively strong relations with the hydrodynamic conditions. Intuitively, years with more intense flood seasons show more migration. Furthermore, for a low average intensity in the flood season, the active channel area decreases. On the other hand, for high average intensities of flood seasons the active channel area increases.

Table 7: Correlation (r) between the different channel stage statistics and metrics. The cells that are marked green are statistically different from zero ($\alpha = 0.05$).

	Max 7-day average	Max 30-day average	Max 4 month average	Max 6 month average	Average over year
Erosion	0.69	0.74	0.89	0.85	0.77
Deposition	-0.44	-0.48	-0.43	-0.36	-0.27
Migration	0.68	0.65	0.83	0.81	0.79
Channel area	0.64	0.69	0.76	0.70	0.62

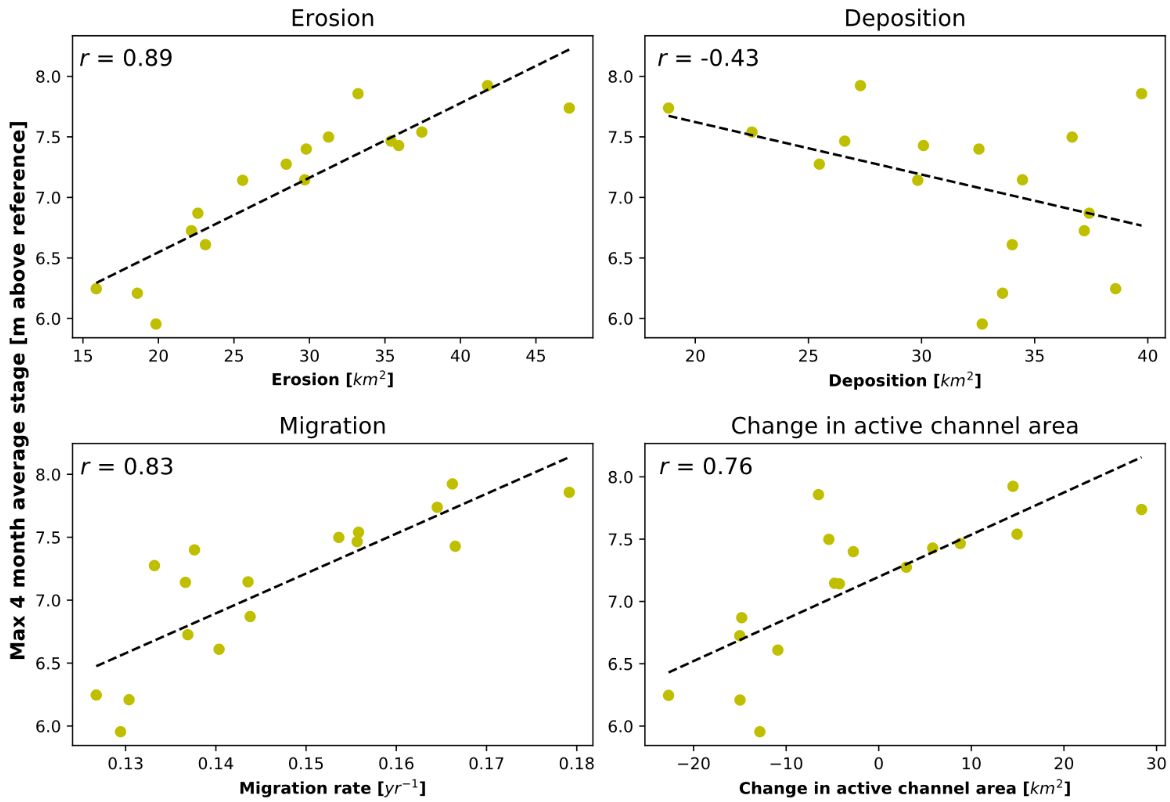

Figure 46: Relation between 4-month average water level, or average flood season intensity, and planform changes measured with detection method 1. Note that the values in the plot are the average values over the samples in Figure 36-Figure 39.

4.3.4 Reducing trend in the active channel area and its relation to the hydrologic regime

The active channel area at bankfull stage reduced over the period of 1988-2019, which was visible over almost the entire river length (see Figure 40, Figure 43). Thus, in total more accretion than erosion is measured between 1988 and 2019. Reach scale changes in planform geometry are often related to changes in the discharge and sediment regime (Xia et al., 2014). Due to the unavailability of data on the sediment regime, there is mostly focussed on data on the hydrologic regime.

From studying the planform dynamics on a yearly time scale a strong relation was found between the average intensity of the flood seasons and the change in active channel area (see Figure 46). A likely reason for the reduction in active channel area is thus related to long term changes in the average flood season intensity. Furthermore, from studying the change in active channel area on a yearly time scale, it becomes clear that an increase in channel area is mostly only occurring during single years, whilst a reduction in channel area takes place over multi-year periods (see Figure 39). Due to this periodicity over multiple years, the measured active channel area is likely a function of the flood season intensity over multiple past years. To consider the flood season intensity of past years, a multi-year moving average is taken. An example of a multiyear moving average is given in Figure 47. The yearly average flood season intensity strongly varies over time, but the 5-year moving average shows a clear trend. Especially during the period of 1998-2010 the 5-year moving average shows a downward trend. This period also shows the largest reduction in the active channel area (see Figure 40).

If the 5-year average flood season intensity is then plotted against the measured active channel area, the relation is further illustrated (see Figure 48). Multiple periods (1-8 years) were considered, but the largest correlation was found between the active channel area and the average flood season intensity over the 5 previous years (r=0.76). The samples of the 5-year average flood season intensity and the active channel area are not independent samples over time, which makes it hard to statistically prove the relation. Nevertheless, a plausible reason for the reduction in active channel area seems to be the relatively calm period from 1998-2010 characterised by a low 5-year average flood season intensity. This reduction in channel area is not yet compensated by the relatively intense period from 2010 onwards.

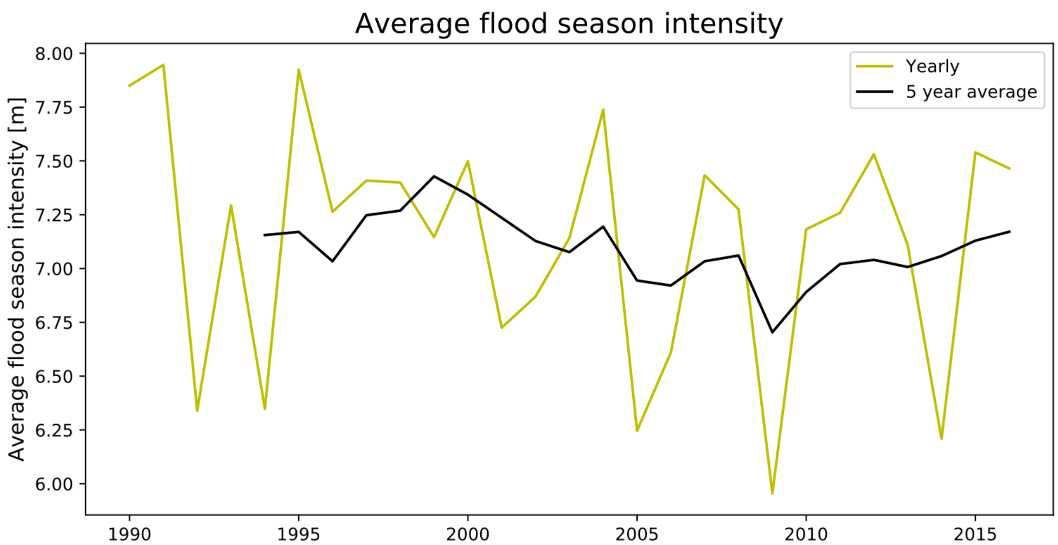

Figure 47: Yearly average flood season intensity and the 5-year moving average. The average flood season intensity is defined as the maximum for 4-month average water level (see section 3.6 for a description).

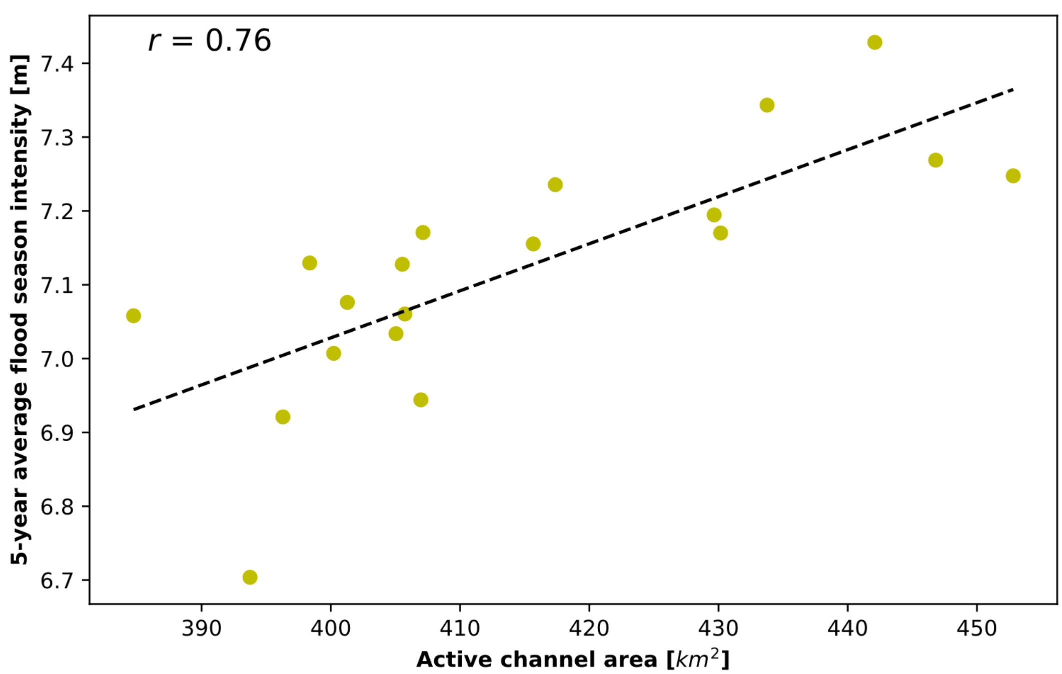

Figure 48: The 5-year average flood season intensity plotted against the active channel area for overlapping data points. It becomes clear that the active channel area is strongly related to the flood season intensities measured over the previous 5 years. The flood season intensity is defined as the maximum for 4-month average water level (see section 3.6 for a description).

4.4 QUANTIFICATION OF LOW STAGE CHANNEL DYNAMICS (CLASSIFICATION METHOD 2)

For the quantification of low stage channel dynamics water level measurements are used. This makes sure that in the used satellite images similar water levels are measured. The water level measurements showed poor spatial correlation and only limited measurement locations are available (see section 3.4.1). Therefore, there was only looked into differences over time, as the investigation of spatial differences is highly uncertain. After this the relation between the measured planform dynamics and the hydrologic regime is discussed.

4.4.1 Differences over time

Some clear differences over time become clear in the morphodynamic metrics (see Figure 49- Figure 53). The red numbers show the number of samples the metric is based on. Note that the samples differ from those in Table 5, which shows the total number of possible samples. Due to limitations in useable memory in Google Earth Engine only a limited number of runs were performed, which means sometimes the number of samples is lower than the maximum achievable samples mentioned in Table 5. Furthermore, the large uncertainty ranges for 2003 are caused by a large variety of water levels that were present in the samples.

In contrast to bankfull channel dynamics that were studied in section 4.3 both erosion and deposition behave comparably. Years with large amounts of measured erosion, also show large amounts of deposition. This can be explained by the different detection method. Comparing the low stage channel over time allows to track the deposition of sediment more directly. Compared to the bankfull channel detection method discussed in the previous section the development of vegetation is not a requirement for the detection of deposition. In terms of sediment balances, this can easily be explained, as erosion of sediment generally leads to deposition of sediment in the same year. This is especially the case if reach scales are investigated as local sediment imbalances do not have a large impact.

This also means that years with large migration rates are when both the measured erosion and deposition are large. The migration rates vary considerably over time. Furthermore, migration rates are much larger compared to those found by the method discussed in the previous section, with an average migration rate of 0.33 yr^{-1}, meaning that on average 33 percent of the low stage channel migrates each year. This is likely caused by the inclusion of sediment bar dynamics within this detection method, next to bankline change. The small ranges in the boxplot of migration rates are explained by the fact that the main uncertainty in this method is caused by the differences in water levels. A higher water level means more measured erosion and less measured deposition and the other way around. Thus, in the migration rate metric the uncertainty in deposition and erosion is partly compensated.

Due to the relatively large uncertainty, and the limited samples it is hard to derive any conclusions regarding trends in the active channel area. An interesting aspect is that both the total active channel area at bankfull stage and total active area at the low stage have reduced over the period of 1999-2003 (see Figure 40 & Figure 53).

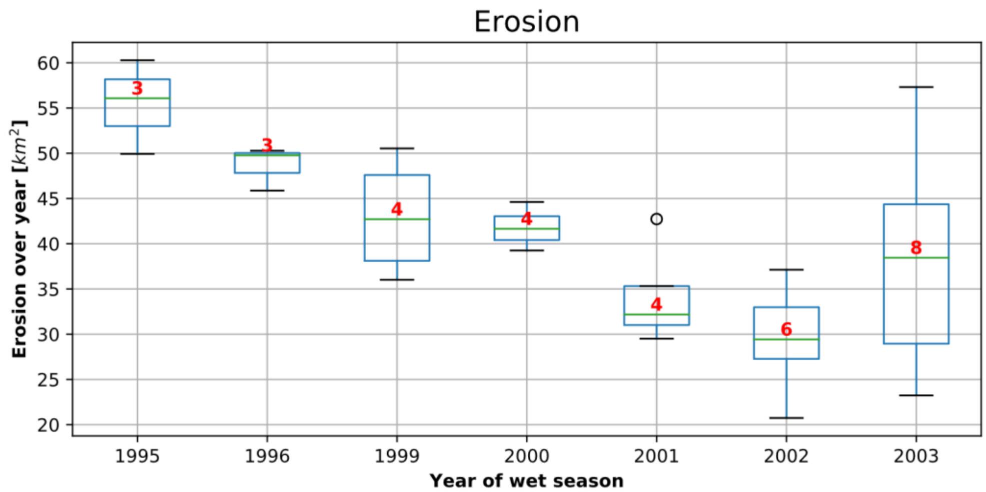

Figure 49: Boxplot of the erosion measured over the entire study area. The red numbers indicate the number of samples.

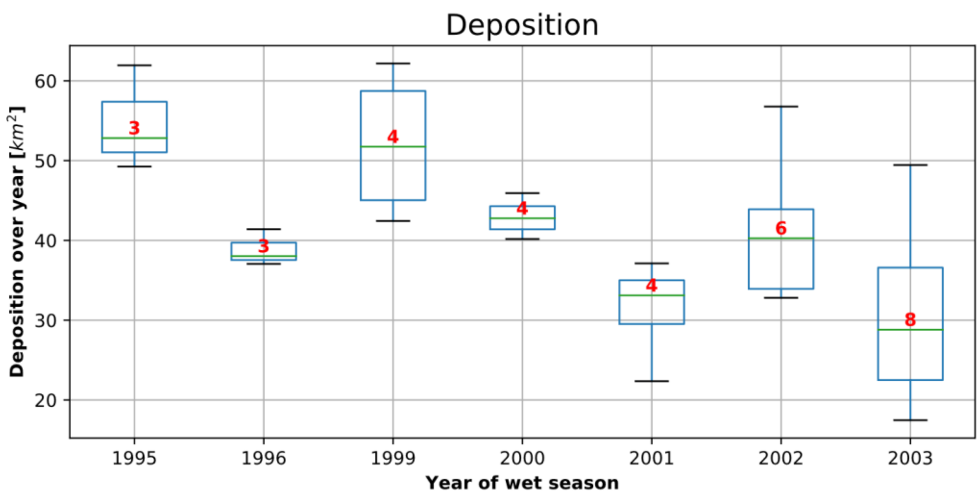

Figure 50: Boxplot of the deposition measured over the entire study area. The red numbers indicate the number of samples

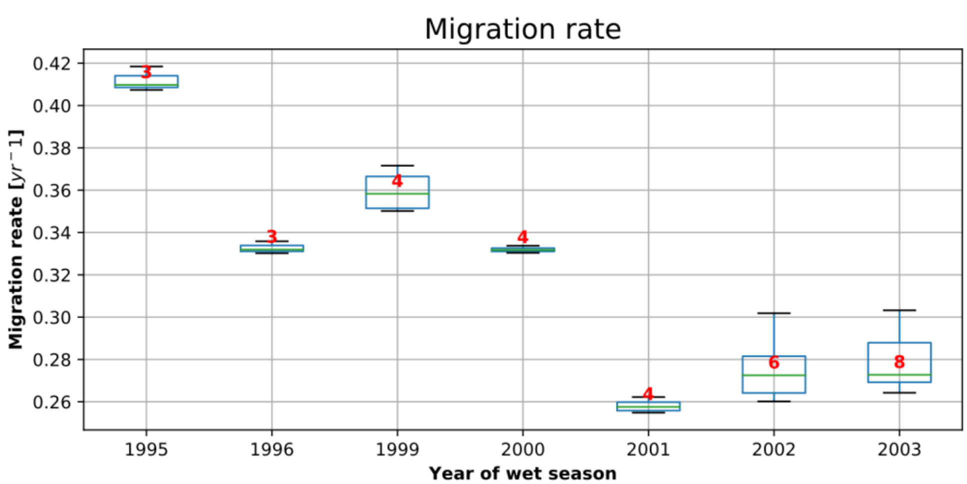

Figure 51: Boxplot of the migration rate measured over the entire study area. The red numbers indicate the number of samples

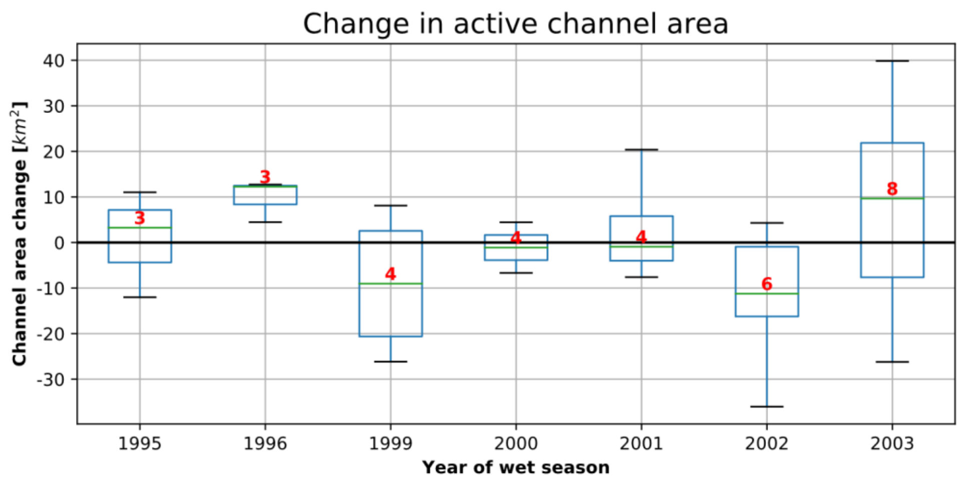

Figure 52: Boxplot of the change in active channel area measured over the entire study area. This is the net difference between erosion and deposition. The red numbers indicate the number of samples.

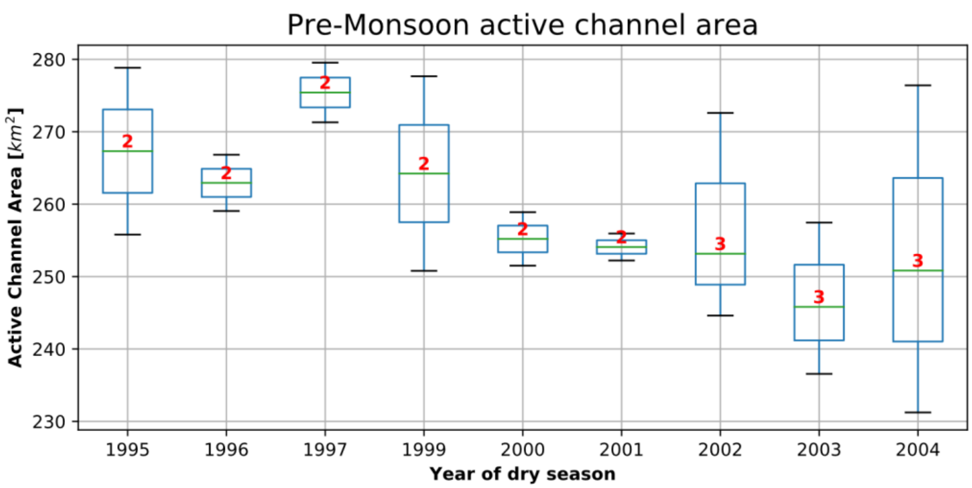

Figure 53: The pre-monsoon channel area. As the active channel area is measured by images from a single year, as opposed to measuring changes where the combination of two years are used, the samples differ from Figure 49 to Figure 52. The relation between Figure 52 and this figure is that Figure 52 shows that over the year 1996 the channel area expanded, which is measured in this figure in the dry season of 1997.

4.4.2 The relation between planform dynamics and the hydrologic regime

Again, relatively strong relations are found between the stage statistics and the planform change metrics (see Table 8, Figure 54). However, as only limited samples were available due to the additional criterium of the water level, only some of the relations of erosion and migration are statistically proven to be different from zero (see Table 8). The calculations of the t-test are given in Appendix E.

Especially migration and erosion of the low stage channel show strong relations with the stage statistics. Mainly the maximum 4-month average water level shows strong relations indicating that again the average flood season intensity is strongly influencing the intensity of both migration and erosion of the low stage channels.

The relations between stage statistics and deposition are not statistically different from zero Nevertheless, the direction of the relation hints towards an interesting dynamic. Oppositely to the method discussed in the previous section, a positive relation is found between deposition and the average intensity of the flood season, meaning that in years with a larger average flood season intensity more deposition is found. The use of a different method detection explains this. The deposition of bars can be measured directly without the need for the development of vegetation. Thus, the eroded sediment during the flood season that is deposited during the same year can be detected, which explains a positive relation.

The change in active channel area shows relatively weak relations with the hydrodynamic conditions. Besides, no clear positive or negative relations are found. The relatively large uncertainty range that is found for change in active channel area (see Figure 53) likely explains the weak relations that are found. This prevents to draw any meaningful conclusions regarding the relation between channel area change and the hydrologic regime.

Table 8: Relation between metrics of method 2 with stage statistics. The cells that are marked green are statistically different from zero ($\alpha = 0.05$).

	Max 7-day	Max 30-day	Max 4-month	Max 6-month	Average over year
Erosion	0.47	0.46	0.87	0.77	0.71
Deposition	0.53	0.57	0.66	0.64	0.42
Migration	0.53	0.56	0.88	0.81	0.65
Channel area	-0.10	-0.16	0.18	0.09	0.28

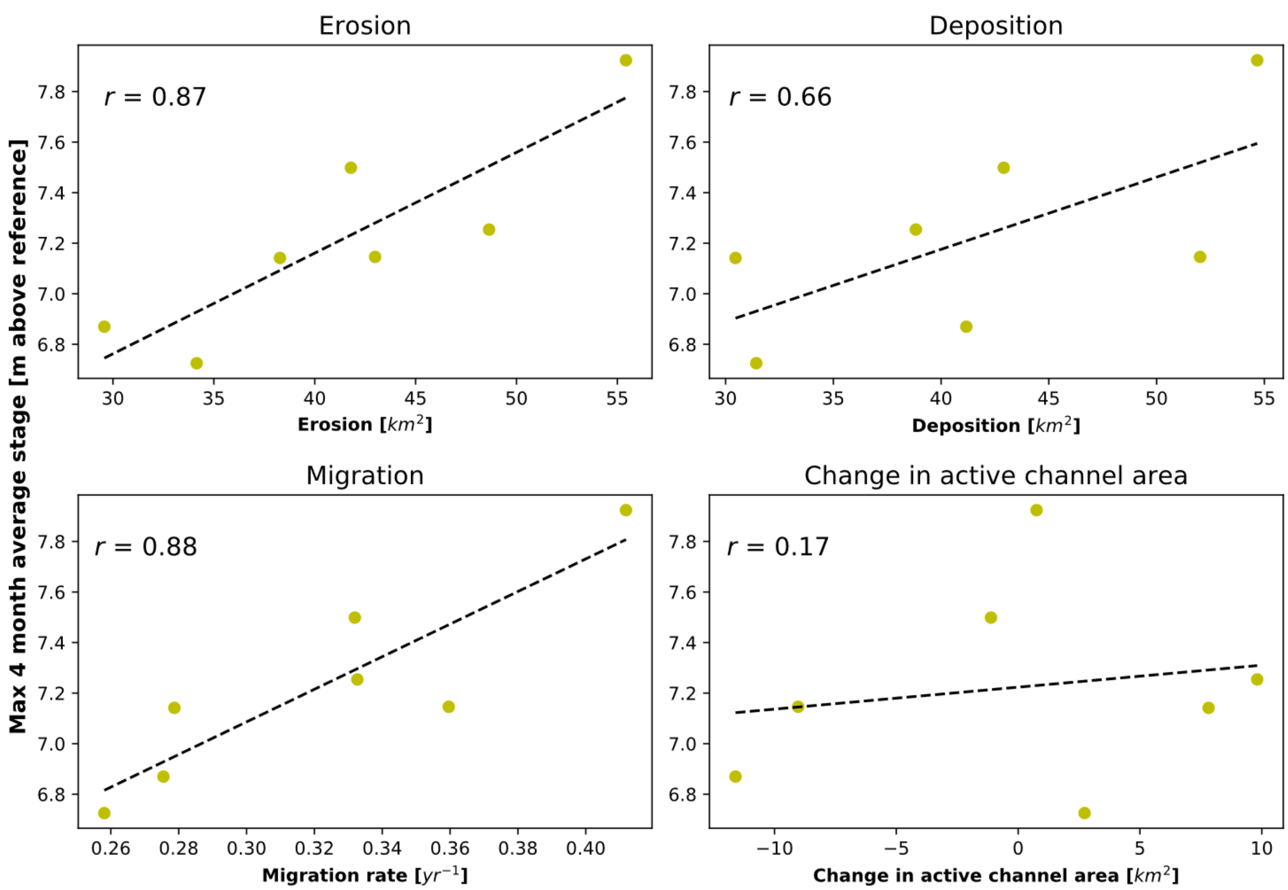

Figure 54: Relation between 4-month average water level, or average flood season intensity, and planform changes measured with detection method 2.

4.5 Differences between method 1 and 2

There exist fundamental differences between the dynamics that are measured with both detection methods. In method 1 the banklines represented by the vegetation boundary are detected. The dynamics that are involved measure the erosion and accretion of vegetated floodplains. The second method detects changes of the low stage channel. The measurements include erosion and deposition of sediment bars. The different dynamics especially become clear in the measurements of deposition/accretion. Method 1 measures floodplain accretion, which is dependent on the growth of vegetation. A negative relation is found between the intensity of the flood season and the measured accretion, indicating that less accretion is measured for more intense flood seasons (see Figure 46). On the other hand, in method 2 a positive relation is found (see Figure 54). Method 2 also includes deposition of bars that are exposed from the water surface. This can be measured independent of vegetation growth. For more intense flood seasons, more deposition is found (see Figure 54).

The ability to compare the results of both methods is thus somewhat limited. Nevertheless, for both methods, the measurements of erosion involve similar dynamics. Increased flow intensity generally leads to more erosion, which is independent of the measurement of erosion of floodplains or sediment bars. Not surprisingly, the measured eroded areas are fairly similar (see left tile of Figure 55). In method 2 consistently more erosion is measured, which is likely related to the fact that bar surfaces erode easier than vegetated surfaces. Nevertheless, the measurements of erosion between both methods clearly covary. The other metrics that are derived, such as change in active channel area and migration rate also depend on the measurements of deposition (see section 3.6 for the definition). As the measurements of deposition of the two detection methods involve different dynamics, these metrics are more difficult to compare. Nevertheless, the measurements of the migration rate in both methods show some covariance. In years with small migration rates measured with detection method 1, also a relatively small migration rates are measured for detection method 2(see right tile of Figure 55). However, due to the inclusion of bar dynamics the migration rates measured with method 2 are much larger than with method 1.

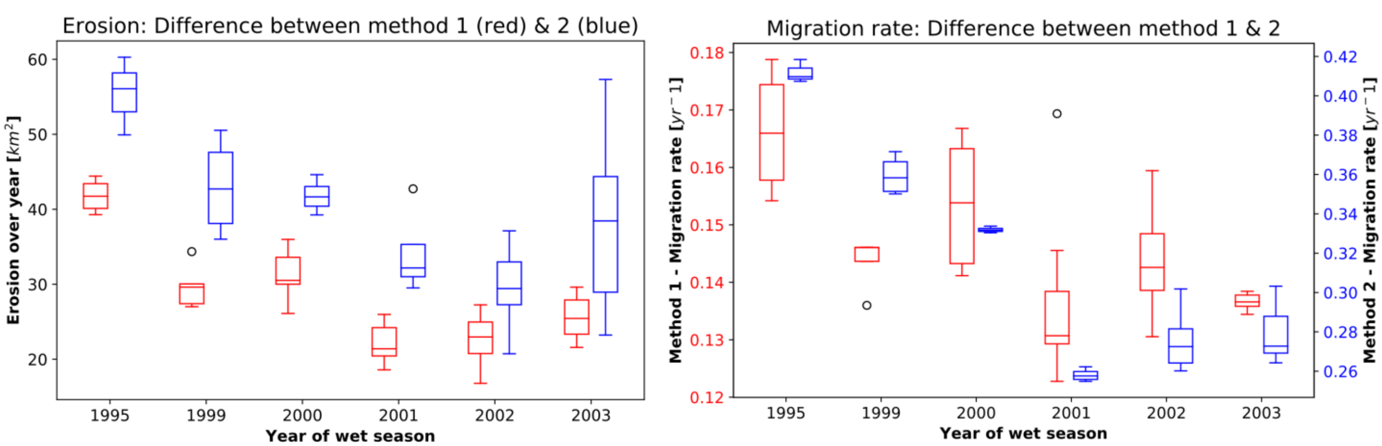

Figure 55: Differences between method 1 (bankfull channel) and method 2 (low stage channel). The left tile gives the differences for the erosion metric and the right tile the difference for the migration rate. Note that for the migration rate the magnitude strongly differs between both methods, which required the use of two different y-axis.

4.6 UNCERTAINTY IN THE QUANTIFICATION OF PLANFORM DYNAMICS

The developed method is able to generate uncertainty ranges by classifying multiple images in each dry season, which allows to detect planform changes between multiple images. The uncertainty ranges mainly show the performance and consistency of the detection method. It does not necessarily give the error of the detection. The error of detection is hard to quantify because, first of all, the absolute definition of a bankline is not straightforward. Secondly, there is no reliable alternative way to estimate bankline locations on a large scale. Therefore, the measurements are hard to validate. However, the uncertainty ranges allow to achieve insight into the main difficulties in detection. As two methods were applied to detect the river surface, they will be treated differently.

4.6.1 Uncertainty in automated detection of method 1

For method 1, the metrics erosion, deposition, migration and active channel area change show considerable uncertainty ranges (see Figure 36 to Figure 40). Nevertheless, due to the large yearly variability in the metrics, clear differences over time can be spotted without the uncertainty ranges overlapping. Going into more detail in the uncertainty of the individual metrics two important details become clear. First of all, the measurements of erosion show relatively small uncertainty ranges. This can be explained by the fact that erosion of the vegetation boundary is easy to detect as it gives fresh deposits. Fresh deposits can be easily detected with the SWIR band, due to strongly different reflection properties from the surroundings. Furthermore, erosion of the vegetation boundary is not common in the dry seasons. Therefore, no erosion of the bank line will be detected over the dry season period in which images are selected. On the other hand, the largest uncertainty is found in the measurement of deposition. Distinguishing old deposits from the initial stages of vegetation development is complicated due to relatively similar reflective properties. This makes it difficult to distinguish a clear vegetation boundary, which can locally lead to poor performance in detection. This results in a relatively large uncertainty in the measurements of deposition, as these measurements depend on the ability to distinguish new vegetation development from sediment bars. Furthermore, vegetation can develop during the dry season and the vegetation boundary can therefore change. As multiple images are selected in each dry season, this increases the uncertainty.

4.6.2 Uncertainty of detection method 2

For method 2 the uncertainty ranges were relatively large. Due to the relative simplicity of the detection of surface water, the detection method itself was found to have little influence on the uncertainty. The largest influence was found to be the stage, which is illustrated in Figure 56. In this figure, the active surface area is plotted against the measured water levels for the years 2002 and 2003. The figure shows that, even though a small range in the water level measurements is present (<1 m), the measured surface area is strongly influenced by the stage. The uncertainty in the measurements of the active surface area is thus strongly linked to the river stage and its variability. The measurements of erosion and deposition are derived by detecting the differences in the planform between 2002 and 2003. However, they also strongly depend on the measured water surface extent, which explains the uncertainty in these measurements. An example can be given to illustrate this. The surface water extent can be larger in 2003 than in 2002, due to a higher water level measured in 2003. In this case, erosion will be measured in 2003, whilst in reality, the higher stage caused part of the changes in the planform. For deposition the opposite is true, and less deposition will be measured due to the effect of the higher measured stage. To conclude, even though the stages were considered and only a limited range was used, it still had a considerable impact on the uncertainty.

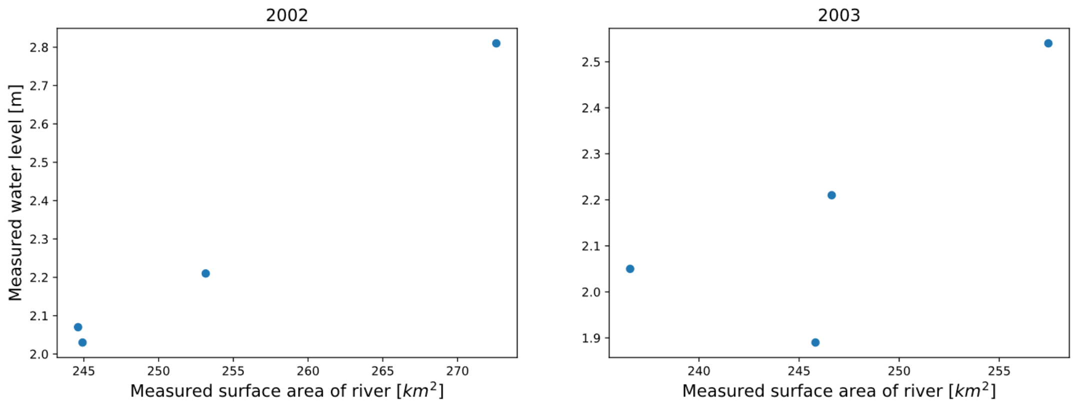

Figure 56: Relation between measured water levels in Zalun (see Figure 18) and surface area. Even though the measured water levels have a small range, the measured surface area strongly varies and clearly depends on the measured stage. Note that for the other locations that were used to select images with similar water levels(see Figure 18) similar relations were found between the measured surface area and the measured water level.

4.7 CONCLUDING REMARKS

This chapter started with listing the relevant characteristics of the river planform. Most of the river length is characterised by relatively stable vegetated islands, which means an anabranching planform seems fitting. Furthermore, the Ayeyarwady river has a strongly seasonally varying discharge and is characterised by a low slope and a wide floodplain, which fits in the description of anabranching planforms.

From visually inspecting the river planform changes, it became clear that significant differences in the characteristics of the planform dynamics are present in the studied river section. Whilst in the northern section lateral migration is limited, it is relatively large in the southern section. Furthermore, the middle section is characterised by intense planform changes, including the formation and abandonment of multiple channels. Regarding the dominating planform dynamics of anabranching planforms, both avulsion and stabilisation of deposits are named as drivers of anabranching planforms (see Chapter 2.1). Both are found in the lower Ayeyarwady river, but stabilisation of deposits seems to be more common.

From the quantification of planform changes, it became clear that there are large differences over time in the metrics of erosion, deposition, migration and change in active channel area. Some years show considerably more change than others. From investigating the differences over space, this pattern was visible over the entire studied river length. Linking the quantified planform dynamics with stage statistics revealed important drivers. The yearly variation of average flood season intensity is a key driver of planform changes in the Ayeyarwady river. This relation is visible for both detection methods, so both bankfull channel changes and low stage channel changes can be linked to the average flood season intensity. Although peak water levels were also found to be related to the measured intensity of the planform dynamics, its relation was much weaker. From studying the trends in the total active channel area, which is used as an expression for the river geometry, an interesting pattern revealed. The active channel area expands during intense average flood seasons, which is followed by multiple years of reduction of the channel area. Furthermore, a relation was revealed where the geometry of the river (total active channel area) is a function of the flood season intensity over the previous 5 years.

Finally, the uncertainty in both detection methods was discussed. In method 1 the uncertainty was found to be the largest for measuring deposition, which is related to difficulties in distinguishing a vegetation boundary. For the second method, the uncertainty was found to be caused by water level differences, rather than uncertainty in the classification of satellite images.

5 DISCUSSION

The discussion is divided into three different parts. The first section discusses the developed methods to detect planform dynamics. The second section discusses the result of the case study and compares the results with other studies. The final section describes both the potential and the general applicability of the developed methods.

5.1 THE DEVELOPED METHOD TO DETECT AND QUANTIFY RIVER CHANGE

To detect planform changes two detection methods were applied. The first method detects the movement of the vegetation boundary, which is assumed to be the river bankline at bankfull stage. It uses relatively simple detection algorithms that combine a water index (NDWI) and the Short-Wave Infrared band. This method can consistently derive channel banklines without the interference of changing water levels. The main assumption behind this method is that the active channel experiences flow and sediment transport which inhibits the growth of vegetation. Although this assumption is very common to extract bankfull channel extents (e.g. Monegaglia et al. 2018; Rowland et al., 2016; Schwenk et al., 2017), it also requires careful consideration. Independent of the detection method that is used, a general downside of the assumption is that there is a dependency on vegetation growth to extract the river banklines. Some areas might not be part of the active channel anymore but are not yet vegetated. This can, for example, occur when the growth rate of vegetation is low. Vegetation growth is thus not necessarily related to areas where deposition or accretion is measured. Besides, there are some limits that are specific to the used detection method in this study. The SWIR band to detect sediment bars was found to be sensitive to misdetections. Especially when the surroundings of the river consist of barren soil, which often occurred late in the dry seasons, or when foggy conditions were present. From the application in the case study, this sensitivity became clear in the large uncertainty ranges in the measurement of deposition. An improvement in the ability to distinguish sediment bars from its surroundings could be the next step to reduce uncertainty in the detection algorithm.

The second method that was applied is selecting images with a similar water level. A large benefit of applying this method is that also dynamics of unvegetated bars are included in the analysis. From applying the method in the case study of the multithreaded Ayeyarwady river several aspects became clear. First of all, the multichannel planform of the Ayeyarwady river, with many bars and low gradient banklines, resulted in a large effect of the water level on the quantification of planform dynamics. This necessitated a strict water level criterium, which reduced the number of samples significantly. Furthermore, even with limiting the water level still a relatively large uncertainty was found in the quantification of planform dynamics. Nevertheless, applying the method in the case study revealed that deposition can be measured more directly. This resulted in a relatively strong positive relation between deposition and the hydrodynamic intensity, which is more in line with actual transport conditions.

If both detection methods are compared, both have their advantages and disadvantages. For resolving the deposition of sediment bars, the second method was found to be more relevant (using images with similar water levels). However, it is difficult to limit the effect of the water level on the analysis of planform dynamics as was shown by the case study. This reduced the potential of the method severely. The vegetation boundary method showed that it can independently and consistently derive planform dynamics. Besides, a relatively large number of samples were available, and due to the independence on water levels, also differences over the spatial domain could be investigated. The deposition metric is less relevant, and also includes vegetation dynamics. This changes the found relationships. Nevertheless, the method allowed to study planform changes extensively for the Ayeyarwady river and find interesting patterns over time.

5.2 THE RESULTS OF THE CASE STUDY

From the quantification of planform changes with satellite images, it became clear that there are large differences over time in the metrics of erosion, deposition, migration and change in active channel area. The yearly variation of average flood season intensity was found to be a key driver of the measured planform changes in the Ayeyarwady river. Studying planform changes also revealed a pattern with single years of net erosion followed by multiple years of net accretion that was visible in most of the studied period of 1988-2019.

A direct comparison of the obtained results of the Ayeyarwady river to most other studies that used remote sensing for studying planform dynamics is not possible. This is due to the fact that a wide range of metrics are studied in literature that are not necessarily comparable (Rowland, et al., 2016). Besides, most studies do not use a yearly time scale (Schwenk et al., 2017). Nevertheless, Schwenk et al. (2017) used similar detection methods of Landsat imagery for the meandering Uyalci river. They investigated a 1500 km reach by detecting the vegetation boundary on a yearly time scale. Due to the focus on a meandering river, most metrics are different from the ones used in this study. Nevertheless, a metric that can be compared is the change in active channel area, or the net difference between erosion and accretion of the floodplain, which is measured the same in both studies. Schwenk et al. (2017) found for the meandering Uyalci river that there was generally a two-year cycle between net erosion and net deposition. For the Ayeyarwady river, generally, a pattern is found with a single year of net erosion of the floodplain, which is followed by a couple of years of net accretion. The different behaviour of the Ayeyarwady river suggests the relative importance of single years with extreme flood seasons on net erosion. Lastly, Schwenk et al. (2017) suggested that the annual flood persistence might be partially responsible for the river's width. A similar relationship was found for the Ayeyarwady river. In this study, the geometry was expressed by the active channel area to account for the complexity of the river planform. Nevertheless, the active channel area at bankfull stage also partly represents the channel's width. A strong relationship was found between the active channel area and the 5-year moving average of the average flood season intensity. This indicates that the river geometry is a function of the flood season intensity of multiple years in the past. Another study that found a similar relationship is performed by Xia et al. (2014). They studied the average river width for a partly braided reach of the Lower Yellow River (China). The river width was found to strongly related to the 4-year moving average of the average flood season discharge.

By generating an improved understanding of the planform dynamics this study also gave some insights on drivers of the anabranching channel pattern of the Ayeyarwady river. Specific to the formation of anabranching planforms, two distinct planform dynamics are mentioned. The first planform dynamic is avulsion and the second is the formation of islands by accretion (Nanson & Knighton, 1996). In both cases, the hydrologic regime is believed to be an important driver. Avulsions are often related to extreme flood conditions (Wang, et al., 2019). For accretion dominated anabranching planforms, the yearly variability in flood discharge is believed to be an important driver, as mid-channel deposits can stabilize during years with lower hydrodynamic intensity (Nicholas et al., 2013). From visual inspection of the planform dynamics, generally, the more accretion-based process seems fitting for the Ayeyarwady river. This is also partly reinforced by the quantification of planform dynamics. The quantification of planform dynamics tracked general planform changes and did not separately track individual mechanics such as avulsion or accretion. Nevertheless, linking the stage statistics with the measured planform changes revealed that the average flood season intensity is strongly related to the measured intensity of the planform dynamics. This indicates that for significant planform changes to occur extreme floods are not required, which would be expected in avulsion dominated anabranching rivers. Furthermore, the importance of flood season variability for the stabilisation of deposits by vegetation was also found in the case study. This dynamic was found by using the method that detects a vegetation boundary. Using this method, a reduction of the active channel area indicates vegetation growth in areas that were a part of the active channel. An interesting pattern revealed, where intense flood seasons show large increases in active channel area, followed by multiple years of reduction of the active channel area. This does not directly represent the stabilisation of bars to islands, as all deposits are included in the metrics. However, it hints in the direction that the yearly variability in flood season intensity might be a key reason for the ability of bars to bars to stabilise to islands. Future improvements in the change detection algorithm to automatically tracks specific dynamics such as avulsion and island formation, might provide additional insights into the drivers of anabranching planforms.

5.3 THE POTENTIAL AND GENERAL APPLICABILITY OF THE DEVELOPED METHODS

In this study, a method was developed to automatically detect and quantify changes of multithreaded river planforms. All of the steps from the filtering of imagery, automated detection of the river channel, and finally change analysis are performed in a single Python script combined with the Earth Engine Python API. The automated detection technique can deal with the complex geometry of a multithreaded planform, which allowed to study planform dynamics on a large spatial scale. At the same time, the automated detection technique allowed the usage of a relatively high temporal resolution with yearly intervals. An additional benefit of the low processing time of the automated detection technique is that it allowed to classify multiple images for each dry season. This created the ability to generate uncertainty ranges, which directly gives insights into the performance and consistency of the detection technique. The usage of automated change detection techniques showed its potential in the case study. The combination of a large spatial scale and relatively small yearly time intervals have proven to be key in the ability to characterise planform dynamics. The case study showed that the yearly time scale gave insights into the effect of flood seasons and their different intensities. This explained the large variability in planform change intensities. Furthermore, the case study showed that manual cleaning of the imagery is not required to be able to characterise planform dynamics, which also reduces the processing time. Although it was not specifically tested in this study, the small processing time illustrates the potential to apply similar methods outside the case study, and on a global scale. This allows to further investigate drivers of planform dynamics for rivers globally.

However, there are several limitations of detecting planform dynamics with satellite images. A general limit of remote sensing studies to study planform changes is that it is difficult to represent the processes of erosion and deposition only based on horizontal changes. It only gives a first indication of volumes, and a real description of volumes would require the height of the cross-sections (Church, 2006). Another limit comes from the resolution of optical satellite imagery. Landsat imagery was used as it has a long-term availability of over 30 years. At the same time, it has a relatively low spatial resolution of 30 meters. This makes it mainly suitable for detecting rivers of at least a couple of pixels in width, which thus restricts the use of this type of imagery to large rivers (Monegaglia et al., 2018). A further complicating factor comes with change analysis. Generally, the ability to detect river planform changes with satellite imagery depends on the rate of channel change, the resolution of the imagery, the time interval between images and the uncertainty in detection (Rowland et al. 2016). In the case study, the yearly time scale has proven to be key in characterising planform dynamics. The applicability of yearly time intervals, however, is still limited to rivers that are dynamic. To detect planform changes, generally, the measured yearly horizontal changes should be more than a pixel size (30 m). Preferably, even large changes are measured to account for uncertainty in detection. On the other hand, with improvements in the detection techniques and with the introduction of higher resolution imagery such as Sentinel-2 in 2015 (10-20 meters (ESA, 2015)), the future possibilities to study long-term changes of smaller and less dynamic rivers are promising. Finally, a limit that is more specifically related to the used detection methods. The method that relies on detecting a vegetation boundary to detect the bankfull channel extent is limited to areas where vegetation growth is common and cannot be applied where vegetation is not present or sparse.

Despite the limitations, the methods showed that planform dynamics of a large dynamic river with a complex multithreaded river planform can be well characterised with satellite images combined with automated detection techniques. Actual occurring planform dynamics can be measured and quantified on a scale that is not achievable with alternative methods such as field studies. The automated detection and change analysis allowed to study planform dynamics on large spatial scales with a high temporal resolution. By quantitatively linking the measured planform dynamics, with commonly available data on the river stage, an improved understanding is generated of the drivers of planform dynamics. With expected future changes in the climate and ever-increasing human influences on the river, due to for example river dams, understanding the drivers of can be key to anticipate future changes.

6 CONCLUSION & RECOMMENDATIONS

This chapter gives the conclusions of this research by answering the research questions. Finally, recommendations for further research are given.

6.1 CONCLUSION

In what ways can satellite images combined with commonly available data assist to create a better understanding of planform dynamics and their controls in multithreaded rivers?

Planform dynamics or planform changes take place at different scales. On reach scales, changes in channel patterns or large-scale changes in channel geometry can occur. Large scale changes of the planform geometry are predominantly caused by changes in the discharge and sediment regime. These changes generally occur on time periods of multiple years to decades. Smaller scale planform dynamics in multithreaded rivers such as channel migration, avulsion and island formation take place at smaller time scales. An important time scale for these dynamics is the flood season. These smaller scale planform dynamics give rise to different channel patterns and geometries, which means understanding the conditions under which these dynamics occur, is key to characterise reach scale planform dynamics. Explaining local planform dynamics with satellite images combined with commonly available data is complicated, as detailed information about local geometry, flow, sediment transport and bank characteristics is required. Nevertheless, if these local dynamics are contextualised on a larger scale, such as a river reach, they can often be linked to the discharge regime. For example, both avulsions and the formation of islands are commonly linked to the yearly variability in the flood regime. Data on the discharge regime, such as water level measurements, are commonly available for most large rivers. To create a better understanding of planform dynamics with satellite images and commonly available data, these findings have important implications. To truly characterise and understand planform dynamics it is key that the time intervals are sufficiently small. Many of the dynamics that characterise multithreaded river planforms, such as avulsions and island formation, take place during a single flood season. To be able to capture these dynamics at least yearly time intervals should be used. At the same time, explaining these dynamics with commonly available data requires to contextualise these dynamics on a large spatial scale. Satellite images and other commonly available data thus show the most potential to assist in the understanding of planform dynamics by studying a large spatial scale on, preferably, yearly time intervals or smaller.

How can river planform dynamics be automatically detected and quantified with satellite imagery on a large scale for multithreaded rivers?

Different automated techniques can be used to detect river morphodynamics over time such as water indices, supervised and unsupervised classification. Independent of the used detection technique, a complicating factor in the analysis of river planform changes is that the water level affects the extent of the water surface. If planform changes are measured by detecting surface water, a similar water level must be present in the images that are used in the analysis. Alternatively, a common approach in literature to eliminate the effect of the water level is detecting a vegetation boundary. Thereby, there is assumed that it represents the bankfull stage boundary. To detect the vegetation boundary often bare sediment and the water surface are considered to be part of the active channel. To quantify river morphodynamics a wide variety of metrics can be derived, for which the distinction between multithreaded rivers and single-threaded (meandering) rivers is key. For meandering rivers, it is common to derive linear rates of change to express channel migration. For multithreaded rivers, these migration metrics do not represent all morphodynamics. For example, the entire channel band might not migrate, whilst within the channel planform morphodynamic change has occurred, such as the migration of bars and islands. A more inclusive approach is to detect the change of all the channel banklines individually, which can be achieved with mask differencing. Mask differencing allows to quantify areas of change that, for example, represent erosion or deposition.

Which planform dynamics and drivers of these dynamics can be identified in the lower Ayeyarwady river with automated classification on satellite imagery and other commonly available data?

Two detection methods were used that both quantified different changes. The first method that was used is tracking the vegetation boundary, which is assumed to be the bankfull channel boundary. Generally, a large variability over time was found for the lower Ayeyarwady river in the measured planform dynamics. The planform dynamics that were measured are erosion, deposition, migration and change in active channel area. Most measured yearly planform dynamics were found to be strongly related to the average flood season intensity. Also, a pattern was revealed of single years with intense changes, followed by multiple years with lower measured intensities of planform change. Furthermore, a similar pattern was found for the active channel area, where single years showed an increase of active channel area which is followed by multiple years of a reduction in active channel area. This revealed the important impact of the yearly variability in flood season intensity on the river geometry. From studying the spatial differences, it became clear that, generally, the entire studied river length of 250 km behaved comparably. Lastly, an interesting decreasing trend in active channel area was found over almost the entire study area. From visualising the planform change, it appeared that in some regions the planform changed to a more single-threaded planform at bankfull stage. A likely reason for the reduction in active channel area in 2019, compared to 1988, is the occurrence of relatively calm flood seasons during the period of 1998-2010, which favoured the abandonment of channels. The second method quantified the water surface change over time by selecting images with a similar water level. This method also allowed to quantify bar dynamics and generated a more accurate representation of deposition. Again, strong relations with the average flood season intensities were found. Also, deposition was found to increase for increased flood season intensities. However, due to the large uncertainty and limited samples that could be used due to an additional criterium of water levels, limited additional insights could be gained into planform dynamics using this method.

Main research question: ***How and to what extent can automated detection techniques with satellite imagery, combined with commonly available data, be used to characterise and explain planform dynamics for large multithreaded rivers?***

For automated detection of river planform dynamics, the varying water levels must be considered. Two methods were used to deal with varying water levels in the case study of the Ayeyarwady river. The first is deriving the bankfull channel extent by detecting the vegetation boundary. The second method is detecting the water surface, whilst using images in which a similar water level is measured. Using water level measurements to select images with similar water levels proved to be difficult in a multithreaded river planform, resulting in a large limitation of the number of samples. The largest potential was found in detecting a vegetation boundary. Using this method in the case study, planform dynamics expressed in metrics such as eroded areas, deposited areas and migration rates could reliably be determined, despite of the complex multithreaded river planform. Furthermore, due to the use of automated detection methods that have low processing times, planform dynamics could be investigated on a large spatial scale, whilst using relatively small yearly time intervals. Quantitatively linking the measured planform dynamics with water level data showed the potential of satellite images combined with commonly available data, to characterize and explain planform dynamics in the case study. The flood season intensity and its yearly variability, which were expressed by water level measurements, explained the varying planform change intensities to a large extent. Furthermore, the automated detection method allowed to spot a decreasing trend in the active channel area measured over the period of 1988-2019. The long-term trends could also be explained by investigating water level statistics. There are still some limitations in the applicability of similar automated detection methods to other rivers. The limitations are mainly caused by the limited spatial resolution of Landsat imagery, the uncertainty in detection methods and the dependency on vegetation growth to extract bankfull channel extent. Nevertheless, this study showed the large potential of automated detection techniques on satellite images combined with commonly available data to generate a further understanding of planform dynamics and their drivers in complex multithreaded river planforms. With increasing pressure on river systems due to climate change and human interventions such as river dams, understanding the controls of planform dynamics is key to successfully manage river dynamics in the future.

6.2 Recommendations

Finally, four recommendations for further research are given based on the findings of this study.

1. Applying similar methods to other cases

Although some initial exploring of the applicability of the methods outside the case study was done, no other case studies were performed. By applying a similar method to different anabranching rivers both materials for comparison are generated and a further understanding of the key drivers of anabranching planforms can be gained. Some interesting anabranching or multithreaded river planforms where similar methods can possibly be applied are: Orinocco river, Ganga river, Brahmaputra river, Rio Inambari and the Maronon river. All of these rivers are characterised by a large width and relatively intense planform changes. Therefore, the developed method in this study, that uses relatively low-resolution Landsat imagery, is likely applicable in these rivers.

2. Improving the current detection algorithm to detect the bankfull channel

In the method that extracts the bankfull channel, a vegetation boundary is detected. This method showed great potential in the case study. Part of the uncertainty in the quantification of planform dynamics was found to be related to the use of the SWIR band to detect sediment bars. In general, the SWIR band combined with a constant threshold was found to give reasonable results. Nevertheless, some difficulties were found in the ability to distinguish sediment bars in late dry seasons. Developing a method that can more reliably detect sediment bars would help to reduce the uncertainty in the developed method. Therefore, it will improve the overall performance in delineating bank lines.

3. Expanding the metrics to quantify planform dynamics

The channel change metrics that are currently derived are all area-based and do not distinguish the type of planform dynamic that is measured. Changes, such as avulsion, bar migration and channel abandonment were all included by quantifying the total change. However, the ability to study key drivers of planforms would be improved if more specific dynamics can be tracked. For example, anabranching rivers are often related to the stabilisation of mid-channel bars or avulsions. If these dynamics can be tracked on reach scales, more information can be gained on conditions in which they occur. This can potentially improve the understanding of drivers of anabranching channel patterns.

4. Resolving bar dynamics

In this study, two methods were applied to detect planform dynamics. One of those methods used water level measurements to select images where the river has a similar water level. By detecting change of the water surface also bar dynamics could be included. In the case study, this method showed the potential to more accurately represent deposition. However, it provided limited additional insights as the water level selection criteria that were required limited the number of available samples severely. Developing a method that can more reliably represent bar dynamics of complex multithreaded planforms is the final recommendation of this study. In many multithreaded river planforms, the formation of mid-channel bars is an important planform dynamic. The ability to track bar dynamics can provide valuable information on the conditions under which large bars form.

REFERENCES

Allen, G. H., & Pavelsky, T. M. (2018). Global extent of rivers and streams. *Science, 361*, 585-588.

Ashmore, P. (1991). How do gravel bed rivers braid? *Canadian Journal of Earth Sciences*(28), 326-341.

Ashraf, M., Bhatti, M. T., & Shakir, A. S. (2016). River bank erosion and channel evolution in sand-bed braided reach of River Chenab: role of floods during different flow regimes. *Arabian Journal of Geosciences*, 140.

Ashworth, P. J., Ferguson, R. I., & Powell, D. M. (1992). *Dynamics of gravel-bed rivers: Bedload transport and sorting in braided rivers .* Chichester.

Baki, A. B., & Gan, T. Y. (2012). Riverbank migration and island dynamics of the braided Jamuna River of the Ganges–Brahmaputra basin using multi-temporal Landsat image. *Quaternary international, 263*, 148-161.

Blom, A., Arkesteijn, L., Chavarrías, V., & Viparelli, E. (2017). The equilibrium alluvial river under variable flow and its channel-forming discharge. *Journal of Geophysical Research: Earth Surface, 122*, 1924-1948.

Brakenridge, G., Syvitski, J., Niebuhr, E., Overeema, I., Higgins, S., Kettner, A., & Prades, L. (2017). Design with nature: Causation and avoidance of catastrophic. *Earth-Science Reviews*, 81-109.

Carling, P., Jansen, J., & Meshkova, L. (2014). Multichannel rivers: their definition and classification. *EARTH SURFACE PROCESSES AND LANDFORMS, 39*, 26-37.

Church, M. (2006). Bed material transport and the morphology of alluvial river channels. *Annual Review of Earth and Planetary Sciences, 34*, 325-354.

Coghlan, M. (2014). Meandering river [Photograph]. Retrieved from https://commons.wikimedia.org/wiki/File:Meandering_River_(14237324394).jpg

Coleman, J. M. (1969). Brahmaputra River: Channel Processes and Sedimentation. *Sedimentary Geology, 3*, 129-239.

Crosato, A. (2008). *Analysis and modelling of river meandering (PhD Thesis).*

Cruciat, D. (2010). Tagliamento river from Aonedis to north [Photograph]. Retrieved from https://commons.wikimedia.org/wiki/File:Tagliamento_da_Aonedis.JPG

Donchyts, G. (2018). *Planetary-scale surface water detection from space (PhD Thesis).* TU Delft. doi:https://doi.org/10.4233/uuid:510bd39f-407d-4bb6-958e-dea363c5e2a8

Donchyts, G., Schellekens, J., Winsemius, H., Eisemann, E., & Giesen, N. V. (2016). A 30 m resolution surface water mask including estimation of positional and thematic differences using Landsat 8, SRTM and OpenStreetMap: A case study in the Murray-Darling Basin. *Remote Sensing, 8*, 386.

DRR. (2015). *DRR-Team Mission Report: Myanmar.*

Eaton, B., Millar, R. G., & Davidson, S. (2010). Channel patterns: Braided, anabranching, and single-thread. *Geomorphology, 120*, 353-364.

ESA. (2015). *Sentinel-2 Spatial Resotution*. Retrieved from Sentinel Online: https://sentinel.esa.int/web/sentinel/user-guides/sentinel-2-msi/resolutions/spatial

Ferguson, R. I. (1987). Hydraulics and sedimentary controls of channel pattern. In K. Richards, *River channels: environment and process* (pp. 129-158). Oxford: Basil Blackwell.

Ferguson, R. I. (1993). Understanding braiding processes in gravel-bed rivers: progress and unsolved problems. *Geological Society, 75*, 73-87.

Feyisa, G. L., Meilby, H., Fensholt, R., & Proud, S. R. (2014). Automated water extraction index: A new technique for surface water mapping using Landsat imagery. *Remote Sensing of Environment, 140*, 23-35. doi:https://doi.org/10.1016/j.rse.2013.08.029

Fisher, A., & Danahar, T. (2013). A water index for SPOT5 HRG satellite imagery, New South Wales, Australia, determined by linear discriminant analysis. *Remote Sensing, 5*, 5907-5925.

Fisher, A., Flood, N., & Danaher, T. (2016). Comparing Landsat water index methods for automated water classification in eastern Australia. *Remote Sensing, 175*, 167-182.

Fisher, G. B., Bookhagen, B., & Amos, C. B. (2013). Channel planform geometry and slopes from freely available high-spatial resolution imagery and DEM fusion: Implications for channel width scalings, erosion proxies, and fluvial signatures in tectonically active landscapes. *Geomorphology, 194*, 46-56.

Geological Survey of Canada. (2008). Braided river in Canada [Photograph]. Retrieved from https://commons.wikimedia.org/wiki/File:Barras_de_Canal.jpg

Google Earth. (2019, July 1). Myanmar. Retrieved from https://www.google.nl/maps/@19.0351334,96.3207503,560958m/data=!3m1!1e3

Gupta, N. (2012). *Channel Planform Dynamics of the Ganga-Padma System, India (PhD thesis).* University of Southampton.

Harmar, O. P., & Clifford, N. J. (2006). Planform dynamics of the Lower Mississippi River. *Earth Surface Processes and Landforms, 31*, 825-843.

Hossain, M. A., Gan, T. Y., & Baki, A. B. (2013). Assessing morphological changes of the Ganges River using satellite images. *Quaternary International, 304*, 142-155.

Huang, C., Chen, Y., Zhang, S., & Wu, J. (2018). Detecting, Extracting, and Monitoring Surface Water From Space Using Optical Sensors: A Review. *Reviews of Geophysics, 56*, 333-360.

Huang, D.-Y., & Wang, C.-H. (2009). Optimal multi-level thresholding using a two-stage Otsu optimization approach. *Pattern Recognition Letters, 30*(3), 275-284.

International Federation of Red Cross And Red Crescent Societies (IFRC). (2004). *Myanmar: Floods - Information Bulletin n° 1*. Retrieved from https://reliefweb.int/report/myanmar/myanmar-floods-information-bulletin-n-1-3

Ivars, B., & Venot, J.-P. (2019). Grounded and Global: Water Infrastructure Development and Policymaking in the Ayeyarwady Delta, Myanmar. *Water Alternatives, 12*(3), 1038-1063.

Jagers, H. R. (2003). *Modelling Planform Changes of Braided Rivers (PhD thesis).* University of Twente.

Jansen, P. P., Van Bendegom, L., Van den Berg, J., & De Vries, M. (1994). *Principles of River Engineering: The non-tidal alluvial river.* Delftse Uitgevers Maatschappij.

Klaassen, G., & Masselink, G. (1992). Planform changes of a braided river with fine sand as bed and bank material. *5th International Symposium on River Sedimentation*, 459-471.

Kleinhans, M. G. (2010). Sorting out river channel patterns. *Progress in Physical Geography, 34*, 287-326.

Kleinhans, M. G., & Van den Berg, J. H. (2011). River channel and bar patterns explained and predicted by an empirical and a physics-based method. *Earth Surface Processes and Landforms, 36*, 721-738.

Ko, K. K. (2016, September 29). Mandalay increases spending to counter riverbank erosion. *Myanmar Times*. Retrieved from https://www.mmtimes.com/national-news/mandalay-upper-myanmar/22787-mandalay-increases-spending-to-counter-riverbank-erosion.html

Kong, D., Latrubesse, E. M., Miaoa, C., & Zhouc, R. (2020). Morphological response of the Lower Yellow River to the operation of Xiaolangdi Dam, China. *Geomorphology, 350*.

Kumar, L., & Mutanga, O. (2018). Google Earth Engine Applications Since Inception: Usage, Trends, and Potential. *Remote Sensing, 10*, 1509.

Langat, P. K., Kumar, L., & Koech, R. (2019). Monitoring river channel dynamics using remote sensing and GIS techniques. *Geomorphology, 325*, 92-102.

Latrubesse, E. M. (2008). Patterns of anabranching channels: The ultimate end-member adjustment of mega rivers. *Geomorphology, 101*, 130-145.

LeFavour, G., & Alsdorf, D. (2005). Water slope and discharge in the Amazon River estimated using the shuttle radar topography mission digital elevation model. *Geophysical Research Letters, 32*(17). doi:10.1029/2005GL023491

Leopold, L., & Wolman, M. (1957). River channel patterns: braided, meandering, and straight. *United States Geological Survey Professional Paper*, 85.

Ligthart, D. (2017). *The physical processes influencing morphodynamics in braided rivers (MSc Thesis).* TU Delft.

McFeeters, S. K. (1996). The use of the normalized difference water index (NDWI) in the delineation of open water features. *International Journal of Remote Sensing*, 1425-1432.

Mertes, L. A., Dunne, T., & Martinelli, L. A. (1996). Channel-floodplain geomorphology along the Solimões-Amazon River, Brazil. *GSA Bulletin*, 1089-1107.

Monegaglia, F., Zolezzi, G., Güneralp, I., & Henshaw, A. J. (2018). Automated extraction of meandering river morphodynamics from multitemporal remotely sensed data. *Environmental Modelling & Software, 105*, 171-186.

Morón, S., Edmonds, D., & Amos, K. (2017). The role of floodplain width and alluvial bar growth as a precursor for the formation of anabranching rivers. *Geomorphology, 278*, 78-90.

Nanson, G. (2013). Anabranching and Anastomosing Rivers. *Treatise on Geomorphology*, 330–345. doi:https://doi.org/10.1016/B978-0-12-374739-6.00244-X

Nanson, G. C., & Knighton, A. D. (1996). Anabranching Rivers: Their Cause, Character and Classification. *Earth Surface Processes and Landforms, 21*, 217-239.

Nicholas, A. P., Ashworth, P. J., Smith, G. H., & Sandbach, S. D. (2013). Numerical simulation of bar and island morphodynamics. *Journal of Geophysical Research: Earth Surface, 118*, 2019-2044.

Nobre, A., Cuartas, L., Hodnett, M., Rennó, C., Rodrigues, G., Silveira, A., . . . Saleska, S. (2010). Height Above the Nearest Drainage – a hydrologically relevant new terrain model. *Journal of Hydrology, 404*, 13-29.

Otsu, N. (1975). A threshold selection method from gray-level histograms. *Automatica, 23*, 285-296.

Park, E., Latrubresse, E., & Aquino, S. (2017). The Irrawady River: An initial Assesments on Suspended Sediments. doi:10.13140/RG.2.2.36614.78407

Peixoto, J. M., Nelson, B. W., & Wittman, F. (2009). Spatial and temporal dynamics of river channel migration and vegetation in central Amazonian white-water floodplains by remote-sensing techniques. *Remote Sensing of Environment, 113*, 2258-2266.

Rinaldi, M., & Darby, S. E. (2007). 9 Modelling river-bank-erosion processes and mass failure mechanisms: progress towards fully coupled simulations. *Developments in Earth Surface Processes, 11*, 213-239.

Robert, A. (2003). *River processes: An intoduction to fluvial dynamics.* Hodder education.

Rowland, J. C., Shelef, E., Pope, P. A., Muss, J., Gangodagamage, C., P.Brumby, S., & J.Wilson, C. (2016). A morphology independent methodology for quantifying planview river change and characteristics from remotely sensed imagery. *Remote Sensing of Environment, 184*, 212-228.

Schumann, G. J., & Moller, D. K. (2015). Microwave remote sensing of flood inundation. *Physics and Chemistry of the Earth*, 84-95.

Schumann, G. J.-P., & Bates, P. D. (2018). The Need for a High-Accuracy, Open-Access Global DEM. *frontiers in Earth Science*.

Schumm, S. (1985). Patterns of alluvial rivers. *Annual Review of Earth and Planetary Sciences, 13*, 5-27.

Schuurman, F. (2015). *Bar and channel evolution in meandering and braiding rivers using physics-based modeling (PhD Thesis).* Utrecht University.

Schwenk, J., Khandelwal, A., Fratkin, M., Kumar, V., & Foufoula-Georgiou, E. (2017). High spatiotemporal resolution of river planform dynamics from Landsat: The RivMAP toolbox and results from the Ucayali River. *Earth and Space Science, 4*, 46-75.

Serra, J. (1983). Introduction to Mathematical Morphology. *Computer Vision, Graphic, and Image Processing, 35*, 283-305.

Słowik, M. (2018). The formation of an anabranching planform in a sandy floodplain by increased flows and sediment load. *Earth Surface Processes and Landforms, 43*, 623-638.

Steijn, R., Huthoff, F., Stoeten, K., Huizer, T., Agerbeek, B., & Sloff, K. (2019). *River Bank and Bed Protection Ayeyarwady River- Nyaungdon.* Arcadis.

Surian, N. (1999). Channel Changes Due to River Regulation: The Case of the Piave River, Italy. *Earth Surface Processes and Landforms, 24*, 1135-1151.

Surian, N. (2015). *Fluvial Processes in Braided Rivers. In: Rivers-Physical, Fluvial and Environmental.* Springer.

Van den Berg, J. (1995). Prediction of alluvial channel pattern of perennial rivers. *Geomorphology, 12*, 279.

Van der Velden, J. (2015). *Understanding the river dynamic of the Ayeyarwady river, Myanmar (MSc Thesis).* Utrecht University.

Van Duijn, D. F. (2018). *The effects of vegetation on riverbank stability in the Ayeyarwady River.* TU Delft.

Wang, D., Ma, Y., Liu, X., Huang, H. Q., Huang, L., & Deng, C. (2019). Meandering-anabranching river channel change in response to flow-sediment regulation: Data analysis and model validation. *Journal of Hydrology, 579*.

Ward, J. O. (1994). The Niger River: geomorphic considerations for future development. In S. A. Schumm, & B. R. Winkley, *The variability of large alluvial rivers* (pp. 423-439). New York: ASCE Press.

Wohl, E., Brian P. Bledsoe, R. B., Poff, N. L., Rathburn, S. L., Walters, D. M., & Wilcox, A. C. (2015). The Natural Sediment Regime in Rivers: Broadening the Foundation for Ecosystem Management. *Bioscience, 65*, Pages 358–371.

WWF. (2019, May 9). *JUST ONE-THIRD OF THE WORLD'S LONGEST RIVERS REMAIN FREE-FLOWING.* Retrieved from WWF: https://www.worldwildlife.org/stories/just-one-third-of-the-world-s-longest-rivers-remain-free-flowing?utm_campaign=freshwater&utm_medium=social&utm_source=twitter.com

Xia, J., Li, X., Li, T., Zhang, X., & Zong, Q. (2014). Response of reach-scale bankfull channel geometry to the altered flow and sediment regime in the lower Yellow River. *Geomorphology*, 255-265.

Xu, H. Q. (2006). Modification of normalised difference water index (NDWI) to enhance open water features in remotely sensed imagery. *International Journal of Remote Sensing, 27*, 3025-3033.

Yang, C., Cai, X., Wang, X., Yan, R., Zhang, T., Zhang, Q., & Lu, X. (2015). Remotely Sensed Trajectory Analysis of Channel Migration in Lower Jingjiang Reach during the Period of 1983–2013. *Remote Sensing, 7*, 16241–16256.

Yang, X., Pavelsky, T. M., G. H., & Donchyts, G. (2019). RivWidthCloud: An Automated Google Earth Engine Algorithm for River Width Extraction From Remotely Sensed Imagery. *IEEE Geoscience and Remote Sensing Letters*.

Yang, Y., Liu, Y., Zhou, M., Zhang, S., Zhan, W., Sun, C., & Duan, Y. (2015). Landsat 8 OLI image based terrestrial water extraction from heterogeneous backgrounds using a reflectance homogenization approach. *Remote Sensing of Environment*, 14-32.

APPENDICES

Appendix A : WATER LEVEL DATA

The water level data was obtained from three different sources:

- The Directorate of Water Resources (DWIR),
- the Department of Meteorology and Hydrology (DMH)
- The Irrigation and Water Utilization Management Department (IWUMD).

The gauges are manually operated and the water levels are read daily. The water levels are measured with respect to a local reference, not with respect to Mean Sea Level (MSL). The datasets that were available generally range from 1990-2017, which is thus most of the period that is studied with satellite images (1988-2019). More information on the water level data is given in Steijn et al. (2019).

Appendix B : ADDITIONAL INFORMATION ON THE USED METHODS

I. FILTERING STEPS

As mentioned in in chapter 3, the scheme of Figure 57 was used to select images for the analysis. This section will go into more details of the selection criteria. First of all, only Tier 1 imagery was used, which are images that have low errors in georegistration[5]. This ensures that the river is located consistently and limits detection errors of river change by improperly georeferenced imagery.

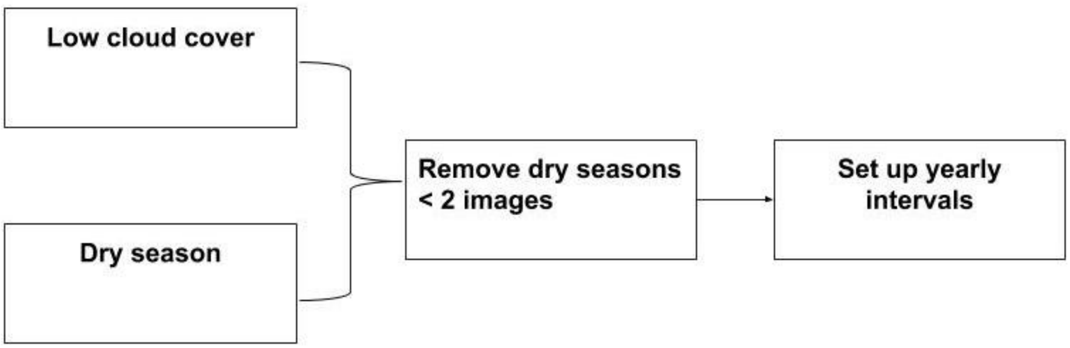

Figure 57: Overview of the filtering steps used in the analysis

Cloud cover

The cloud cover in the study area was minimised. It was found that both the detection of surface water and the detection of sediment bars were heavily impacted by cloud cover. The cloud score was determined with the simpleCloudScore[6] algorithm, which detects clouds by using a combination of several infrared bands. The cloudy pixel percentage was determined by selecting by drawing the river contour with about 2 km's of buffer on either site. This makes sure that cloud directly influencing the classification of the river surface were limited. Finally, the cloud pixel percentage was set to lower than 5 percent.

Dry season

Generally, the period with the lowest water levels ranges from January to April (see Figure 13). It was found that in late dry seasons the ability to distinguish sediment bars from more barren areas was troublesome. Areas that are normally vegetated become more barren in late dry seasons. Therefore, there was opted to limit the period from January- March

The final lists of selection criteria is as follows:

- Landsat 4, 5, 7 and 8.
- Top of Atmosphere or TOA
- Only Tier 1 images
- Rows 47 and 48 +path 133
- Cloud cover in the direct surrounding of the river lower than 5 percent.

---

[5] https://www.usgs.gov/land-resources/nli/landsat/landsat-collection-1?qt science_support_page_related_con=1#qt-science_support_page_related_con
[6] https://developers.google.com/earth-engine/landsat#simple-cloud-score

- Only the dry season, specifically the months Jan-March to improve the performance

II. ADDITIONAL FILTERING STEPS FOR METHOD 2 OF DETECTION (EQUAL WATER LEVELS)

Several additional steps were taken to make sure the water levels were similar. As the water level data showed poor spatial correlation, a combination of multiple measurement locations is used. Data from 4 measurement locations is available (see Figure 58). To represent the northern part of the study area, only a single location (Seiktha) is available. In the southern part Zalun, Danubyu and Nyaungdon are available. Nyaungdon is on the outer edge of the study area, which was therefore not included in the analysis. Thus, a combination of Seiktha, Zalun and Danubyu was used to try to reduce the effect of the water level on the analysis. From the spatial correlation in the measurement data it was found that Danubyu and Zalun can sometimes have a low spatial correlation even though they are only 20 km apart. This can be due to local outliers. However, as outliers are not straightforward to identify they were both included in the selection of satellite images.

For each station a histogram was made of the water level data in the dry season (January- April). Based on this, the most common water levels are derived. As mentioned in the main text, the range was set to 1 meter which was found to both give enough samples and reduce the effect of the water level on the change metrics. An example of the procedure is given in Figure 58. The range with the most common occurrence is between 2 and 3 meter above local reference.

The next step is to couple the images to the measured water levels on the day of acquisition. Finally, by using a combination of the general filtering steps and the water level criteria the images are selected (see Figure 59).

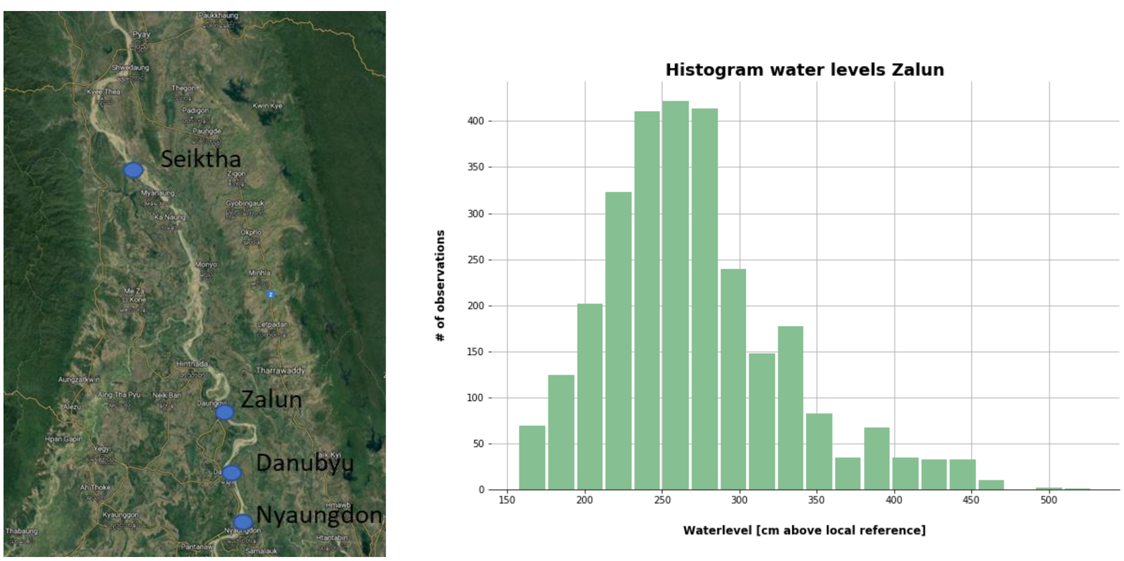

Figure 58: Measurement locations and an example of the histogram for the water level location of Zalun.

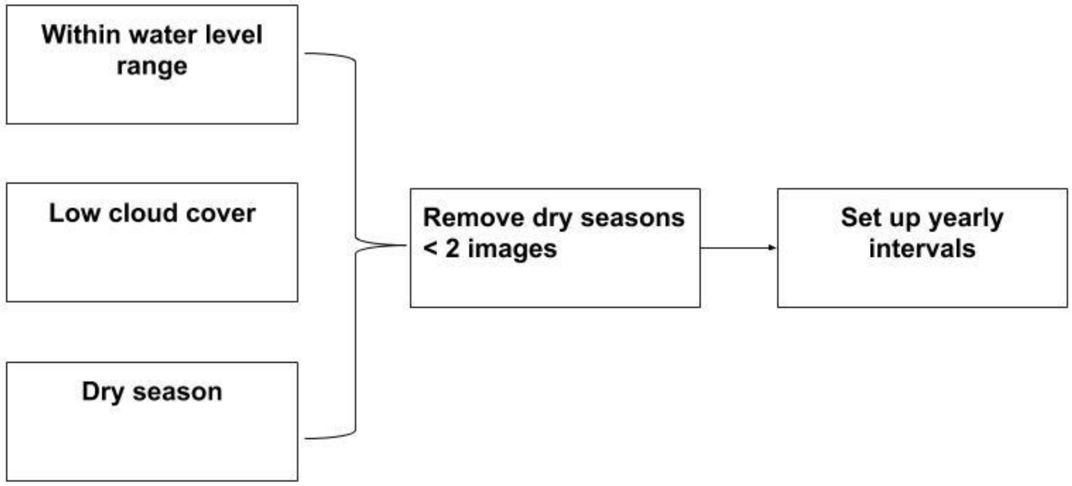

Figure 59: All filtering steps for the second method of detection (equal water level)

III. Differences between the NDWI and the mNDWI

It is not straightforward to determine which water index performs best, as the performance largely depends on local conditions. Therefore, both the NDWI and the MNDWI were tested. A characteristic of the Ayeyarwady river is the presence of a lot of areas with shallow water and many land water boundaries around sediment bars. For the detection of surface water the performance around these areas is critical. The main difference between the mNDWI and the NDWI is the use of the NIR band and the use of the SWIR band.

$$NDWI = \frac{Green - NIR}{Green + NIR}$$

$$mNDWI = \frac{Green - SWIR}{Green + SWIR}$$

The histograms of Figure 60 show a clear difference between the two indices. The NDWI shows two wide peaks and a narrower peak. The narrower peak accounts for the bar surfaces. This shows that the NDWI is relatively sensitive to sediment. On the other hand, the MNDWI only shows two peaks and is insensitive to sediment. Due to the insensitivity it is more easily able to distinguish a land and a water class. However, the downside is that shallow water pixels near sediment bars and mixed pixels around sediment bars are not detected as water. This effect is illustrated by Figure 61. In detection method 1 both bars and the water surface are combined into a single river mask. The usage of the MNDWI create large unwanted gaps in the river mask. This is why there was opted for the NDWI, despite the fact it can less easily distinguish a land and a water class.

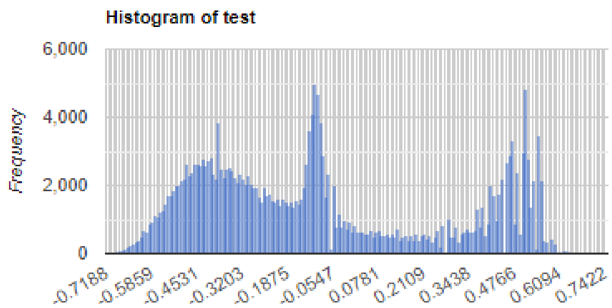

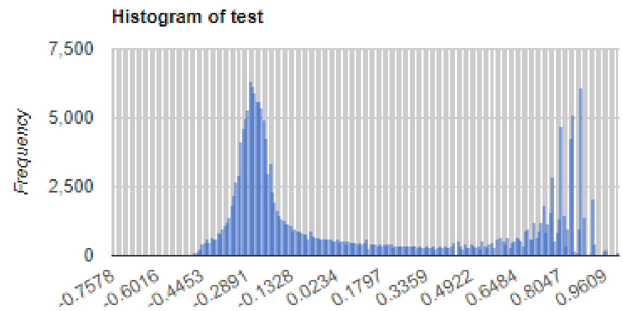

Figure 60: Histograms of NDWI and mNDWI

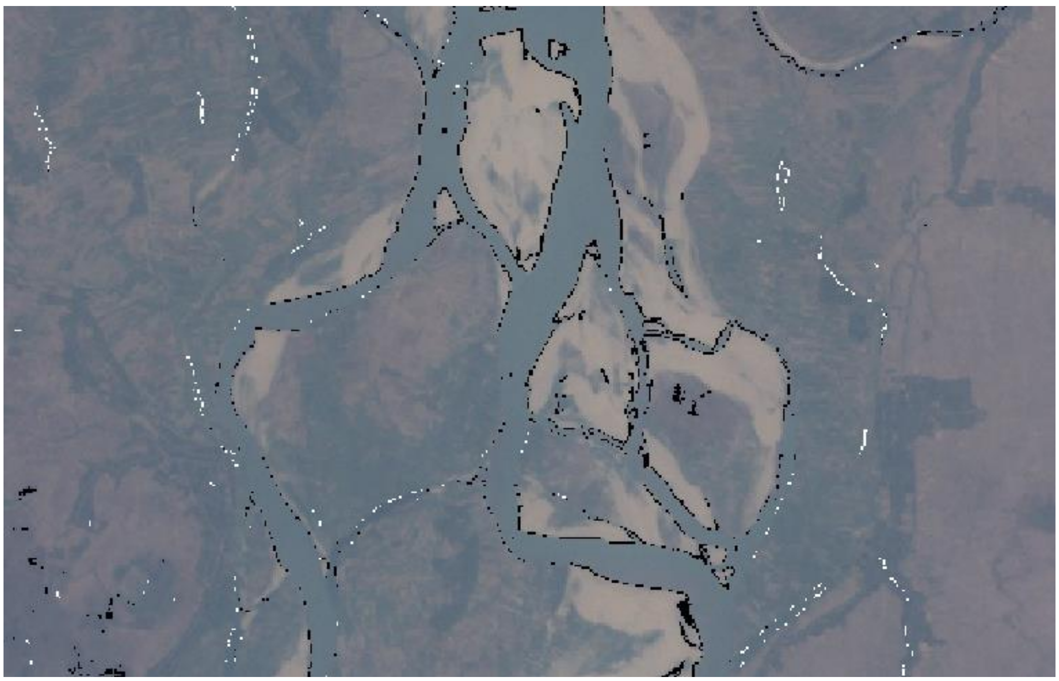

Figure 61: Difference between MNDWI and NDWI. The black pixels indicate where the NDWI has detected water but the mNDWI did not. As is visible differences mainly occur between edges of water and sediment. For edges with vegetation both the MDNWI and the NDWI are equal

IV. THRESHOLDING

Surface water

The used method is largely based on the developed method of Donchyts (2018). For a more elaborate description this is referred to his study. Some modifications were done for the applications in the Ayeyarwady river. In short, to determine the threshold for water, first of all a region of interest is drawn, which is in this case the lower Ayeyarwady river. Then all the river edges are determined with a canny edge filter, which detects sharp changes between reflections which are present between land and water. Then a buffer around the river edges was made, to ensure the inclusion of sufficient pixels of land and water. The pixels inside this buffer served as input for the Otsu thresholding method. This should optimize the threshold to also take into account the edges of the river. Furthermore, this makes sure that an optimal distribution of water and non-water pixels are used, which preferably gives a bimodal distribution of reflections. The steps are illustrated in Figure 62.

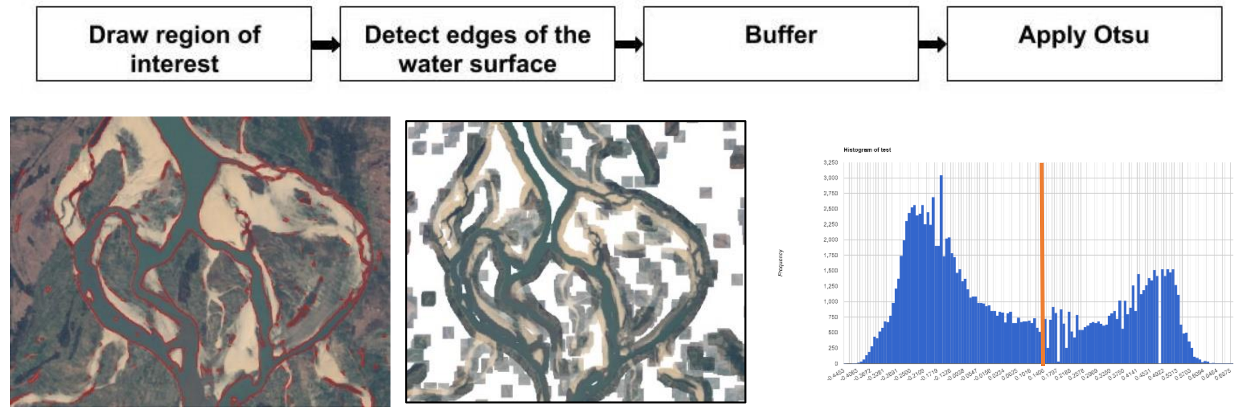

Figure 62: Illustration of the Otsu thresholding method applied for the case study of the Ayeyarwady river. From left to right the images represent: The detection of the surface water edges. Generating a buffer to serve as input for Otsu thresholding. Applying Otsu thresholding.

Sediment bars

An example of a typical cross section of the river and the reflective properties in the Short Wave Infrared band (B7 in LS5 ,7 and 8) and is given in Figure 63. It shows three different classes which from left to right represent water, vegetation and sediment bars. The original two class Otsu thresholding algorithm (Otsu, 1979) requires a bi-modal distribution (Donchyts, 2018), which is clearly not present. There have been developed multiclass approaches, e.g. the often cited paper by Huang & Wang (2009). However, the selection of adequete input for the algorithm is still complicated. Sediment bars genereally have a relatively small surface area compared to other surfaces such as water and vegetation and migrate.

In the end there was therefore opted to manually select a constant threshold by studying the reflectence properties over time such as in Figure 63. Although foggy condtions changed the reflective properties somewhat, it was found that a threshold of **0.25** provided sufficient result over the period of 1988-2019.

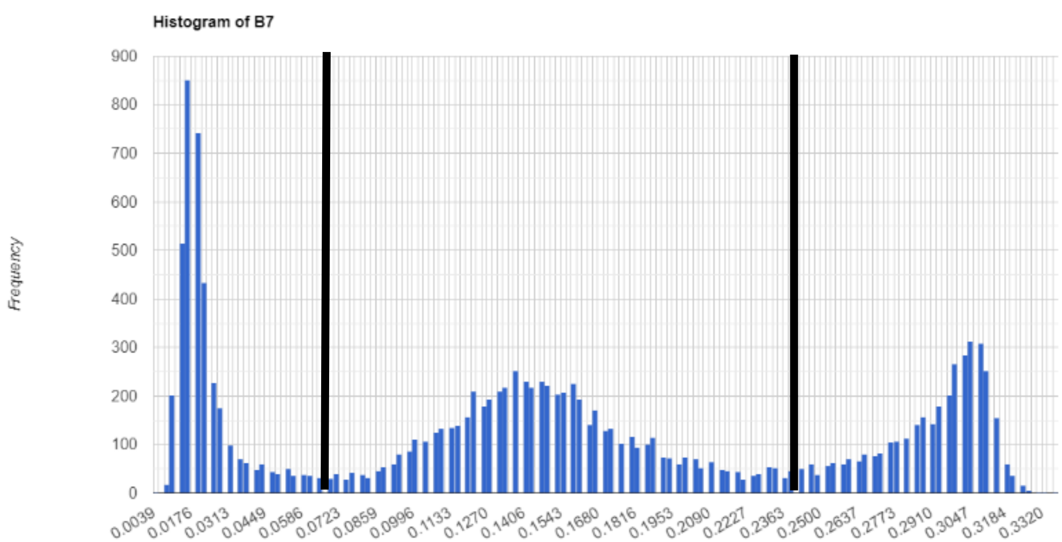

Figure 63: An example of the measured reflectance in the SWIR band (B7) in a typical cross-section of the Ayeyarwady river. Three classes are visible, from left to right: Water, vegetation and bars. Setting a threshold of 0.25 allows to distinguish the bar class.

V. Generating different river sections for detection of spatial differences

A polygon was made which was divided into 15 different sections. The procedure to derive a polygon used several steps:

- First of all, all classified river masks were used and combined into a single mask that represents all locations of the river from 1988-2019.
- All islands were removed to create a river polygon.
- The resulting polygon was smoothed with a gaussian filter.
- A buffer was taken to ensure all river areas are included.
- A centreline was generated by making use of Voronoi diagrams.
- Orthogonal lines were generated based on the centreline at 15 intervals.
- Finally, using the orthogonal lines and the polygon representing all locations of the river 15 polygons were generated of that represent a river length of roughly 20 km.

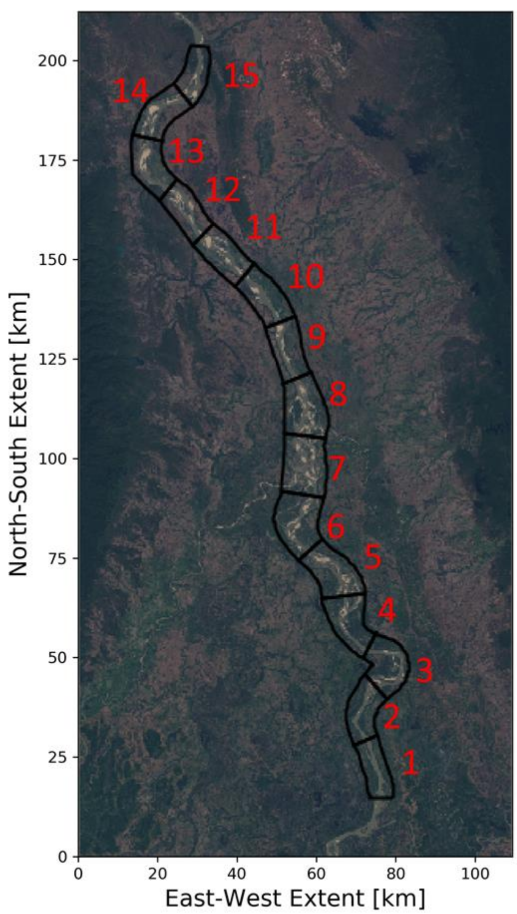

Appendix C : IMAGE ID'S

All used images including their ID number in Google Earth Engine that are used to derive the bankfull channel extent (method 1) are given in Table 9. Compared to Table 4, the number of pairs correspond to the number of images that are mentioned there. Each pair of row 47 and 48 is considered as 1 single image. In Table 10 all images for the method that detects the low stage channel are given.

Table 9: All images including their ID numbers for bankfull stage channel detection

Dry season year	Pair number	Pairs of rows 47 and 48
1988	1	LANDSAT/LT05/C01/T1_TOA/LT05_133048_19880207; LANDSAT/LT05/C01/T1_TOA/LT05_133047_19880207
	2	LANDSAT/LT05/C01/T1_TOA/LT05_133048_19880223; LANDSAT/LT05/C01/T1_TOA/LT05_133047_19880223
1989	1	LANDSAT/LT04/C01/T1_TOA/LT04_133048_19890116; LANDSAT/LT04/C01/T1_TOA/LT04_133047_19890116
	2	LANDSAT/LT04/C01/T1_TOA/LT04_133048_19890201; LANDSAT/LT04/C01/T1_TOA/LT04_133047_19890201
	3	LANDSAT/LT05/C01/T1_TOA/LT05_133048_19890209 ; LANDSAT/LT05/C01/T1_TOA/LT05_133047_19890209
	4	LANDSAT/LT04/C01/T1_TOA/LT04_133048_19890217 ; LANDSAT/LT04/C01/T1_TOA/LT04_133047_19890217
1995	1	LANDSAT/LT05/C01/T1_TOA/LT05_133048_19950314; LANDSAT/LT05/C01/T1_TOA/LT05_133047_19950314
	2	LANDSAT/LT05/C01/T1_TOA/LT05_133048_19950330 ;LANDSAT/LT05/C01/T1_TOA/LT05_133047_19950330
1996	1	LANDSAT/LT05/C01/T1_TOA/LT05_133048_19960229; LANDSAT/LT05/C01/T1_TOA/LT05_133047_19960229
	2	LANDSAT/LT05/C01/T1_TOA/LT05_133048_19960316; LANDSAT/LT05/C01/T1_TOA/LT05_133047_19960316
1998	1	LANDSAT/LT05/C01/T1_TOA/LT05_133048_19980202; LANDSAT/LT05/C01/T1_TOA/LT05_133047_19980202
	2	LANDSAT/LT05/C01/T1_TOA/LT05_133048_19980306; LANDSAT/LT05/C01/T1_TOA/LT05_133047_19980306
	3	LANDSAT/LT05/C01/T1_TOA/LT05_133048_19980322; LANDSAT/LT05/C01/T1_TOA/LT05_133047_19980322
1999	1	LANDSAT/LT05/C01/T1_TOA/LT05_133048_19990120; LANDSAT/LT05/C01/T1_TOA/LT05_133047_19990120
	2	LANDSAT/LT05/C01/T1_TOA/LT05_133048_19990309; LANDSAT/LT05/C01/T1_TOA/LT05_133047_19990309
2000	1	LANDSAT/LT05/C01/T1_TOA/LT05_133048_20000123; LANDSAT/LT05/C01/T1_TOA/LT05_133047_20000123
	2	LANDSAT/LT05/C01/T1_TOA/LT05_133048_20000224; LANDSAT/LT05/C01/T1_TOA/LT05_133047_20000224
	3	LANDSAT/LE07/C01/T1_TOA/LE07_133048_20000303; LANDSAT/LE07/C01/T1_TOA/LE07_133047_20000303
2001	1	LANDSAT/LT05/C01/T1_TOA/LT05_133048_20010125; LANDSAT/LT05/C01/T1_TOA/LT05_133047_20010125
	2	LANDSAT/LT05/C01/T1_TOA/LT05_133048_20010226; LANDSAT/LT05/C01/T1_TOA/LT05_133047_20010226
	3	LANDSAT/LE07/C01/T1_TOA/LE07_133048_20010306; LANDSAT/LE07/C01/T1_TOA/LE07_133047_20010306
2002	1	LANDSAT/LE07/C01/T1_TOA/LE07_133048_20020205; LANDSAT/LE07/C01/T1_TOA/LE07_133047_20020205

	2	LANDSAT/LE07/C01/T1_TOA/LE07_133048_20020221; LANDSAT/LE07/C01/T1_TOA/LE07_133047_20020221
	3	LANDSAT/LE07/C01/T1_TOA/LE07_133048_20020309; LANDSAT/LE07/C01/T1_TOA/LE07_133047_20020309
	4	LANDSAT/LE07/C01/T1_TOA/LE07_133048_20020325; LANDSAT/LE07/C01/T1_TOA/LE07_133047_20020325
2003	1	LANDSAT/LE07/C01/T1_TOA/LE07_133048_20030208; LANDSAT/LE07/C01/T1_TOA/LE07_133047_20030208
	2	LANDSAT/LE07/C01/T1_TOA/LE07_133048_20030224; LANDSAT/LE07/C01/T1_TOA/LE07_133047_20030224
	3	LANDSAT/LE07/C01/T1_TOA/LE07_133048_20030312; LANDSAT/LE07/C01/T1_TOA/LE07_133047_20030312
2004	1	LANDSAT/LT05/C01/T1_TOA/LT05_133048_20040306; LANDSAT/LT05/C01/T1_TOA/LT05_133047_20040306
	2	LANDSAT/LT05/C01/T1_TOA/LT05_133048_20040322; LANDSAT/LT05/C01/T1_TOA/LT05_133047_20040322
2005	1	LANDSAT/LT05/C01/T1_TOA/LT05_133048_20050205; LANDSAT/LT05/C01/T1_TOA/LT05_133047_20050205
	2	LANDSAT/LT05/C01/T1_TOA/LT05_133048_20050309; LANDSAT/LT05/C01/T1_TOA/LT05_133047_20050309
2006	1	LANDSAT/LT05/C01/T1_TOA/LT05_133048_20060224; LANDSAT/LT05/C01/T1_TOA/LT05_133047_20060224
	2	LANDSAT/LT05/C01/T1_TOA/LT05_133048_20060312; LANDSAT/LT05/C01/T1_TOA/LT05_133047_20060312
2007	1	LANDSAT/LT05/C01/T1_TOA/LT05_133048_20070110; LANDSAT/LT05/C01/T1_TOA/LT05_133047_20070110
	2	LANDSAT/LT05/C01/T1_TOA/LT05_133048_20070126; LANDSAT/LT05/C01/T1_TOA/LT05_133047_20070126
	3	LANDSAT/LT05/C01/T1_TOA/LT05_133048_20070227; LANDSAT/LT05/C01/T1_TOA/LT05_133047_20070227
	4	LANDSAT/LT05/C01/T1_TOA/LT05_133048_20070315; LANDSAT/LT05/C01/T1_TOA/LT05_133047_20070315
	5	LANDSAT/LT05/C01/T1_TOA/LT05_133048_20070331 ; LANDSAT/LT05/C01/T1_TOA/LT05_133047_20070331
2008	1	LANDSAT/LT05/C01/T1_TOA/LT05_133048_20080301; LANDSAT/LT05/C01/T1_TOA/LT05_133047_20080301
	2	LANDSAT/LT05/C01/T1_TOA/LT05_133048_20080317; LANDSAT/LT05/C01/T1_TOA/LT05_133047_20080317
2009	1	LANDSAT/LT05/C01/T1_TOA/LT05_133048_20090131; LANDSAT/LT05/C01/T1_TOA/LT05_133047_20090131
	2	LANDSAT/LT05/C01/T1_TOA/LT05_133048_20090216; LANDSAT/LT05/C01/T1_TOA/LT05_133047_20090216
	3	LANDSAT/LT05/C01/T1_TOA/LT05_133048_20090304; LANDSAT/LT05/C01/T1_TOA/LT05_133047_20090304
	4	LANDSAT/LT05/C01/T1_TOA/LT05_133048_20090320; LANDSAT/LT05/C01/T1_TOA/LT05_133047_20090320
2010	1	LANDSAT/LT05/C01/T1_TOA/LT05_133048_20100203; LANDSAT/LT05/C01/T1_TOA/LT05_133047_20100203
	2	LANDSAT/LT05/C01/T1_TOA/LT05_133048_20100219; LANDSAT/LT05/C01/T1_TOA/LT05_133047_20100219
	3	LANDSAT/LT05/C01/T1_TOA/LT05_133048_20100323; LANDSAT/LT05/C01/T1_TOA/LT05_133047_20100323
2014	1	LANDSAT/LC08/C01/T1_TOA/LC08_133048_20140214; LANDSAT/LC08/C01/T1_TOA/LC08_133047_20140214
	2	LANDSAT/LC08/C01/T1_TOA/LC08_133048_20140302; LANDSAT/LC08/C01/T1_TOA/LC08_133047_20140302

	3	LANDSAT/LC08/C01/T1_TOA/LC08_133048_20140318; LANDSAT/LC08/C01/T1_TOA/LC08_133047_20140318
2015	1	LANDSAT/LC08/C01/T1_TOA/LC08_133048_20150217; LANDSAT/LC08/C01/T1_TOA/LC08_133047_20150217
	2	LANDSAT/LC08/C01/T1_TOA/LC08_133048_20150305; LANDSAT/LC08/C01/T1_TOA/LC08_133047_20150305
	3	LANDSAT/LC08/C01/T1_TOA/LC08_133048_20150321; LANDSAT/LC08/C01/T1_TOA/LC08_133047_20150321
2016	1	LANDSAT/LC08/C01/T1_TOA/LC08_133048_20160220; LANDSAT/LC08/C01/T1_TOA/LC08_133047_20160220
	2	LANDSAT/LC08/C01/T1_TOA/LC08_133048_20160307; LANDSAT/LC08/C01/T1_TOA/LC08_133047_20160307
	3	LANDSAT/LC08/C01/T1_TOA/LC08_133048_20160323; LANDSAT/LC08/C01/T1_TOA/LC08_133047_20160323
2017	1	LANDSAT/LC08/C01/T1_TOA/LC08_133048_20170206; LANDSAT/LC08/C01/T1_TOA/LC08_133047_20170206
	2	LANDSAT/LC08/C01/T1_TOA/LC08_133048_20170222; LANDSAT/LC08/C01/T1_TOA/LC08_133047_20170222
	3	LANDSAT/LC08/C01/T1_TOA/LC08_133048_20170310; LANDSAT/LC08/C01/T1_TOA/LC08_133047_20170310
	4	LANDSAT/LC08/C01/T1_TOA/LC08_133048_20170326; LANDSAT/LC08/C01/T1_TOA/LC08_133047_20170326
2018	1	LANDSAT/LC08/C01/T1_TOA/LC08_133048_20180225; LANDSAT/LC08/C01/T1_TOA/LC08_133047_20180225
	2	LANDSAT/LC08/C01/T1_TOA/LC08_133048_20180313; LANDSAT/LC08/C01/T1_TOA/LC08_133047_20180313
	3	LANDSAT/LC08/C01/T1_TOA/LC08_133048_20180329; LANDSAT/LC08/C01/T1_TOA/LC08_133047_20180329
2019	1	LANDSAT/LC08/C01/T1_TOA/LC08_133048_20190228; LANDSAT/LC08/C01/T1_TOA/LC08_133047_20190228
	2	LANDSAT/LC08/C01/T1_TOA/LC08_133048_20190316; LANDSAT/LC08/C01/T1_TOA/LC08_133047_20190316

Table 10: All images including their ID numbers for low stage channel detection

Year of dry season	Pair number	Pairs of row 47 and 48 (ImagesID's GEE)
1995	1	LANDSAT/LT05/C01/T1_TOA/LT05_133048_19950109 LANDSAT/LT05/C01/T1_TOA/LT05_133047_19950109
	2	LANDSAT/LT05/C01/T1_TOA/LT05_133048_19950210 LANDSAT/LT05/C01/T1_TOA/LT05_133047_19950210
1996	1	LANDSAT/LT05/C01/T1_TOA/LT05_133048_19960229 LANDSAT/LT05/C01/T1_TOA/LT05_133047_19960229
	2	LANDSAT/LT05/C01/T1_TOA/LT05_133048_19960316 LANDSAT/LT05/C01/T1_TOA/LT05_133047_19960316
1997	1	LANDSAT/LT05/C01/T1_TOA/LT05_133048_19970114 LANDSAT/LT05/C01/T1_TOA/LT05_133047_19970114
	2	LANDSAT/LT05/C01/T1_TOA/LT05_133048_19970303 LANDSAT/LT05/C01/T1_TOA/LT05_133047_19970303
1999	1	LANDSAT/LT05/C01/T1_TOA/LT05_133048_19990120 LANDSAT/LT05/C01/T1_TOA/LT05_133047_19990120
	2	LANDSAT/LT05/C01/T1_TOA/LT05_133048_19990309 LANDSAT/LT05/C01/T1_TOA/LT05_133047_19990309
2000	1	LANDSAT/LT05/C01/T1_TOA/LT05_133048_20000224 LANDSAT/LT05/C01/T1_TOA/LT05_133047_20000224
	2	LANDSAT/LE07/C01/T1_TOA/LE07_133048_20000303 LANDSAT/LE07/C01/T1_TOA/LE07_133047_20000303
2001	1	LANDSAT/LT05/C01/T1_TOA/LT05_133048_20010226 LANDSAT/LT05/C01/T1_TOA/LT05_133047_20010226
	2	LANDSAT/LE07/C01/T1_TOA/LE07_133048_20010306 LANDSAT/LE07/C01/T1_TOA/LE07_133047_20010306
2002	1	LANDSAT/LE07/C01/T1_TOA/LE07_133048_20020205 LANDSAT/LE07/C01/T1_TOA/LE07_133047_20020205
	2	LANDSAT/LE07/C01/T1_TOA/LE07_133048_20020221 LANDSAT/LE07/C01/T1_TOA/LE07_133047_20020221
	3	LANDSAT/LE07/C01/T1_TOA/LE07_133048_20020309 LANDSAT/LE07/C01/T1_TOA/LE07_133047_20020309
	4	LANDSAT/LE07/C01/T1_TOA/LE07_133048_20020325 LANDSAT/LE07/C01/T1_TOA/LE07_133047_20020325
2003	1	LANDSAT/LE07/C01/T1_TOA/LE07_133048_20030123 LANDSAT/LE07/C01/T1_TOA/LE07_133047_20030123
	2	LANDSAT/LE07/C01/T1_TOA/LE07_133048_20030208 LANDSAT/LE07/C01/T1_TOA/LE07_133047_20030208
	3	LANDSAT/LE07/C01/T1_TOA/LE07_133048_20030224 LANDSAT/LE07/C01/T1_TOA/LE07_133047_20030224
	4	LANDSAT/LE07/C01/T1_TOA/LE07_133048_20030312 LANDSAT/LE07/C01/T1_TOA/LE07_133047_20030312
2004	1	LANDSAT/LT05/C01/T1_TOA/LT05_133048_20040102 LANDSAT/LT05/C01/T1_TOA/LT05_133047_20040102
	2	LANDSAT/LT05/C01/T1_TOA/LT05_133048_20040219 LANDSAT/LT05/C01/T1_TOA/LT05_133047_20040219
	3	LANDSAT/LT05/C01/T1_TOA/LT05_133048_20040306 LANDSAT/LT05/C01/T1_TOA/LT05_133047_20040306

Appendix D : DERIVATION OF SURFACE WATER SLOPE

To get an estimation of the surface water slope SRTM DEM is used. SRTM data with a horizontal resolution of 30 meters is used. Reports of the vertical accuracy of SRTM DEM range from 5-10 meters (Schumann & Bates, 2018), however, LeFavour & Alsdorf (2005) show that it can give a reasonable estimation of the water surface slope. To derive the slope several steps were taken:

- Manually draw a river centreline based on the river surface in 2000 (SRTM DEM is created in 2000)
- Divide the centreline into equal intervals of roughly 1 km
- Read the elevation from SRTM DEM in Google Earth Engine at each interval.

Appendix E : STATISTICAL SIGNIFICANCE OF FOUND CORRELATIONS

Method 1 of detection (vegetation boundary):

The following steps were performed to test the statistical significance of the found relations:

- 19 samples are in the dataset
- The degrees of freedom are 19-2 = 17
- Using a two-tailed t-test with $\alpha = 0.05$ this gives :
  - $t_{crit} = 2.110$
- Assumption: Independent samples
- The t value is calculated by:
  - $t = \frac{r\sqrt{n-2}}{\sqrt{1-r^2}}$

The correlations that were found and the according t-values and their statistical significance are given in Table 11 & Table 12.

Table 11: Correlations method 1 of detection

	Max 7-day average	Max 30 day average	Max 4 month average	Max 6 month average	Average over year
Erosion	0.69	0.74	0.89	0.85	0.77
Deposition	-0.44	-0.48	-0.43	-0.36	-0.27
Migration	0.68	0.65	0.83	0.81	0.79
Channel area	0.64	0.69	0.76	0.70	0.62

Table 12: T-values method 1 of detection (marked green are > $t_{crit} = 2.110$)

	Max 7-day average	Max 30 day average	Max 4 month average	Max 6 month average	Average over year
Erosion	3.93	4.54	8.05	6.65	4.98
Deposition	-2.02	-2.26	-1.96	-1.59	-1.16
Migration	3.82	3.53	6.14	5.69	5.31
Channel area	3.43	3.93	4.82	4.04	3.26

Method 2 of detection (equal water levels):

Using the same steps:

- 7 samples are in the dataset, and the degrees of freedom are 5
- This gives: $t_{crit} = 2.571$

The correlations that were found and the according t-values and the statistical significance are given in Table 13 & Table 14

Table 13: Correlations method 2 of detection

	Max 7-day average	Max 30 day average	Max 4 month average	Max 6 month average	Average over year
Erosion	0.47	0.46	0.87	0.77	0.71
Deposition	0.53	0.57	0.66	0.64	0.42
Migration	0.53	0.56	0.88	0.81	0.65
Channel area	-0.10	-0.16	0.18	0.09	0.28

Table 14: T-values method 2 of detection (marked green are >$t_{crit} = 2.571$)

	Max 7-day average	Max 30 day average	Max 4 month average	Max 6 month average	Average over year
Erosion	1.19	1.16	3.95	2.70	2.25
Deposition	1.40	1.55	1.96	1.86	1.03
Migration	1.40	1.51	4.14	3.09	1.91
Channel area	-0.22	-0.36	0.41	0.20	0.65

Appendix F : SCRIPTS

An online example of the used script is given in the following link:

https://code.earthengine.google.com/bcc7296eaa9bd69176b5bda87ae31361

This script is an example of classification method 1, which detects the vegetation boundary to generate river masks. Method 2 that uses images with similar water levels, largely uses the same methods so a separate script is not provided. The main text elaborates on the differences between both methods. For quantifying and analysing the planform changes an offline Python script is used, combined with the Earth Engine Python API[7].

[7] https://developers.google.com/earth-engine/python_install